FOG

Freiberg Online Geoscience

FOG is an electronic journal registered under **ISSN 1434-7512**

2015, Volume 43

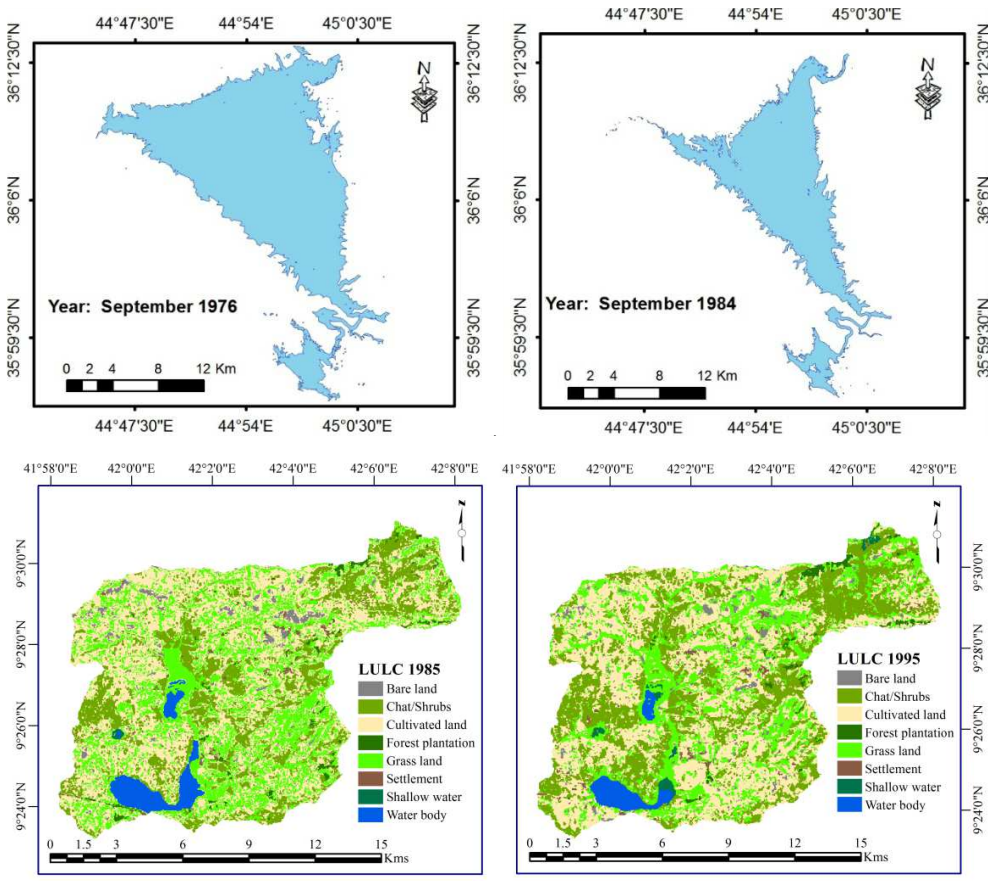

Broder Merkel & Mandy Hoyer (Eds.)

FOG special volume: Man-made changes in land cover, water quality and quantity – three case studies

61 pages, 3 contributions

List of contents

The images on the cover page are clippings taken from the papers from Al-Saady et al. and Gebere et al. They show the following features:

Upper images:	Change in the spatial extension of Dokan Lake in the Little Zab River Basin in Kurdistan Region between September 1976 and 1984
Lower images:	Land use and land cover changes in the dry Lake Haramaya Watershed in eastern Ethiopia between 1985 and 1995

Land use and land cover (LULC) mapping and change detection in the Little Zab River Basin (LZRB), Kurdistan Region, NE Iraq and NW Iran

Al-Saady, Younus — Department of Geology, College of Science, University of Baghdad, Baghdad, Iraq. Email: younusalsaady@yahoo.com

Merkel, Broder — Department of Hydrogeology, Institute of Geology, Technische Universität Bergakademie Freiberg, Gustav-Zeuner Str. 12, 09599 Freiberg, Germany. Email: merkel@geo.tu-freiberg.de

Al-Tawash, Balsam — Department of Geology, College of Sciences, University of Baghdad, Baghdad, Iraq. Email: balsamsalim@yahoo.com

Al-Suhail, Qusay — Department of Geology, College of Science, University of Basrah, Basrah, Iraq. Email: quab65@gmail.com

Abstract: The aim of this study was to investigate the effect of land use expansion on the natural environment of the Little Zab River basin (LZRB). The specific objectives were to: (i) prepare a land use land cover (LULC) map for the LZRB; (ii) detect changes between five dates within the time period 1976-2014 and to identify spatial and temporal changes that occurred within this time period using image indices; (iii) assess LULC classes results and compare the differences between them.

Different remote sensing and GIS techniques were applied, such as digital image processing using supervised classification and image indices. Supervised classification using a maximum likelihood algorithm was only applied on the Landsat 8 OLI data (September 2014) to classify the LULC map. The classified image was modified with the help of image indices and visual interpretation to produce a more accurate map. The image obtained with supervised classification has an overall accuracy of 83.43 % and an overall Kappa coefficient of 0.811. The results were validated using 507 ground truth points distributed all over the study area. Six Landsat images from September 1976, 1984, 1990, 2000 and two Landsat 8 OLI 2014 images from April and from September were georeferenced, radiometrically and atmospherically calibrated to detect the changes in the LZRB and to identify seasonal changes. Changes have been calculated for the vegetation cover (natural vegetation vs. cropland and pasture), surface water features and urban and built-up land. Change detection of the LZRB was performed using three indices: the Normalized Difference Vegetation Index (NDVI), the Normalized Difference Water Index (NDWI) and the Normalized Difference Built-Up Index (NDBI). From the results from supervised classification six main LULC classes have been distinguished in the LZRB. They involve barren land, agricultural land, natural vegetation, urban and built-up land, burned land and water. Barren land is the main class in the basin; it is subdivided into six subclasses. Agricultural land is the second largest class; it is subdivided into three subclasses. In this study, change detection analysis over the period (1976-2014) has revealed highly dynamic interchanges between the LULC classes. The change detection results show a rapid increase in urban and built-up land. A significant increase of the population number, the migration from small villages to the main cities and economic growth has fueled the rise of the urbanization rate within the last decades. Surface water features were shown to shrink mainly due to the shrinkage of Dokan Lake

under the pressure of climate change and due to the construction of dams in the upper watershed area of the LZRB. The natural vegetation displayed a wavy or irregular trend while cropland and pasture showed an increasing trend.

With the NDVI two classes of natural vegetation, and one cropland and one pasture class have been identified based on reflectance values. Areas with relatively high NDVI values indicate the cropland and pasture class, while lower values represent natural vegetation. Two spectral water index methods were employed in this study, an NDWI (Ji et al. 2009), which was applied on Landsat 8 OLI and TM5 images and an NDWI (El-Asmar et al. 2013), which was only applied on Landsat MSS images. Different water indices have been applied for the MSS sensor due to the large difference in the spectral range between MSS bands and other Landsat sensor bands. Both NDWI indices were successfully applied to extract water features. Finally, the NDBI changes were calculated based on visual interpretation.

Keywords: Remote sensing, supervised classification, LULC, change detection NDVI, NDWI, NDBI.

1 Introduction

Little Zab River is one of the most important tributaries of Tigris River. In the last decade, the Little Zab River Basin (LZRB) underwent many changes concerning land use expansions as a result of rapid urbanization, increasing population, and climate change. Consequently, the demand for water supply increased and the necessity for water quality monitoring and basin management became urgent. The urbanization in the Kurdistan region of Iraq and in the LZRB as a part of this region has been increasing rapidly within the last decade. Therefore, it is important to identify different LULC categories and to evaluate the magnitude and spatial extent of changes within the basin to ensure best future planning and management.

A supervised classification with the maximum likelihood algorithm was used to classify the LULC of the Landsat 8 OLI images. Different supervised classification methods have been applied and tested extensively for land use planning and management in arid and semi-arid environments (Ulbricht et al. 1993; Del Valle et al. 1998).

LULC mapping of the river basin is a useful tool that can be used for good planning and management of urbanization, agricultural practices and other human activities. Landsat data is ideal for LULC mapping and for change detection studies of large basin areas such as the LZRB. Landsat satellite data was chosen because of its open accessibility, suitability for the aim of the study, its long time of observation and its good spectral and spatial resolution for LULC analyses. Mapping LULC is presently the standard method and most common approach to monitor land use changes and developments (Mancino et al. 2014). Especially when LULC classes and their spatial and temporal changes are to be determined for categories of small geographic extent in vast areas, high-resolution satellite images are needed (Reed et al. 1996). The terms land use and land cover have been used interchangeably in many publications despite the difference between these two terms. In general land cover refers to natural biophysical covers such as forest, water bodies and barren land, while land use refers to the human utilization of land for different purposes like agriculture and settlements, which lead to altering biogeochemical, physiographical and hydrological conditions (Di Gregorio and Jansen 2000).

Despite the importance of the LZRB, little is known about the LULC change dynamics and its influence on environment and water quality. No effort has been made to evaluate the effects that agricultural land use, urban- and built-up expansion or municipal wastewater effluents could have on water quality of this

river. Identifying the dynamic change in water usage and scientifically interpreting the reasons for these changes will lead to best management of the basin environment (Nian et al. 2014).

LULC can be considered as one of the most important determinants for the quality of water resources (Griffith et al. 2002). Agricultural activities are the pollution sources most commonly mentioned in literature because of their contribution in increasing the sediment load and nutrient input to water resources (Cooper 1993). Besides that they directly contribute to the input of pesticides, pathogens and hormones. Land use practices directly influence the hydrochemistry and quality of water and then the aquatic organisms in receiving waters (Environment Canada, 2001). New techniques including geographical information systems (GIS), geo-statistics, and remote sensing provide new opportunities for the research on land surface processes. Strong population growth and consequently an increased demand for food, grazing land and fodder as well as increasing industrial activities have essentially led to the rapid change in LULC patterns. Agriculture, especially annual crops represent a large portion of the land use in the LZRB. Runoff from agricultural land could have a major and direct impact on the river water quality. The other major threat to this river is the release of municipal wastewater from the cities and towns.

1.1 Study area

The LZRB is located in the northeastern Iraq and northwestern Iran territories (Fig. 1). It stretches out between (35° 10′ 00′′ - 36° 55′ 00′′) latitude and (43° 25′ 00′′ - 46° 20′ 00′′) longitude, encompasses an area of 19,860.6 km^2 and comprises a wide variety of landscapes. The Little Zab River (LZR), which is also known as Lower Zab or sometimes Lesser Zab River is the largest tributary of Tigris River with about 71 % of its basin situated in Iraq and the rest in Iran. The LZR is an 8th order river that flows from northeast to southwest. It feeds Dokan Lake Reservoir and flows further into Tigris River. The river is fed by rainfall, snowmelt and many springs resulting in a high discharge in spring and low discharge in summer. The average annual discharge of the LZR is 7.17 km^3, of which 5.07 km^3 are retarded every year since the construction of Dokan Dam (Frenken, 2009). The climate of the basin varies from semi-arid in the north and northeastern parts to arid in the south and southwestern part. Areas of higher elevation in the north and northeast of the basin receive substantial rainfall quantities with a mean annual precipitation of up to 850 mm. This decreases notably to less than 315 mm/a in the area of lower elevation in the south and southwest of Dokan Lake until the confluence with the Tigris River. Many different geological units are exposed in the Little Zab River basin with ages ranging from Jurassic to Quaternary. The upper part of the basin area is located within the highly folded zone and Zagros Suture Zone (Jassim and Goff, 2006). It is characterized mainly by alternation of different rock types with different lithological properties, while the lower part of the basin is located within the foot hills zone, which is characterized by clastic unresisting rocks (Aziz 1983).

2 Materials and methods

2.1 Remote sensing imagery data

Satellite imagery was used from the Landsat Multispectral Scanner System (Landsat2-MSS L1T) acquired in September 1976, from Landsat 5 Thematic Mapper (TML1T) acquired in September 2000, 1990 and 1984 and from Landsat 8 OLI acquired in April 2014 and September 2014. All this data was obtained from the USGS archive (http://earthexplorer.usgs.gov/). The downloaded bands of Landsat 8OLI, TM and MSS scenes were superimposed (excluding the thermal band) to form multispectral images using ENVI5.1 software. After the acquisition of the images seven bands of OLI8, five bands of TM, four bands of MSS except the thermal bands of each image scene were superimposed to form a single multispectral image dataset using the "layer stack" function. From the acquired data, if possible, only those images without cloud cover were selected. The Universal Traverse Mercator (UTM) system

with the datum of WGS84 and Zone 38 was selected as projection for all data. The QuickBird satellite collects image data with a pixel resolution of 0.65 m. Images from this satellite are an excellent basis for identifying LULC classes. QuickBird images were used in order to effectively identify the spatial distribution characteristics of urban and built-up land and other unspecified objects in Landsat images. This data was also used to investigate and provide data (e.g. ground truth points) for areas that are inaccessible, to refine the classification of the satellite images and as reference image for geo-referencing.

2.2 Radiometric calibration and atmospheric correction

The radiometric calibration, atmospheric correction, and other preprocessing steps were done to prepare the satellite images for LULC classification and change detection. The satellite image scenes were first converted to radiances; then each image scene was converted to satellite reflectance using the Landsat calibration tool in ENVI 5.1. The necessary information such as acquisition date and sun elevation was obtained from the Landsat header files while the average elevation of each image scene was obtained from digital elevation data (DEM). Multi-temporal multispectral digital images collected by Landsat satellites for more than 38 years were utilized for preparing the LULC maps and change detection maps.

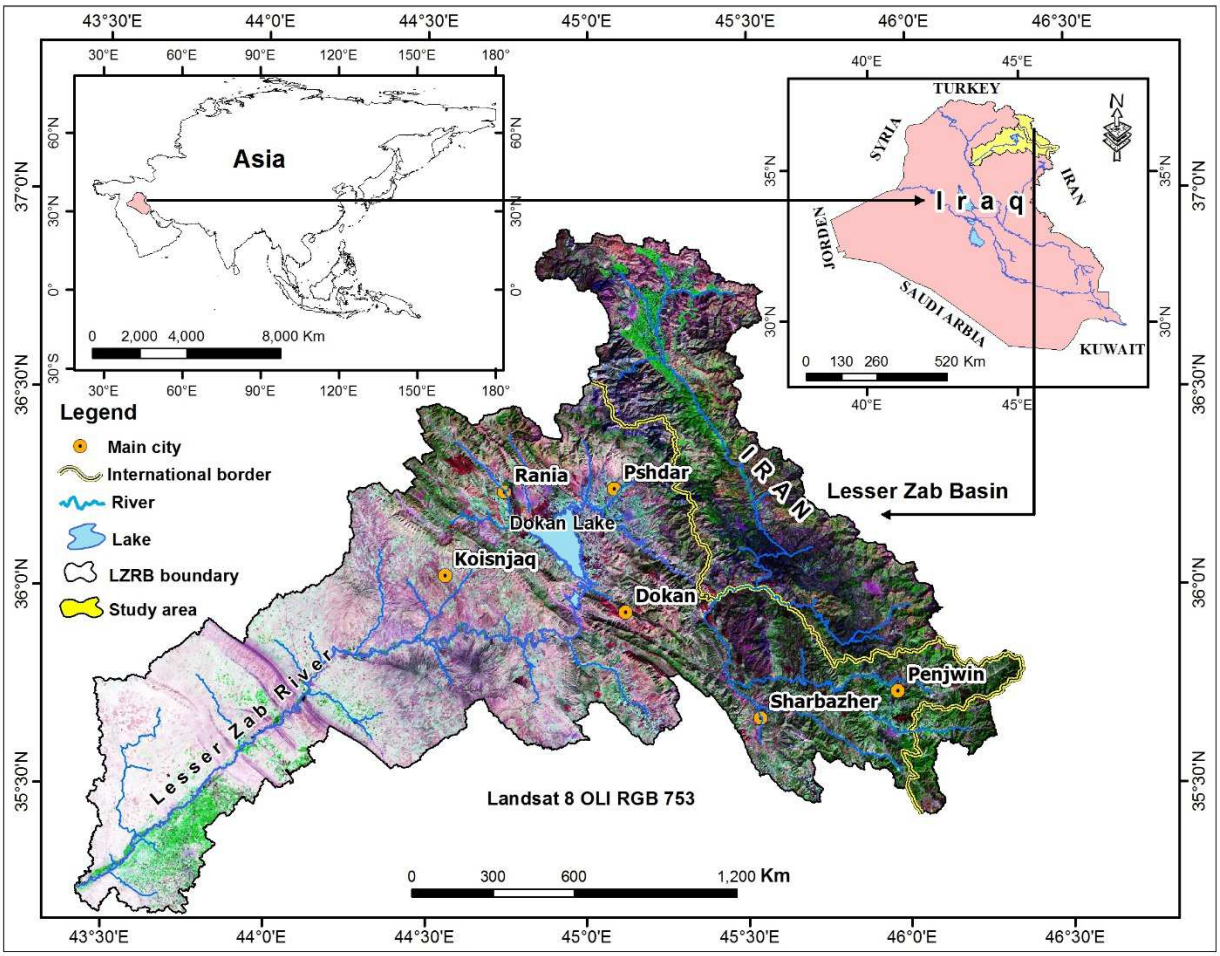

Figure 1: Location map of the study area

The correction itself involves the conversion of digital number (DN) values to spectral radiance (at the sensor), the conversion of spectral radiance to apparent reflectance (at the sensor) and finally the removal of atmospheric effects, which result from absorption and scattering (atmospheric correction) (Lillesand et al. 2014; Cui et al. 2014; Chander and Markham 2003). The spectral radiance is usually converted to reflectance because spectral radiance depends on the degree of illumination of the feature (irradiance), which is affected by many variables such as time of the day, season, latitude, etc. Whereas reflectance provides a standardized measure, which directly allows comparing images. Thus all images were radiometrically corrected.

Atmospheric corrections are unnecessary for maximum likelihood image classification of a single date image (Singh 1989; Song et al. 2001). It is, however, necessary for minimizing reflectance variations within the individual LULC classes before image classification and the detection of changes between images from different dates. Jeffries-Matusita distance is one of the spectral separability measures commonly used in remote sensing applications. It is used to quantify the spectral separability during target detection (Santillan et al. 2011). In this study, radiometric calibration and atmospheric correction have been necessary because multi-temporal data was utilized. These corrections are used to remove atmospheric interferences and to put multi-temporal data to the same radiometric scale in order to detect and monitor terrestrial surface cover changes (Chen et al. 2005; Song et al. 2001; Serra et al. 2003).

2.3 Geo-referencing of images

From comparing the results of the satellite data with the ground truth points and QuickBird data, it was observed that all data is acceptable and compatible except for the Multispectral Scanner (MSS) sensor scenes, from which selected points did not exactly fit the corresponding ground control points and ground features. Thus MSS scenes were corrected by using the image-to-image geo-referencing operation tool of ENVI based on ground control points. The Landsat MSS scenes were geo-referenced with a root mean square error of less than 0.5 pixels. Several control points were selected for geo-referencing each MSS scene with the reference image. Subsequently, the images of each year were mosaicked to generate new images covering the entire study area. For this purpose, the mosaicking tool based on geo-referenced images was used. Then the MSS images were reprojected to the Universal Transverse Mercator grid using the nearest neighbor resembling method. Finally, subsets of the images of the LZRB were created using the region of interest (ROI) layer tool of ENVI.

2.4 Field data (ground truth points) and auxiliary data

Field surveys of LZRB were conducted during wet season (April) and dry season (September) 2014 to identify the LULC and detect changes in water and vegetation cover between spring and summer using Landsat 8 OLI imagery. The global position system (GPS) Garmin and Nikon Camera were used during the collection of ground truth points. In addition to this data the available ground control points and photos from previous field surveys are also used in this work.

Existing auxiliary data comprising topographical maps, QuickBird satellite images, digital spatial geological data, laboratory reports and thematic layers were prepared as well. This data was employed to facilitate fieldwork, help with the interpretation of remote sensing data and to validate the results of LULC mapping and change detection assessments. There are 507 ground truth points from which 288 points were collected during the field survey of the study period and from previous field surveys on the study area. The rest of the ground control points were collected based on the auxiliary data (Figure 2). The ground truth points were subdivided into two groups, one group for selecting training sites for the supervised classification and the second group for the assessment of the accuracy of the image index results.

2.5 Images processing and interpretation

Image pre-processing, supervised classification, accuracy assessment and change detection using image indices was performed.

2.5.1 Supervised classification

In this study a supervised classification using maximum likelihood was applied based on the spectral differences between different classes. These differences were used to subdivide the LULC of the LZRB into separate classes. Prior knowledge is utilized to execute supervised classification, depending on previously collected training sites from certain areas of known LULC. In order to execute a supervised classification, it is necessary to collect spectral signatures from training areas, which are then used to "train" the classification algorithm (Chen and Stow 2002; Jusoff et al. 2009). Several training site were collected from different places of the study area depending on the collected ground control points, field observations and the auxiliary data. Training sites for each LULC class were collected by selecting many training sites for the same class considering their spatial distribution. Based on the statistics of these training sites, each pixel in the classified image of the LULC map was then assigned to these training sites.
The LULC map for the LZRB was generated based on the pixel-by-pixel supervised classification using Landsat 8OLI images from September 2014. Classes have been separated by selecting the spectral signatures of each class from different image sites, using the seed properties method that is provided in ERDAS Imagine V.11 software. The results were manually corrected by ArcGIS, using mainly OLI8 images of 30 meter spatial resolution. The image was improved and enhanced using digital image enhancement processing techniques to highlight some LULC classes before interpretation. Image enhancement processes alter the impression of the image on the viewer. In Erdas software different enhancement techniques are available: contrast enhancement, linear and nonlinear contrast stretching, density slicing, Gaussian stretching and so forth. Because the enhancement distorts digital pixel values, supervised classification was carried out on the original images.

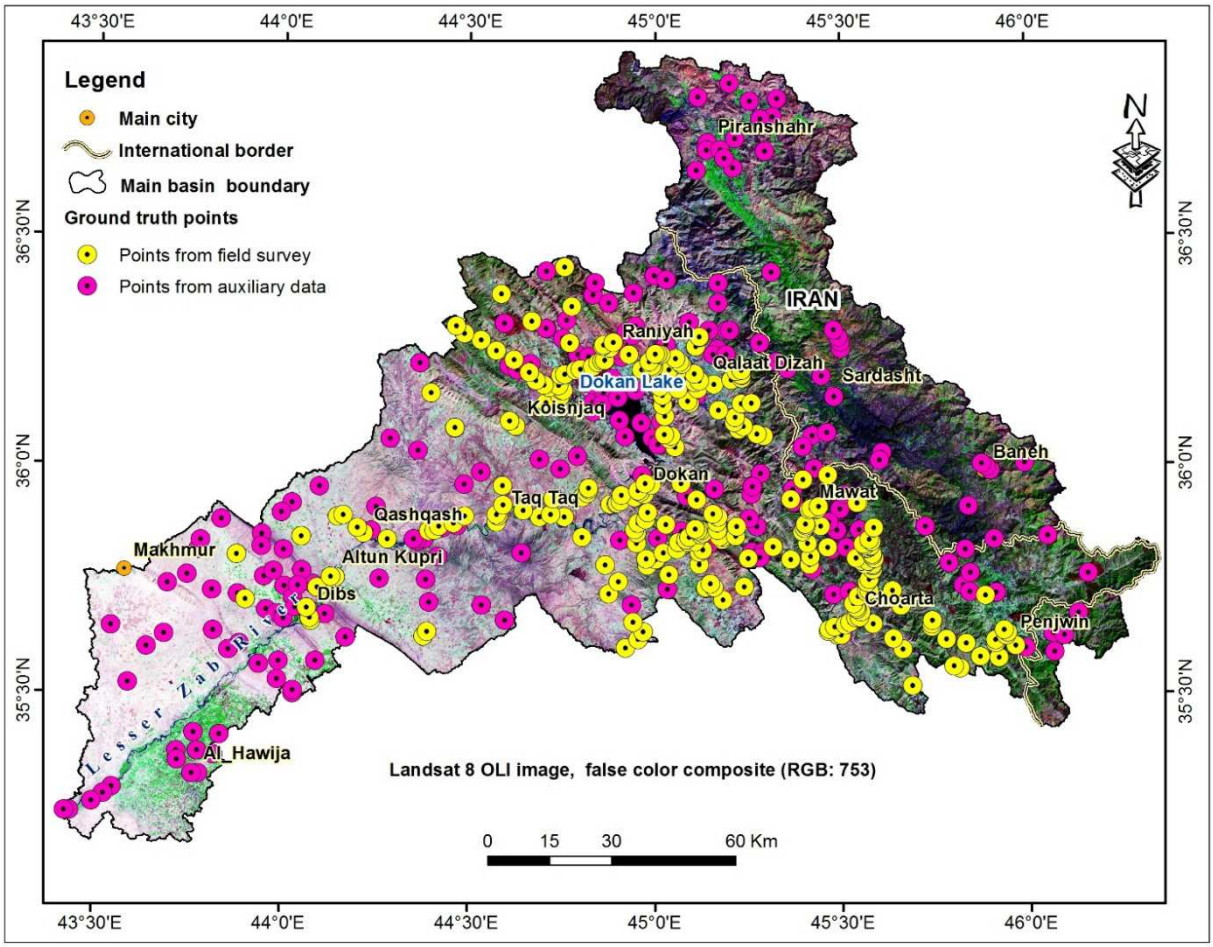

Figure 2: Ground control points used for verifying the accuracy of the LULC map

Integrating the supervised classification results of the Landsat 8 OLI and QuickBird data offered the most satisfactory results. A QuickBird image (2006) was used when detailed information was required; otherwise Landsat data was used. Several steps were used in order to improve the classification and to resolve interference problems between classes depending on visual interpretation with the help of auxiliary data and QuickBird images. The main interference existed between the urban and the built-up land class with the barren land subclasses particularly in small residential areas such as villages and towns. The misclassification in residential areas is due to the heterogeneous composition of buildings, roads, and wooded and non-wooded areas (Ward et al. 2000). After supervised classification, all images were vectorized into polygons to modify the classified image results for more accuracy using several methods such as band ratio, and visual digitizing. The spatial extents of LULC were calculated in Arc Map for each subbasin based on their derived extents and the produced LULC map. The classification of the LULC was produced according to a modified USGS classification (Anderson et al. 1976) to be more compatible with the goal of the study and the environmental conditions of the LZRB area. Finally, a set of 13 LULC classes and subclasses were recognized in the LZRB area.

2.5.1.1 Accuracy assessment

The increasing use of satellite data in different scientific fields in the last decades is because of its low costs, and also because it provides faster and more powerful results. However, results obtained from satellite data are accompanied by a certain error probability. Accuracy is considered to be the degree of closeness of the results to values accepted as true. To evaluate the quality of thematic maps produced

from raster images, examining the accuracy of the classification and evaluating the agreement of the resulting map for the particular purpose is the main approach (Foody, 2008). The accuracy of the classification is assessed by comparing the classification results with known information. The minimum level of interpretation accuracy in the identification of LULC categories from remote sensor data should be at least 85 % (Wright and Morrice 1997; Anderson et al. 1976). According to Thomlinson et al. (1999) the target should be an overall accuracy of 85 % with no class less than 70 % accuracy. Despite the attractiveness of having a target value and a standard method for accuracy assessment, it appears the remote sensing researchers are not achieving the typically specified targets yet (Foody, 2002).

There are many factors that can affect the accuracy value such as the characteristics of the satellite data, the scale of the study area, and the details in the LULC classes. Thematic maps extracted from remote sensing data should undergo a statistically rigorous accuracy assessment before being used for scientific investigations (Stehman and Czaplewski 1998). Accuracy in this study was evaluated with an error matrix or so-called confusion matrix. An error or confusion matrix is among the most common approaches used for calculating the accuracy of thematic maps derived from multispectral imagery (Smits et al. 1999; Congalton and Green 2002; Liu et al. 2007). An error matrix displays the results from the comparison of reference class labels of the LULC categories with the real results (Stehman and Czaplewski 1998).

For accuracy assessment, the overall accuracy, the producer's accuracy, the user's accuracy and the overall kappa coefficient was calculated. The user's accuracy was calculated by dividing the number of correctly classified pixels for each LULC class by the total number of pixels in the classified image. The producer's accuracy refers to the number of correct pixels in the classified image for each LULC class divided by the total number of pixels in the reference data. Accordingly, the user's accuracy reflects that a given pixel can be identified on the earth surface as it is in the classified image, whereas producer's accuracy refers to the percentage of a given class that is correctly identified on the map. The overall accuracy is computed by dividing the total number of correctly classified pixels by the total number of reference pixels (Congalton 2001; Rogan et al. 2002). In this study, the accuracy assessment of the final classified image was validated against earth surface features using randomly distributed ground truth points. These points were considered as references for examining the accuracy of the LULC map of LZRB and the change detections results. The accuracy assessment was conducted for each classification result. Agreements and disagreements of the classification have been assessed by using an error matrix and simple descriptive statistics (Table 1).

The Kappa index was also calculated for the classified image to measure the accuracy of the results. The Kappa statistics of the LULC map result after classification is 0.811. The Kappa coefficient expresses the proportionate reduction of the errors generated by a classification process compared with the error of a completely random classification (Forghani et al. 2007). A Kappa value of 1 indicates perfect agreement, and a value of 0.811 expresses that the produced LULC map avoided 81.1 % of the errors. The accuracy achieved for the LULC map of the LZRB is well accepted amongst remote sensing specialists and GIS practitioners (Forghani et al. 2007; Zhang et al. 2002; Harris and Ventura 1995).

2.5.2 Change detection (image indices)

One of the most important applications of satellite data is to detect the changes for the same object between different seasons and different years. The process by which variation in an object at different times or changes that occur in LULC are monitored and identified over a certain number of years is known as change detection (Singh 1989,Tewolde and Cabral 2011). Changes in LULC result in changes in radiance values and these changes will be largely related to radiance changes but also to other factors (Ingram et al. 1981). The impact of these factors such as differences in atmospheric conditions, Sun angle and soil moisture can partially be reduced by selecting suitable data (Singh 1989; Jensen, 1983).

Table 1: Accuracy assessment of the LULC map of the LZRB, reference totals is the total number of tested pixels in the reference image, classified totals is the number of classified pixels in the classified image, number correct is the number of correctly classified pixels, which agree with the pixels in the reference image. The producer's, the user's and the overall accuracy are explained in paragraph 2.5.1.1.

LULC units	Reference totals (true)	Classified totals (predicted)	Number correct	Producer's accuracy	Users accuracy
Water	22	22	20	90.9	90.9
Urban and built-up Land	41	29	29	70.7	100
Natural vegetation	26	24	19	73.1	79.2
Cropland and pasture	40	36	35	87.5	97.2
Cultivated land	37	37	26	94.6	74.3
Harvested land	40	33	29	72.5	87.9
Burned land	17	6	5	29.4	83.3
Igneous and/or metamorphic rocks	36	32	27	75	84.4
Carbonate rocks	26	36	24	92.3	66.7
Clastic rocks	47	54	46	97.9	85.2
Conglomerate	21	24	21	100	87.5
Bare soil	22	23	21	95.5	91.3
Mixed barren land	132	151	121	91.7	80.1
Totals	507	507	423		
Overall classification accuracy = 83.4 %, Overall Kappa statistics = 0.81					

Change detection analysis is used to determine the nature; extent and rate of land cover changes through spatial and temporal variations (Rogan and Miller 2006; Zubair 2006). Information from change detection can be used for land management and future planning by linking many important variables such as urbanization, water management, deforestation and land degradation (Mancino et al. 2014). Image differencing is executed by subtracting images from two different time periods of the same location or scene (Fox et al. 2007). Spectral radiance values of satellite data can be analyzed individually for each band or for a combination of many bands (Singh, 1989). The difference image for two or more dates shows either an increase or a reduction of particular LULC categories and displays also the variation in their spatial distribution. Many indices have been developed and utilized to detect changes in different locations and under different environmental conditions around the world. The Normalized Difference Water Index (NDWI) and the Normalized Difference Vegetation Index (NDVI) have been widely used to produce useful time series results. Multi-temporal satellite images are commonly used to identify and monitor spatial and temporal changes in water and vegetation cover. In this study, the threshold of the reflectance of each index was determined by manually checking the index values and comparing the results with false-color images. All index equations were run using the 'Model Maker' in Erdas Image software. The size of the all LULC classes and the image index areas in the different years have been computed in ArcGIS. Integrating remote sensing and GIS technologies was proven to be very useful for detecting changes.

3 Results and discussion

3.1 Land Use Land Cover map classes

Thirteen LULC classes and subclasses have been identified in the LZRB; these are: urban and built-up land, barren land, which involves 6 subclasses (igneous and/or metamorphic rocks, carbonate rocks, clastic rocks, mixed barren land, bare soil and conglomerate), agricultural land, which involves three categories (cropland and pasture, cultivated land and harvested land), natural vegetation, burned land and water. The spatial distribution of the LULC classes is illustrated in Figure 3. The covered area and

percentage that each LULC class covers are shown in Table 2. Figure 4 shows which percentage of the LZRB each class covers.

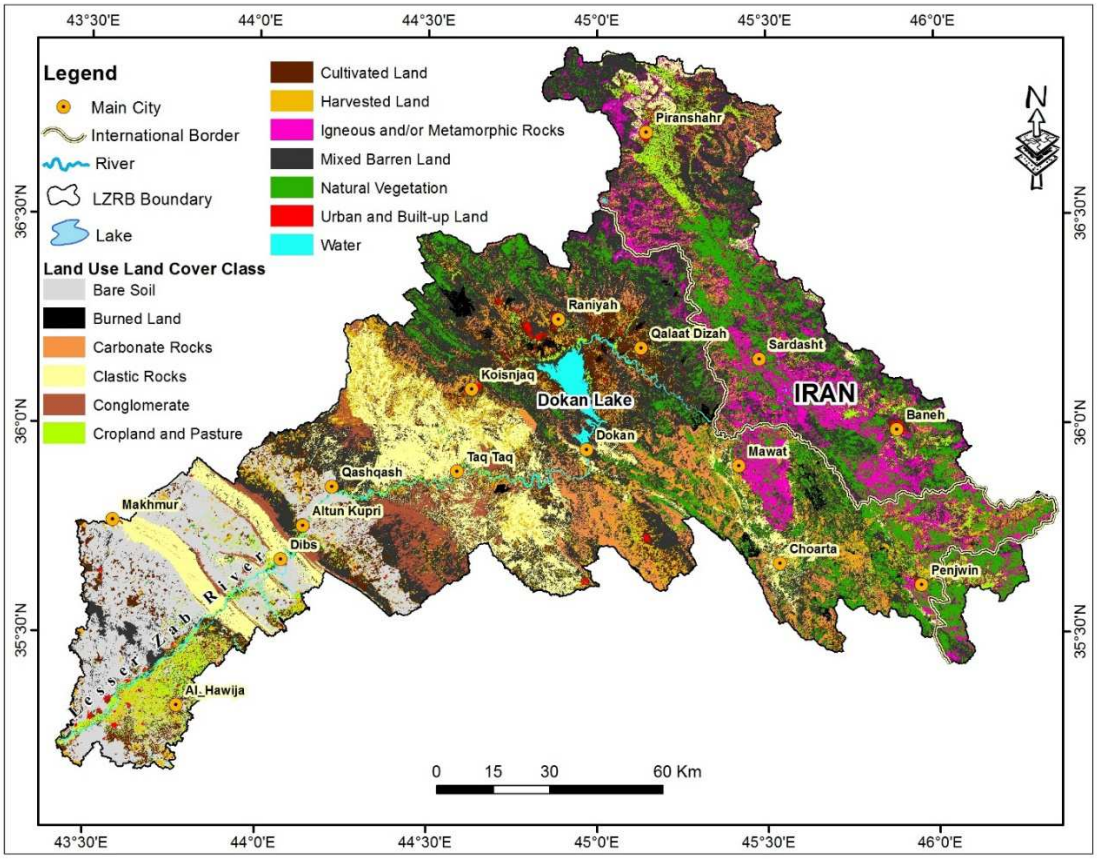

Figure 3: LULC map of the LZRB (Landsat 8OLI, September 2014)

Table 2: Area and percentage that each LULC class covers in the classified image of the LZRB (Landsat 8 OLI, September 2014)

LULC class and subclass		LZRB (km^2)	% of the LZRB
Igneous and/or metamorphic rocks		1293.3	6.5
Carbonate rocks	Barren land*	1207.1	6.1
Clastic rocks		2103.1	10.6
Conglomerate		566.3	2.9
Bare soil		2036.3	10.3
Mixed barren land		6841.1	34.5
Cropland and pasture	Agricultural land**	783.3	3.9
Cultivated land		980.2	4.9
Harvested land		1322.9	6.7
Urban and built-up land		113.2	0.6
Natural vegetation		2278.1	11.5
Burned land		187.1	0.9
Water		148.6	0.8
percent		19860.7	100

* Total barren land 14047.3 km^2 with 70.7 % of the total area,
**Total agriculture land 3086.45 km^2 with 15.5 % of the total area

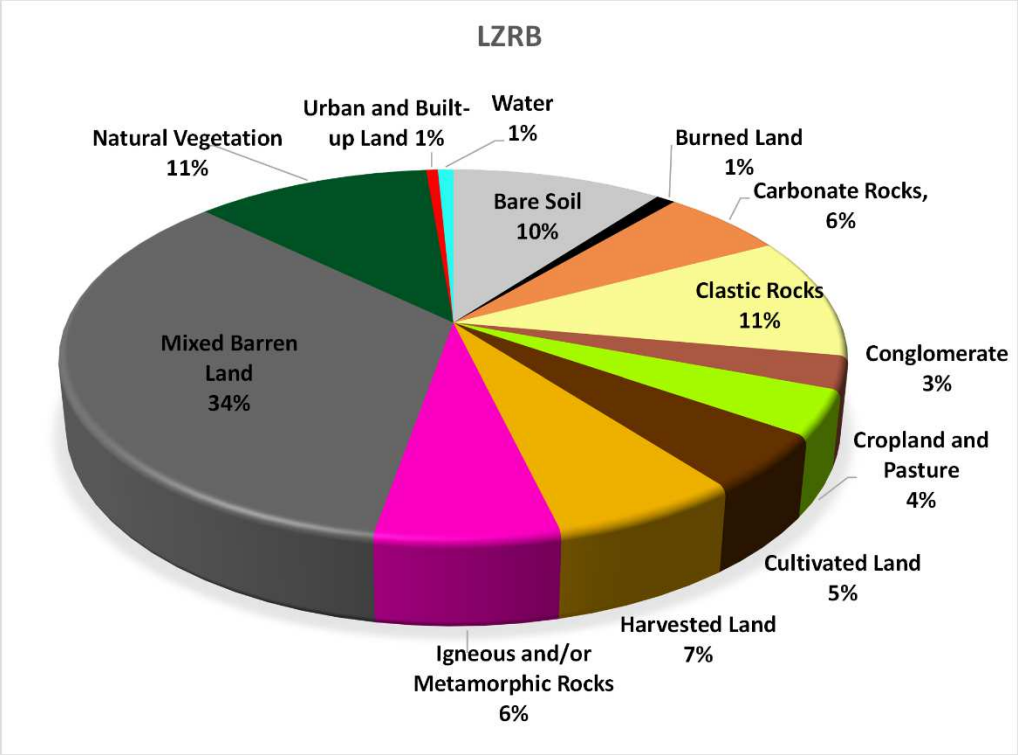

Figure 4: Pie chart of the LULC classes in percent of the total area of the LZRB

3.1.1 Urban and built-up land

Within the last years, urban and also rural areas in the LZRB have grown rapidly due to the significant economic growth in Kurdistan Region in Iraq as a whole and the higher demand for living space due to the population increase. This trend has been most pronounced in cities, towns and villages that are located in relatively flat areas. There are different approaches for mapping urban and built-up land such as visual interpretation of aerial and satellite data, digitizing topographic map and digital interpretation using satellite image processing techniques (Wang et al., 2010). The huge urbanization in the map area is represented by many cities and towns like Koisanjaq, Raniyah, Qal`at Dizah, Taq Taq, Altun Kupri, Hawija, Chuwaarta and Penjween within the territory of Iraq and Piranshar, Pasveh, Baneh and Sardasht in the Iranian territory. Additionally, villages and scattered houses are distributed all over the map area. The built-up land extracted using Landsat 8OLI 2014 occupies the smallest class with only 113.2 km^2, i.e. not more than 0.57 % of the total area (Table 2). It is difficult to determine urban areas in the LZRB solely by digital image processing due to the use of various kinds of building materials. This results in the confusion with other LULC classes as most of the villages are made of rocks and clay derived from surrounding areas. In addition, the low spatial and spectral resolution of the images and the uncertainty of spectral characteristics add to the obstacles in distinguishing this class. The spectral signature of villages in the area is very difficult to separate from fallow land. Thus the classification was complemented by the visual interpretation of QuickBird data using ArcGIS. Combining visual interpretation and digital image processing leads to the best results (Jensen, 2000). The determined urban and built-up land is highlighted in reddish blue to bluish pink color in 753 RGB in the Landsat 8 OLI image (Figure 5, A and B).

3.1.2 Natural vegetation

Natural Vegetation includes all vegetation cover that grows naturally, like forests, shrubs, perennial herbs, and grasses. Orchards that produce various fruits and nuts are also included in this class because of their limited spatial extension. It is distributed mainly in the high-mountains area of the basin and has the same spectral signature as sparse trees and forest patches. Consequently, the LZRB provides valuable information for assessing the relation between topography, morphometry, climate type and soil characteristics and their effect on the diversity and composition of the vegetation. The vegetation cover in arid and semiarid regions more strongly depends on the environmental conditions than in humid regions (Böer & Sargeant, 1998). The environmental factors that change the composition of the vegetation in arid and semi-arid regions include the geological and topographical situation, the climate conditions, the soil type and grazing. They all lead to a variation in spatial and temporal changes in the composition of the vegetation. The morphometric characteristics of the river basin have a direct effect on the spatial distribution of plant communities (Al-Rowaily et al. 2012). The northern and north eastern parts of the main basin receive the highest annual rainfall with an average of about 783 mm/a. The rainfall in the lowland (west and northwest) gradually decreases; the average annual rainfall there is about 308 mm/a. Generally, native vegetation and orchards are distributed in the high mountains in the north- and northeastern parts of the main basin north of and around Dokan Lake (Figure 5, C and B). There are different types of hazel filbert, nut trees, and fruits in the mountainous area. Shrubs mostly comprise herbaceous plant species that mostly do not grow higher than 1 m and are distributed as scattered plants or small communities throughout the LZRB. Several springs exist in the high-relief areas; they are surrounded by different types of vegetation cover. The present study also showed that most mixed forests exist in the northern and north eastern part of the LZRB and are associated with higher precipitation than in the lower part of the main basin. The natural vegetation of the LZRB covers an area equal to 2278.07 km^2, i.e. 11 % (Table 2) of the LULC map area.

3.1.3 Agricultural land

Agricultural land includes all types of agricultural land that can be distinguished at the acquisition date of satellite image. The availability of water is the main factor controlling the distribution of species in arid and semiarid regions as a result of the limited amount of precipitation and frequency of droughts (Zheng et al. 2013). Agricultural lands are permanently changing at various spatial and temporal scales in response to human activity and environmental factors.

The agricultural landscapes of the LZRB area are dominated by the farming of cereal crops. The agricultural land in the low-relief area is based mainly on the production of cereals like barley and wheat.

The agricultural lands of the LZRB are mainly distributed in the flat terrain, low-relief land and hilly terrain area but also along the flood plain of the main river course and its tributaries and alluvial fans around Dokan Lake. Thus the variation of this land use along the main river from high-altitude mountainous area to flat and hilly terrain has a direct influence on the vegetation's composition and diversity. The types of the agricultural land are:

3.1.3.1 Cropland and pasture

The cropland component of the agricultural land must be given significant attention to because its frequently undergoes spatial and temporal changes which directly influence the biogeochemical and hydrologic cycles of the land cover patterns (Wardlow et al. 2007). Cropland and pasture involve many components in agricultural studies such as harvested cropland, cropland used only for pasture, the alternation between crops and pasture, and land more or less permanently used for one of the purposes, cropland or pasture (Anderson et al. 1976). The alluvial fans that surround Dokan Lake are fertile with dense agricultural activities, where different crops grow on the large wheat farms in the summer season.

Most of the croplands that are mainly irrigated by precipitation are distributed in the northern and northeastern parts of the main basin area, because the precipitation there is higher than in the southern part, which is almost dry throughout the year. The LULC in the mountainous areas is characterized by scattered cropland patches along narrow flood plains and Piedmont plains.

Farmland can be distinguished from natural vegetation by distinctive geometric features and lighter color than natural vegetation (Figure 5, E and F). The red/green ratio was used to distinguish forests from croplands. As the red band (0.64–0.67 μm) is the red-color absorption band of the chlorophyll of healthy green vegetation and the green band (0.53–0.59 μm) represents the radiation reflected from leaf surfaces this ratio can be used to discriminate broad classes of vegetation. Croplands appeared as lighter (brighter) tone and forests appeared as darker tone and also the SWIR 2 /green ratio could be used to distinguish forests from croplands. But it could not distinguish forests from water bodies. Consequently, different attempts have been made in this research to discriminate natural vegetation from agriculture land; band-ratio visual interpretation by manual class identification using ground survey data and mask creation around agriculture land have been performed. The main obstacles in the separation of cropland from pasture are that both classes have the same reflectance and both are growing close to each other or as mixture on the same agriculture land. As it was apparent that the spectral signatures of these two classes cannot be distinguished from each other they were merged.

The lower part of the LZRB is fertile and most wheat farms are found in this plain particularly in Al-Haweja District in the lowest part of the basin. Cropland and pasture in the LZRB cover an area of about 786.73 km^2 which represents 3.96 % of the LULC classes of the basin (Table 2 and Figure 4).

3.1.3.2 Cultivated land

Cultivated lands are prepared and improved lands for agricultural purposes to grow crops for food production purposes. Leaving land unplanted for most of or for an entire growing season to enhance the soil's fertility for crop production in the following year is known as fallowing (Havlin et al. 1995). Fallow land is included in the cultivated land class because it is difficult to discriminate between them. This can also be justified by the fact that fallow land occurs only at a limited spatial extent in the basin area because of the high fertility of the soil there.

The cultivated lands have different spectral signatures in different parts of the LZRB, depending on the type and source of the soil material, which impacts the color and also some other properties of soil, like its moisture content and texture. Agricultural lands are characterized by their regular geometric shape and their location along road networks. These properties help to identify this land cover type when looking at it from the aerial perspective.

Cultivated lands cover approximately the same area as cropland and pasture; it amounts 980.21 km^2, i.e. 4.94 % of the map area (Table 2 and Figure 4). The spatial extent of cultivated lands is shown in Figure 3. In some locations, there are large areas in which barren land and cultivated land are significantly mixed. This is because they are composed of the same materials. So, they had to be separated based on the visual interpretation of the filed reconnaissance survey. Cultivated land has a dark brown to brown color with dark maroon color in the multispectral arrangement RGB753 of Landsat 8OLI (Figure 5 G and H).

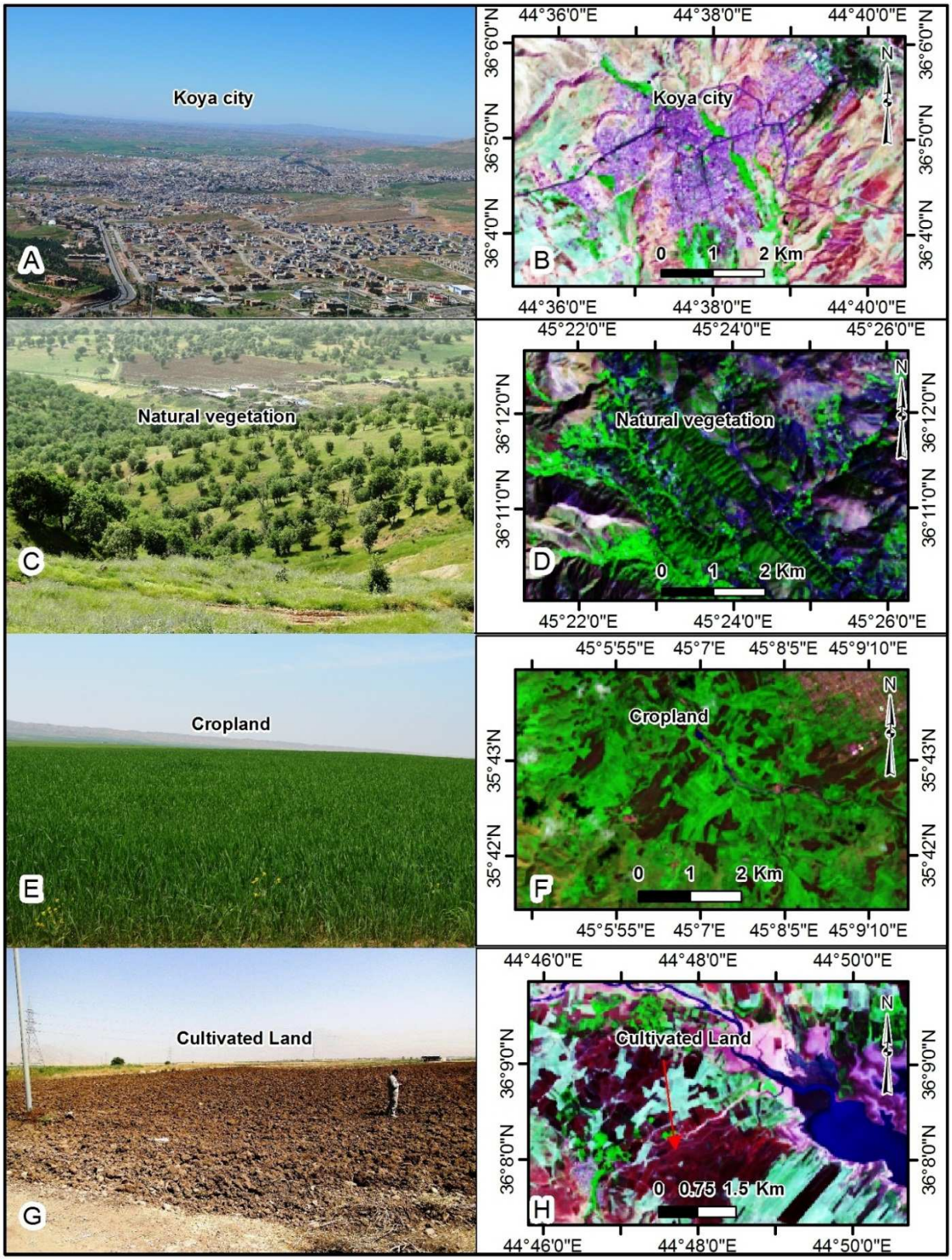

Figure 5: Built-up land (A and B), natural vegetation (C and D), cropland (E and F) and cultivated land (G and H), The images on the left show photos of the LULC type and the right image represent false-color composites RGB753 of the Landsat image OLI 8.

3.1.3.3 Harvested land

The satellite images acquired stem from the end of the dry season (after harvesting season). The lands that are classified and named as harvested land reflect the non-vegetated spectral response of the soil and crop residues from the fields of wheat and barley in the LZRB area. Wheat and barley are usually planted in November and December and are harvested in May or June. Therefore, they cover the land until the harvesting time.

In the basin area dry herbaceous are widely distributed. As they have the same spectral reflection as harvested land, these two land cover types can easily be confused (Figure 6A). Therefore, most of the agricultural lands and dry herbaceous in the low relief land appeared almost the same as bare land with the typical bright cyanic color on the RGB754 false color composite (Figure 6B). The results of the field work showed that the bright cyanic color belongs to stubbles or other remnants of the harvested crops. Harvested land covered about 1322.93 km^2 of the LZRB area, i.e. 6.66 % of the map area (Table 2).

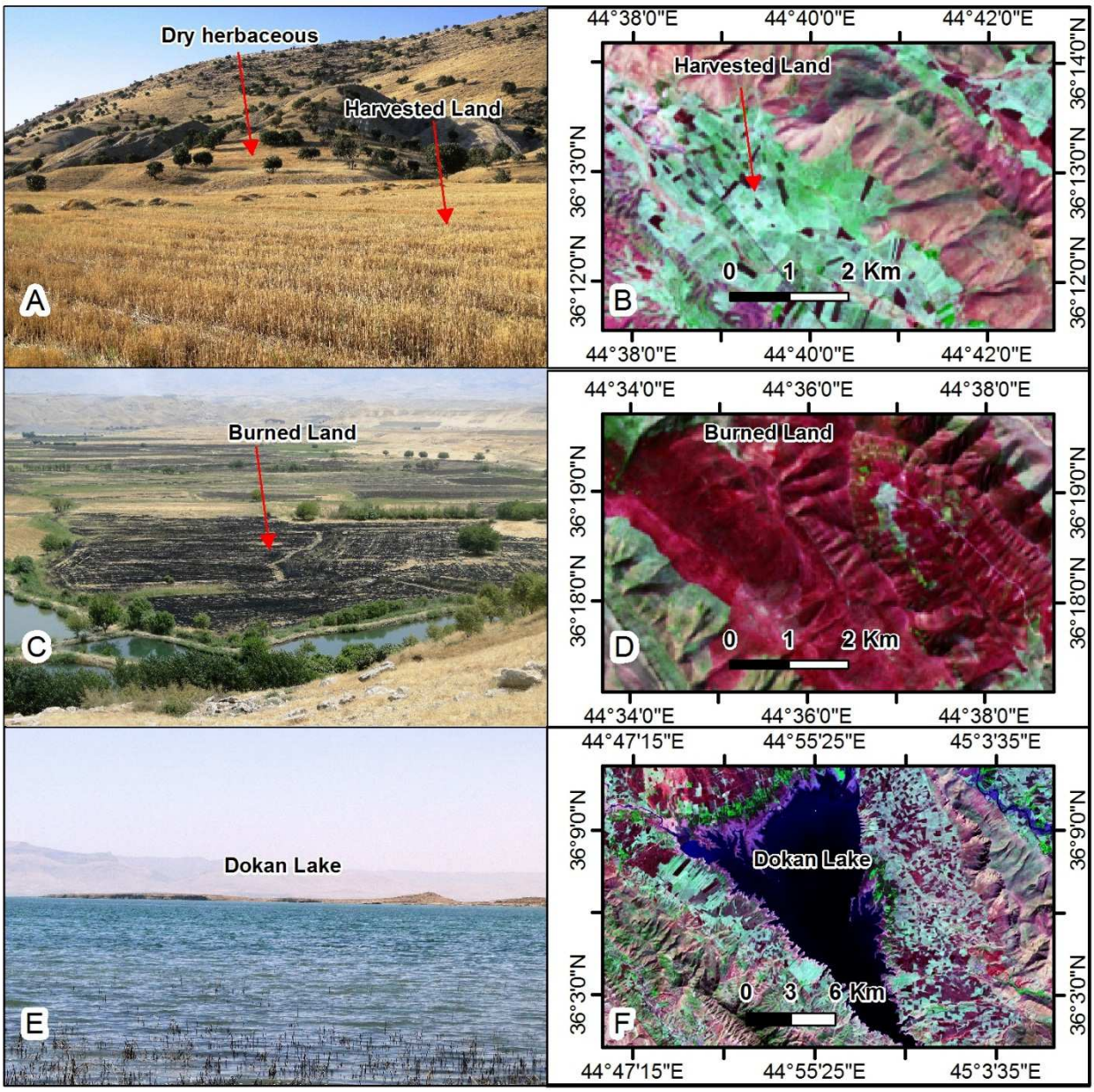

Figure 6: Harvested land (A and B), burned land (C and D) and water (E and F), The left image shows photos of the LULC type and the right image represents false-color composites of the Landsat 8 OLI, RGB753 image.

3.1.4 Burned land

Burning land is a traditional way that aims to prepare the agricultural land before cultivation by removing stubble residues or the remnants of harvested crops from the previous crop season (Figure 6C). It is an annual practice for easily clearing the land for cultivation. Furthermore, burning harvested fields is done to get rid of the rodents from farmlands before the next crop season (Eiumnoh and Shrestha 2000).

Burn agriculture is widely used in the territory of Iraq and particularly in the Kurdistan region in the north of Iraq. Harvested land and pastures are burnt regularly to improve their quality (Lindell 2011). Although the chemical changes resulting from burning can contribute to an improvement of the soil's fertility, this effect is only temporal (Hölscher et al. 1997). Fires in some cases get out of control, expand to areas of natural vegetation and consequently affect areas that the farmer actually did not want to burn. The adverse effects of the burn agriculture, like land degradation and erosion, need to be understood by the people in order to prevent this bad practice. Repeated burning on slopes caused an increase in the erosion rate (Scotter 1972) and subsequently, surface runoff. The increase in the spatial extent of bare rock and soil can be better explained by the burning of bushes on slopes. The geochemical effect of burning organic material in the topsoil is a lack of important nutrients such as C, N and S by volatilization processes (Giardina et al. 2000; Sommer et al. 2004; Ewel et al. 1981). Several studies report the resulting ash from burn land to reduce soil acidity as burning also increases the amount of one or several exchangeable base cations such as magnesium and calcium. Moreover, burn agriculture impacts the C cycle and consequently affects global climate. Information on the occurrence of burned land can help agricultural scientists and local authorities to monitor this problem and its effect on the ecosystem. Stone (1971) states that after twelve years of burning there is no difference in grain productivity on the site where wheat straw has been burned. These burned lands can be identified by their distinct maroon color in the Landsat 8 OLI, RGB 753 image (Figure 6D). Burned lands are distributed in many parts of the basin (Figure 3). They cover an area of about 187.13 km^2 in LZRB, i.e. 0.94 % of the total map area (Table 2, Figure 4).

3.1.5 Water

The water category comprises water bodies, streams, canals, and other linear water bodies, lakes, reservoirs, bays and estuaries (Anderson et al. 1976). Water bodies in the LZRB are represented by Dokan Lake and LZR which appear as linear features surrounded by strips of agricultural lands, particularly in low-relief areas. The delineation of water areas depends on the scale of the data presentation and the resolution characteristics of the satellite data used for preparing the LULC map (Anderson et al. 1976). There are also some permanent tributaries and many intermittent and ephemeral streams, which are usually active during rainy season. During heavy rain most of the valleys are flooded. Some of them are flash-flooded during strong rain storms and supply huge amounts of water to the LZR.

Dokan Lake is an artificial reservoir mainly supplied by water from the LZR. It represents an important reservoir for the storage of water for agricultural land irrigation, drinking water supply, power generation, and flood control. Additionally, it is surrounded by fertile agricultural land extending over the surface of alluvial fans (Figure 6E and F.). Although the variation of the spatial extent of water bodies and the water level of the lake are artificially controlled by the dam, the climatic conditions, particularly the fluctuation of the rainfall rate is also crucial for the assessment of the amount of water in the lake. The fluctuation of the water level is directly reflected by the surface water body's spatial extension. Consequently, the artificially controlled Dokan dam at least partly affected the statistical calculation of the water class in the LULC map.

There are many other water resources in the LZRB such as natural springs that are distributed in different places particularly in the mountainous area. Wetlands in the LZRB are also included in the water class. It is mainly represented by bogs in high mountain area, and small backswamps nearby the main river and around some springs. Wetlands occur only to a very limited extent and are hard to be depicted in the LULC map, due to scale limitations. The area covered by water in the LZRB accounts for about 148.6 km^2 which is 0.75 % of the total map area (Table 2 and Figure 4).

3.1.6 Barren land

The land that is not used for any purpose is commonly known as barren land. Barren land categories are used to classify lands with a limited capacity to support life and having less than 5 percent vegetative cover (scattered vegetation) (Lillesand et al. 2014). Generally, the surface of barren land is covered by salt flats, sand dunes, mud flats, beaches, bare exposed rock, bare soil, or by salt-affected soils (Anderson et al. 1976).
Barren land is more vulnerable to erosion than vegetated land which is more resistant to and protected against soil erosion (Iqbal and Khan 2014). Barren land occurred everywhere in the study area. The data reveals that the total area of barren land covers 14047.3 km^2 which corresponds to 70.73 % of the total map area (Table 2 and Figure 4). The subcategories of barren land in the LZRB include mixed barren land, igneous and/or metamorphic rocks, clastic rocks, carbonate rocks, conglomerates and bare soil. Remote sensing data and techniques supply means for successfully distinguishing between and mapping of exposed rock classes and other associated weathering products. They provide information that is very useful in addition to geological maps of the bedrocks (Leverington and Moon 2012). Landsat 8 OLI images have been successfully used to map the exposed rocks within the LZRB. Bare exposed rocks in the LZRB are subdivided into igneous and/or metamorphic rocks, carbonate rocks, and clastic rocks, which are described hereinafter.

3.1.6.1 Igneous and/or metamorphic rocks

The application of Landsat 8 OLI satellite data to identify the types of igneous and metamorphic rocks was successful. Mafic and ultramafic rocks can easily be discriminated because fresh mafic rocks have a higher reflectance than fresh ultramafic rocks (Macias 1995). There are many factors that pose obstacles to the mapping of rocks like extensive vegetation covers or dry herbaceous, soil and weathering products. The spectral reflectance of geological materials can be controlled by surface alteration rather than by the material's fresh internal mineralogy (McSween et al. 2009). Thus, the characteristics of the rock's spectral reflectance are strongly impacted by the physical and chemical conditions of the rock outcrops.

Landsat 8 OLI images allow the effective discrimination between ultramafic rocks and mafic rocks. Mafic rocks have lighter colors than ultramafic rocks due to their relatively high silica content, which has a high spectral reflectance. Mafic rocks have magenta color in the mutispectral band composite image 753 RGB while ultramafic rocks have dark violet to bluish color in that image image (Al-Rubaiay et al. 2010). The same results are obtained from the Landsat 8 OLI image (Figure 7B). Igneous and metamorphic rocks are characterized by the distinct and multispectral reflections, which are merge to one class after classification.

Igneous and metamorphic rocks occupy 1293.3 km^2, i.e. 6.51 % (Table 2 and Figure 4) of the LZRB. They are located in the complex mountainous area in the north and north east of the LZRB (Figure 3). This class comprises different types of igneous and metamorphic rocks with some sedimentary rocks that belong to the Qandil Metamorphosed Series (Cretaceous), Shalair Series (Early-Late Cretaceous), Katar Rash (Volcanic) Group (Late Cretaceous), Intrusive Complex (Earl-Late Cretaceous) and the Walash Volcanic Rock Group (Paleocene/Eocene -Oligocene). An example for igneous and metamorphic rocks within the basin are mafic or basaltic lava, laminated and andalusite schist, gneiss, phyllites, serpentinite, quartzite, recrystallized and massive metamorphosed limestone, andesites, diorite, granodiorite, syenite, nepheline syenite (Sissakian 1993; Ma'ala 2007). The Mawat Ophiolite succession from the bottom upwards consists of ultramafic rocks (Figure 7A), gabbro, spilitic basalt and metabasalt (Al-Mehaidi 1974). There are also different igneous and metamorphic rocks mapped and reported in geological maps of Mirwan and Mahabad in Iran territory such as pyroxene hornfelse facies, homogenous phyllite, gneiss, acidic volcanic rocks, andesitic to basaltic volcanic rocks with pillow structures, spotted slate, andalusite and chiastolite schist, ophiolite, marble, serpentinite, gabbro, diorite and so forth.

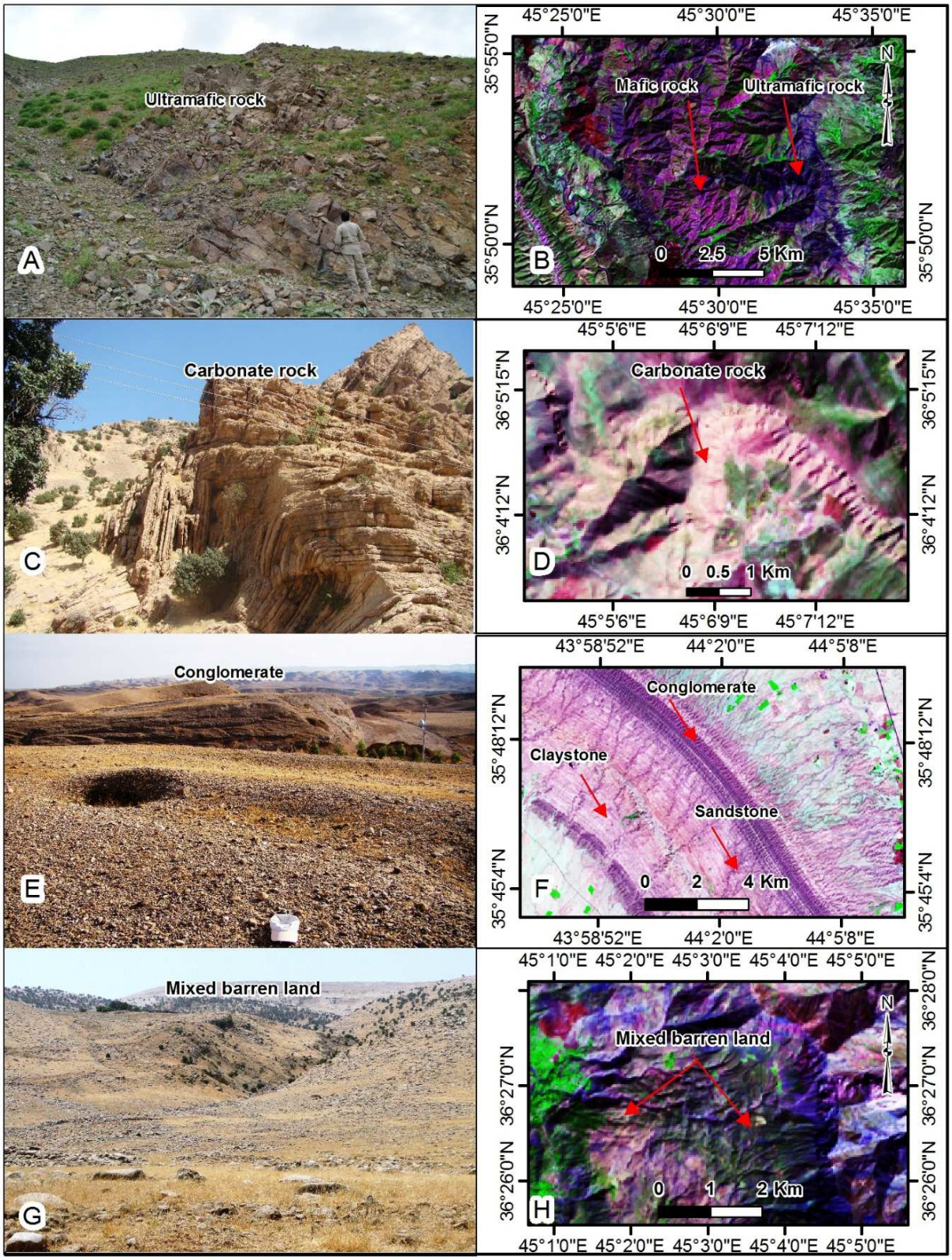

Figure 7: Mafic and ultramafic rocks (A and B), carbonate rocks (C and D), conglomerates (E and F) and mixed barren land (G and H), the images on the left show photos of the LULC type and the right images represent false-color composites of the Landsat 8 OLI, RGB753 image.

3.1.6.2 Sedimentary rocks

The LZRB area is mainly covered by sedimentary rocks. They primarily comprise clastic rocks (sandstones, siltstones and shales) and carbonates. Sedimentary rocks are exposed in different parts of the LZRB area. In the central and upper part of the basin, mainly carbonate rocks are present; south and southwest of Dokan Lake clastic rocks are most common. The lithological classification based on satellite image interpretation was combined with the digitized results from the GEOSURV-Iraq geological maps. Three types of sedimentary rocks were differentiated in the map area; they are described hereinafter.

- Carbonate rocks

Carbonate minerals have diagnostic absorption features in their reflectance spectra in the SWIR and TIR band due to electronic and vibrational processes, so that the spectra can be used to discriminate carbonate minerals from other minerals (Van Der Meer and de Jong 2001; Clark 1999; Russ 2011).

The exposed carbonate rocks of different geological formations appear in a light pinkish color in the band combination of 753 RGB in the Landsat 8 OLI image (Figure 7D). The high spectral reflection of these rocks is due to their light color (Figure 7C). The carbonate rocks that appear in a dark color are grouped together with the mixed barren land subclass, because they are covered by thin weathered horizons, soil, vegetation, or affected by different coloring constituents. Carbonate rocks cover an area of about 1207.1 km^2, ie. 6.08 % of the total LZRB area (Table 2 and Figure 4). The carbonate rocks identified from Landsat 8 OLI are mainly present around Dokan Lake and in the northeastern part of the main basin (Figure 3).

- Clastic sedimentary rocks

Clastic rocks such as sandstones, siltstones and claystones or other unconsolidated materials belong to different formations such as the Fatha, Injana, Mukdadiyah and the Bai Hassan Formations in Iraq and the Ruteh, Parut and the Lulan Formations in Iran (Figure 3). These sediments are mainly distributed in the central and southwestern parts of the LZRB and to a limited extent also in the north eastern part of the main basin. Clastic rocks in the central and southwestern parts are exposed in the anticline and syncline on both sides of the LZR. These rocks can be discriminated by their spectral signatures depending on the spectral response of the contained materials. They exhibit different color variations ranging from violet, pink to light pinkish for sandstones, siltstones and claystones, respectively, on Landsat 8 OLI RGB753 color composite images (Figure 7F). Clastic rocks that are predominantly composed of sandstone are characterized by darker color shadings than those composed of siltstone and claystone. In the LZRB, clastic sedimentary rocks cover an area of about 2103.1 km^2 which corresponds to 10.59 % of the map area (Table 2 and Figure 4).

- Conglomerates

The conglomerate subclass has been separated from the clastic rocks because they are widely distributed and easily distinguishable in the Landsat data. The coarse-grained sedimentary rocks (conglomerates) generally show dark magenta color shades in the Landsat 8 OLI, RGB 753 color composite images (Figure 7F). They also exhibit spectacular dendritic drainage patterns in highly dissected badland terrain morphology. Moreover, the hills within badland areas consist of conglomerates characterized by smooth surfaces (Figure 7E). Conglomerates are separated from other clastic rocks because they can easily be distinguished using the Landsat data. Conglomerates are distributed mainly in the south and south west of Dokan Lake on the flanks of some anticlines and along the main river course.

The exposed conglomerates in the LZRB mainly belong to the Bai Hassan Formation, recent Quaternary sediments of river terraces and recent valley fill sediments. The river terraces consist of different

lithologies eroded from high-slope landscapes. They are generally composed of unconsolidated coarse-grained sediments. The valley fill sediments consist of alluvial material from mass wasting, surface runoff from highlands and sediment load of rivers and valleys. The size of the gravels generally varies from few mm up to boulders and locally blocks of up to 2 m were noticed in the upper reaches of some streams. In the lower reaches of the valleys the size of gravel range from fine pebbles to up to 20 cm, often mixed with a sand matrix. This class occupies 566.28 km^2, i.e. 2.85 % of the LZRB (Table 2 and Figure 4).

3.1.7 Bare soil

Bare soil is restricted mainly to the lower part of the LZRB in the foot hill zone, which appears at the surface of piedmont, sheet run off and polygenetic sediments. Bare soil stretches out on both sides of the LZR's course and is almost utilized for agricultural purposes. The main agricultural areas are widely distributed within this part of the region due to gentle slopes and fertile soils. Furthermore, irrigation canals are distributed within this part particularly in the south and southeast of LZR in the surrounding of Al-Haweja Town. In the areas of bare soil that are located on the southwestern side the agricultural activity is lower than on the opposite side because of limited or abandoned irrigation canals (Figure 3).

Generally, bare soils consist of eroded materials (silty and clayey materials with sandy and gypsiferous admixtures) that cover the pre-Quaternary rocks. Bare soil is distinguished from other barren land because it has a different spectral signature that makes it possible to discriminate it from the surrounding areas. In many areas the bare soils can be recognized on the basis of their light color shade caused by its soft texture. The high spectral reflectance of some areas is caused by the fine sediments that make up the soil's surface or dry bare soil with sparce vegetation cover. The variation of the physical properties (such as moisture content) of the bare soils is the reason for the variation of the reflectance of this class. Bare soils cover an area of about 2036.3 km^2 which corresponds to 10.25 % of the LZRB (Table 2, Figure 4).

3.1.8 Mixed barren land

The class mixed barren land is used when a mixture of different barren land features occur and the most dominant land use occupies less than two thirds of the area (Anderson et al. 1976). The mixed barren land in the LZRB is represented mainly by the products of denudation and is largely composed of unconsolidated or semi-consolidated recent alluvial, argillic, sandy alluvial and fluvial sediments of weathered friable loose formations (Figure 7G). Mixed barren land is the largest LULC class in the LZRB, representing 34.44 % and occupying 6841.1 km^2 of the total LULC map (Table 2 and Figure 4). The mixed barren land is classified on the basis of its spectral reflection and field checking. Different shades of this class on the Landsat 8 OLI, RGB 753 color composite images are present due to big differences between the source materials (Figure 7H). These differences comprise the sediments' environment, variations in texture, the type of lithology, the degree of consolidation and so forth. Moreover, many formations are grouped together in this category because they are composed of different types of materials.

3.2 Change detection using image indices

In this research, the NDWI and NDVI were calculated from Landsat 8OLI 2014 images in wet (April) and dry (September) season while from TM5 (2000), TM5 (1990), TM5 (1984) and MSS (1976) the indices were calculated only for the dry season. Satellite images were utilized to determine the spatiotemporal changes in natural vegetation, cropland, surface water, and urban and built-up land. Changes in NDBI were identified using visual interpretation. The wet season in the LZRB extends from

October to April and the dry season extends from May to September. Therefore, the selected months for the analysis of seasonal changes in the LZRB were April (wet or high-runoff season) and September (dry season). Water features were manually identified and NDVI thresholds were manually applied to classify thematic images into two classes, land and water. The best fit for the water features and the NDVI thresholds for each index were determined using visual interpretation of the color composites of the satellite data and also using the field work data.

3.2.1 Calculation of magnitude and percentage of changes

The magnitude and percentage of the changes detected represents the degree of spatial expansion or reduction of the area occupied by the respective LULC class. Positive values indicate increases while negative values indicate decreases of the spatial extent of the regarded LULC class. The magnitude of change is calculated by subtracting the area of the respective class for each recent satellite image date from that of the first image date. The value of change is calculated by subtraction between the recent and first image and also between each successive date (Table 3). The percent of change (P) is then calculated according to the following equations:

$$RF = \mathrm{R} - \mathrm{F} \quad (eq.1)$$

$$\mathrm{SD} = \mathrm{R} - \mathrm{O} \quad (\mathrm{eq.}\,2)$$

$$\mathrm{P} = \frac{\mathrm{R}-\mathrm{F}}{\mathrm{F}} * 100\% \quad (\mathrm{eq.}\,3)$$ (Abubakar and Anjide 2012)

Where: RF is the recent reference, R is the recent date (2014, 2000, 1990, 1984), F is the reference (First) date (1976), SD is the Successive Date, O is the Old date**,** P is the percentage of change relative to the reference date (1976).

The NDWI, NDVI and NDBI indices are extracted from the surrounding area depending on the defined thresholds and masks. In this study, changes in spatial extent of water and vegetation cover as well as urban and built-up land between the earliest and latest image data and also between successive image periods were calculated. An increase in the spatial extent is marked as positive (+).Change detection identifies changes in terms of location and extent which are then utilized to generate spatial distribution maps of the image indices.

Table 3: Change detection in the LZRB using image indices: A: area in km^2 for each index, SD: the difference in km^2 for each index between successive dates, i.e. recent date (R) minus old date (O), RF: the difference in km^2 for each index between an image date and the reference date (1976), P: percent of change relative to the reference date.

Year	A	SD	RF	P	Year	A	SD	RF	P
NDBI (urban and built-up land)					NDVI (natural vegetation)				
					2014 April	3283.2			
2014 Sept.	113.2	52	102.3	9.4	2014 Sept.	2278.1	-726.9	-368.5	-0.14
2000	61.2	20	50.3	4.6	2000	3005	-69.7	358.4	0.14
1990	41.2	15	30.3	2.8	1990	3074.6	699.7	428	0.16
1984	26.2	15.4	15.4	1.4	1984	2375	-271.6	-271.6	-0.1
1976	10.9	0	0	0	1976	2646.6	0	0	0
NDWI (surface water bodies with Dokan Lake)					NDVI (cropland and pasture)				
2014 April	230.7				2014 April	5134.1			
2014 Sept.	148.6	-12.9	-155.2	-162.1	2014 Sept.	783.3	65.1	204.5	0.35
2000	161.5	-55.5	-149.2	-0.5	2000	718.3	-21.5	139.5	0.24
1990	217	25.1	-93.7	-0.3	1990	739.8	119.1	161	0.28
1984	191.9	-118.8	-118.8	-0.9	1984	620.7	41.9	41.9	0.07
1976	310.7	0	0	0	1976	578.8	0	0	0
NDWI (Dokan Lake only)									
2014 April	156.31				SD = R - O				
2014 Sept.	110.6	-27.6	-131.8	-0.5	RF: R-F				
2000	138.1	-53.1	-104.2	-0.4	P = (R-F)/F*100%				
1990	191.3	57.6	-51.1	-0.2	(-): decreasing trend				
1984	133.7	-108.7	-108.7	-0.5					
1976	242.4	0	0	0					

3.2.2 NDBI

The fast expansion and changing pattern of NDBI reflects the changing economic and social conditions and the increasing population. Several NDBI indices have been applied but they only gave results of low accuracy. Therefore the NDBI was extracted mainly based on the visual interpretation of images by on-screen digitizing of the urban areas for 1976, 1984, 1990, 2000 and 2014. The delineation of urban and built-up land was performed using ArcGIS software. In the LZRB there are mainly urban settlements, but also many rural settlements like towns and villages along the main river course. The total built-up land area in 2014 was 113.2 km^2, which is only 0.57 % of the total LZRB area. It has increased to 102.3 km^2 from 1976 to 2014 i.e. by 9.39 %. The largest increase in built-up land area occurred from 2000 to 2014 (Table 1 and Figure 8). The distributions of urban and built-up land in the LZRB vary strongly. The increase in their spatial extent goes step by step, which can be seen when comparing images from successive dates (Figure 9).

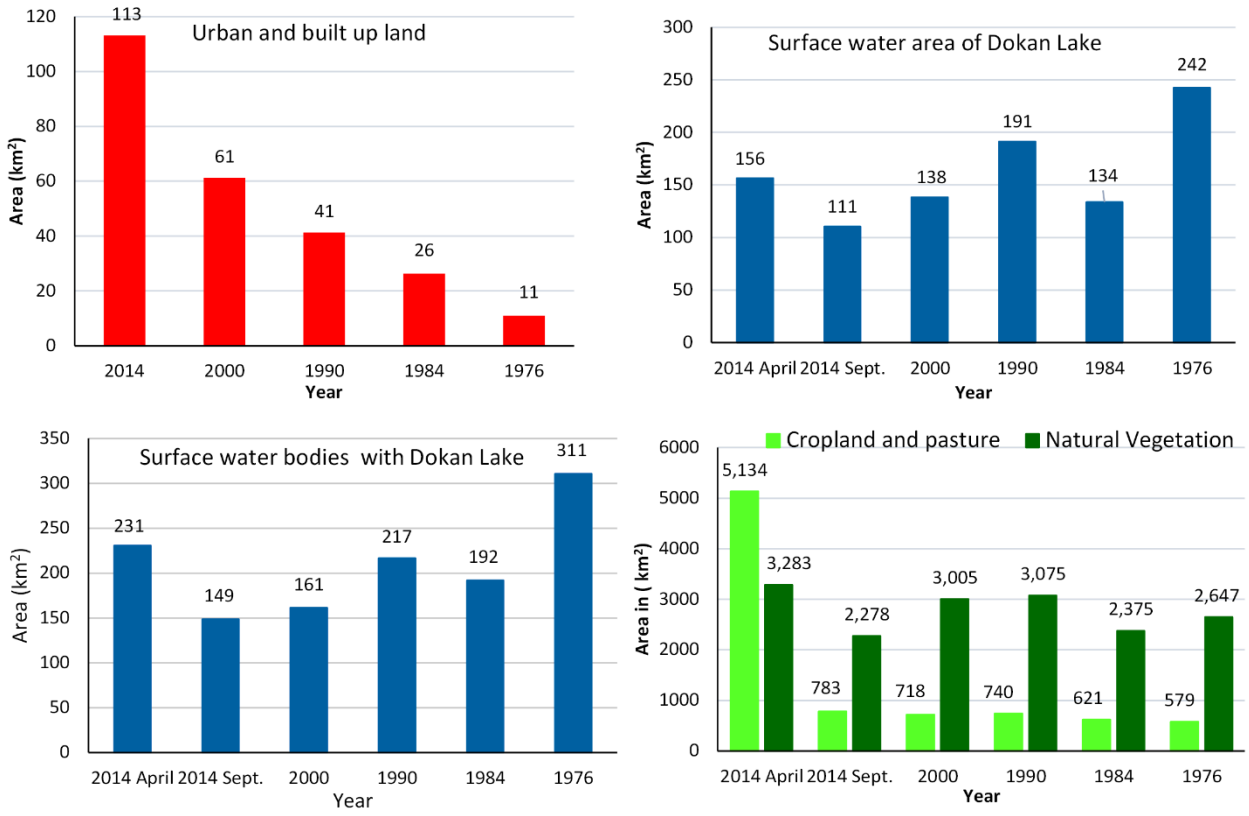

Figure 8: Changes in image indices within the time period 1976-2014 and seasonal change between April and September in 2014

3.2.3 NDWI

Remote sensing satellite data is widely used in water resources monitoring and management. It supplies more accurate and convenient information for mapping surface water bodies and for monitoring the dynamics of water (Ji et al.2009) .In this study the NDWI was applied to identify surface water using the method of extracting thematic images from band ratios [equation 4 (Ji et al. 2009)] and [equation 5 (El-Asmar et al. 2013)].

$$\text{NDWI for Landsat8 and TM5} = \frac{(\rho Green - \rho SWIR)}{(\rho Green + \rho SWIR)} \quad (eq.4) \quad \text{4 (Ji et al. 2009)}$$

$$\text{NDWI for MSS} = \frac{(\rho\text{Green} - \rho\text{NIR (B4)})}{(\rho\text{Green} + \rho\text{NIR (B4)})} \quad (eq.5) \text{ (El-Asmar et al. 2013)}$$

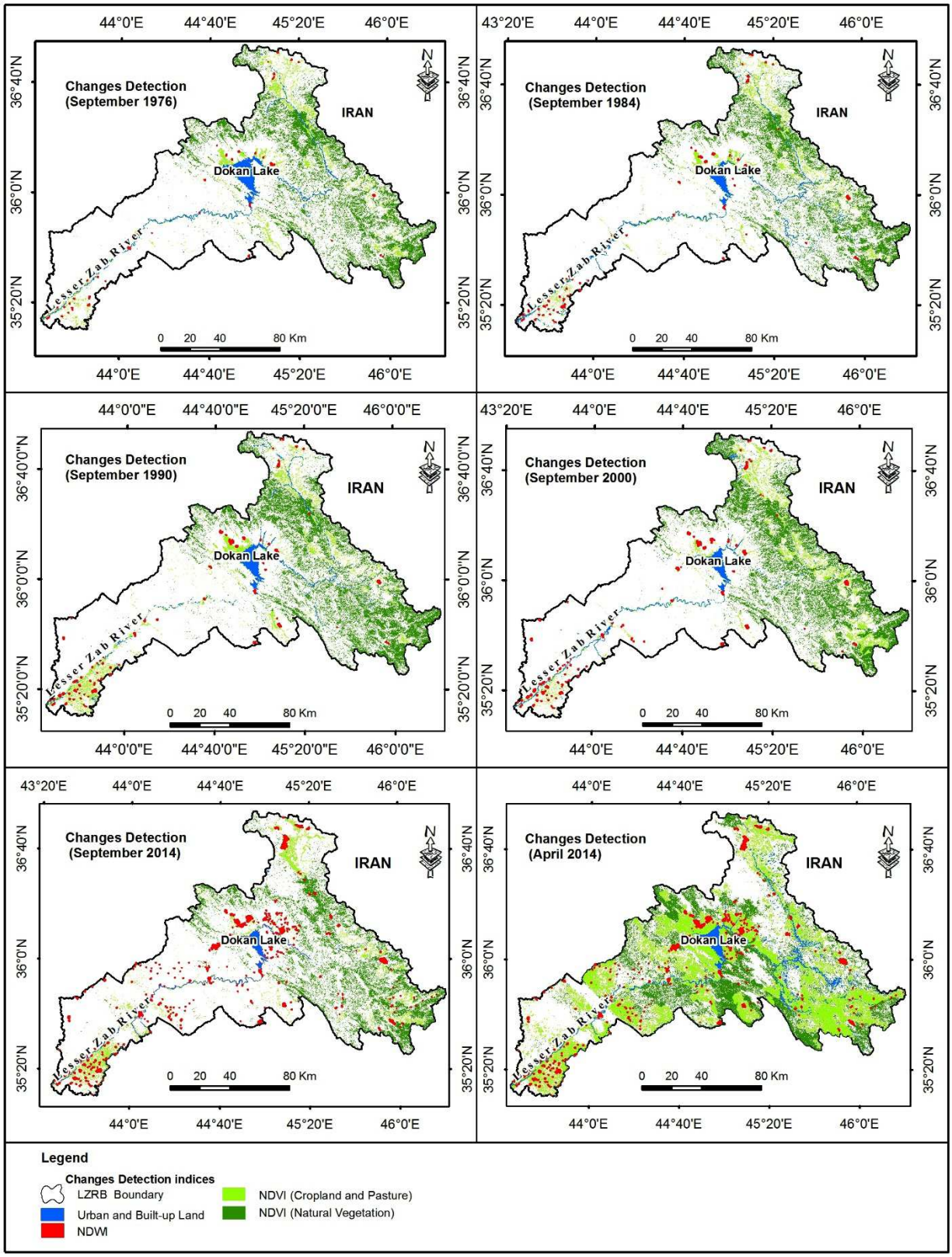

Figure 9: Change detection map for September 1976, 1984, 1990 and 2000, April 2014 and September 2014

There are different image indices that have been calculated and examined to delineate surface water; the aforementioned equations were found to be the most applicable and most accurate for determining the spatial and temporal changes of the water features.

The NDWI has successfully been used to extract surface water features from Landsat 8 OLI and TM5 and MSS images. Several image indices have been applied to extract water bodies from the MSS satellite sensor but none of them produced convincing results because MSS images lack a shortwave (SWIR) band. Therefore, different NDWI have been proposed to determine the best performing index and to establish appropriate thresholds for the MSS for clearly identifying water features. The resulting NDWI images highlight water bodies that are present in the study area. the NDWI index ranges from -1 to +1 with water bodies represented by high values (El-Asmar et al. 2013).

The reflectance of clear water is high in the green band and low in the near infrared because water is characterized by strong absorption in the near infrared wavelengths range and beyond. Therefore, for calculating the NDWI two bands are used: green (0.5-0.6 μm) and near infrared (0.8-1.1 μm). In this study it was found that the above-mentioned equations are best for calculating the NDWI. Water features in MSS images show positive NDWI values; a threshold of ≥ 0.13 was found to be the most suitable and most accurate. Modeling spectral reflectance curves is not enough for water extraction because there are many spectral mixtures that have the same spectral reflectance as water. The modeling was done using the model maker in Erdas imagine software. Mixtures of water pixels with some other objects' pixels have been identified and processed depending on the matching between NDWI results with ground truth points, field surveys, QuickBird image data and other axillary data using GIS.

There are also interferences between water identified with the NDWI applied on MSS images and the ultramafic rocks exposed in the north eastern part of the basin. These rock exposures have the same spectral characteristics as water and the same threshold value. By examining the NDWI in detail it was observed that shadows are also mixed with extracted water features in some places. The interface areas have been removed using GIS by converting the NDWI result to polygons and manually removing it based on visual interpretation. Finally, the thresholds for finding water features were identified by visual analyzing the band composition of Landsat 8 OLI, TM5 and MSS. The extracted results were validated with ground-truth observations throughout the LZRB by field surveys and collected training sites. The NDWI in the LZRB is mainly represented mainly by the linear features of the LZR, its main permanent tributaries and Dokan Lake. The spatial variations of the NDWI during the (1976-2014) period are illustrated in Figure 9. There is a dramatic decrease in the extent of the surface water in the LZRB (Table 3 and Figure 8). The change in NDWI during the period of 1976-2014 can be attributed mainly to the variation in the storage of Dokan Lake which depends on the climatological conditions and the management of Dokan Dam Reservoir (Table 3 and Figure 10). In this study, the surface area changes of Dokan Lake during the period of 1976–2014 were investigated. Dokan Lake is one of the largest water storage lakes in Iraq. The water storage of Dokan Lake is of economic importance for the power generation and also provides a suitable place for recreation. There are huge variations in the spatial extent of Dokan Lake between April and September that reflect the difference between wet (rainy) and dry season (Figure 10). Times series of the spatial extension of Dokan Lake are displayed in Figure 10. Dokan Lake is in a critical situation now as a result of decreasing surface water area with time and increased water demand for agricultural and domestic uses. It is necessary to monitor the decrease of the Dokan lake surface area regularly to understanding the main factors influence on the lake and to provide the best management.

3.2.4 NDVI

The NDVI is the basic index for measuring the vegetation cover and for distinguishing vegetation from other earth surface covers. NDVI calculations are based on the fact that the chlorophyll in living plants strongly absorbs radiation in the visible range of red light and strongly reflects radiation in the near-infrared range of the spectrum (Tucker 1979; Mather and Koch 2011). Although, there are many new indices that have been developed to distinguish vegetation from non-vegetated lands and some of them also take into account the soil's behavior, the NDVI is still the most commonly used index (Forkuo and

Frimpong 2012). Changes in the vegetation cover (natural vegetation, cropland and pasture) of the LZRB were detected using the NDVI in five observation times within the period of 1976-2014. Different sensors are sensitive to different wavelengths in the bands that were used to determine NDVI values. Therefore, there are systematic differences in the NDVI values derived from different sensors (Ouyang et al. 2012).

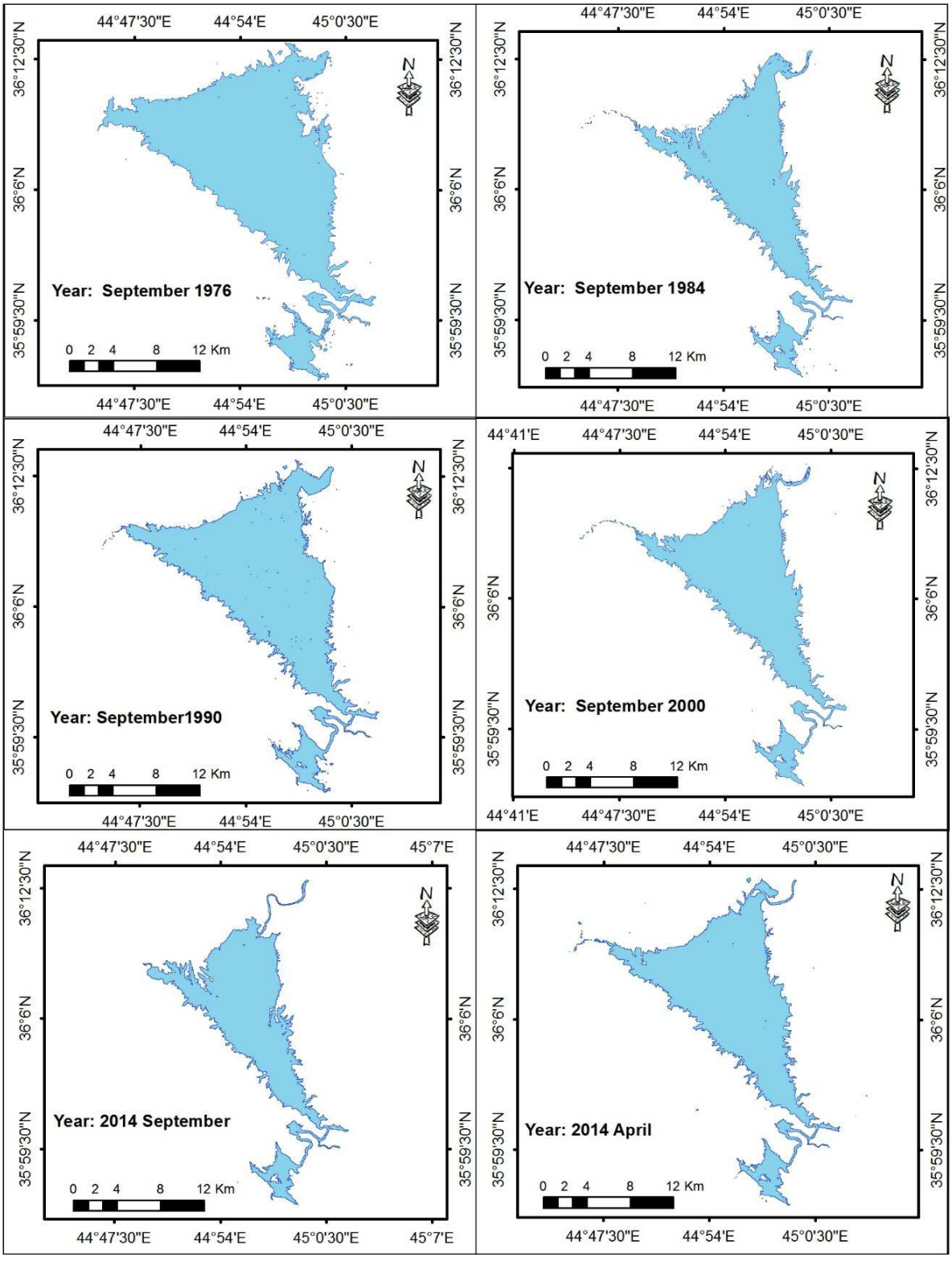

Figure 10: Change in the spatial extension of Dokan Lake during the period of 1976-2014 and the seasonal change between April and September in 2014 based on the NDWI index results.

Hence, there are some slight differences in the NDVI thresholds between the different Landsat sensors. Changes in vegetation cover during the analysis period (1976-2014) were detected using the NDVI differencing images technique. First, the NDVI indices were calculated from the Landsat images during the analysis period (1976-2014) using NDVI depending on the general normalized difference between near infrared (NIR) and visible red (RED) (eq. 6). The resulting NDVI images were subtracted between each successive date (i.e. 1976-1984, 1984-1990, 1990-2000 and 2000-2014 (Table 3)). NDVI images with positive values indicate increasing vegetation while negative NDVI values indicate decreasing vegetation cover. The use of the NIR and the red band was shown to be significantly correlated with the amount of green leaf area or green leaf biomass (Tucker 1979; Singh 1989).

$$NDVI = \frac{\rho\mathrm{NIR} - \rho\mathrm{Red}}{\rho\mathrm{NIR} + \rho\mathrm{Red}} \qquad (eq.6)$$

The results from applying equation 6 are NDVI images in which areas of sparse to none vegetation correspond to lower values and vegetation to high values (Myneni et al. 1995). In the present study, the best fit threshold values for vegetation cover identification were based on comparing image indices with visual analyses of satellite data of RGB color composite images and field surveys. Determining the spatial extension of cropland areas and separating them from natural vegetation was done by clipping the NDVI image using a mask polygon for the cropland areas in the LZRB which represented the actual cropland area extension. This can be considered as a possible representation of the cropland's extension during the period of 1976-2014. Several masks have been prepared for each date's image depending on the geometric shape of the farmland's physiographic character, its spatial characteristics, the color shade of the image, the vegetation pattern and field surveys. Finally, the natural vegetation has been separated from cropland for each date using GIS according to the aforementioned indicators. The reflectance of surface vegetation covers depends on their spectral response characteristics, structural properties of the vegetation and the underlying soil (Myneni et al. 1995). There was no visible difference between the vegetation extracted using the NDVI and that extracted based on the supervised classification of the Landsat 8 OLI image from September 2014.

The NDVI of the natural vegetation displays an oscillating pattern during the period of 1976-2014 with a maximum decrease in the image from 2014, while the NDVI of the cropland and pasture displayed only slight variations during the same period (Table 3 and Figure 8). The variation in the spatial extent of the NDVI of natural vegetation contributes mainly to the fluctuations of the climatological factors such as the intensity and the frequency of the precipitation (Figure 9). The pasture land has a limited extent and is mainly restricted to the seasonal river courses and the bank of the main river because the satellite images were acquired in the end of the dry season. There are huge differences in the vegetation cover between dry and wet seasons due to climatological and anthropogenic effects. During wet season there are large farmland areas of wheat and barley even in hilly terrains that grow together with grass and pastures in spring. The summer season is characterized by summer croplands of limited spatial extent that mainly depends on the irrigation with water from the LZR and groundwater wells.

4 Conclusions

LULC change detection studies have to be performed and updated regularly to support a variety of future planning activities and to resolve environmental issues. This research combined remote sensing, GIS, and detailed ground information to produce LULC maps and to evaluate and detect changes in the LZRB between 1976, 1984, 1990, 2000 and two dates in 2014 – one in April and one in September to compare seasonal changes. From the LULC map of the LZRB thirteen classes and subclasses have been extracted based on supervised classification. Barren land is the dominated class covering an area of about 14,047.26 km^2 with a percentage of 70.7 %. The mixed barren land is the largest category of the barren land class occupying 34.4 % of the main basin; the natural vegetation is the second largest class occupying 11.5 %. The change detection results for the (1976-2014) period show that the area of the urban- and built-up lands has increased from 10.9 km^2 in 1976 to 113.2 km^2 in 2014 due to the population increase and the

economic growth in the last decade. The NDWI shows a negative trend, it has decreased from 310.7 km^2 in 1976 to 148.6 km^2 in 2014. The negative trend of the NDWI is correlated mainly with the shrinkage in the Dokan Lake area. The vegetation cover of the basin has been classified into two groups; NDVI (cropland) and NDVI (natural vegetation). The NDVI (cropland) shows a positive trend during (1976-2014) while the NDVI (natural vegetation) shows no clear trend during the same period. The increasing of the agricultural land area is due to the increasing agricultural practices to meet the growing local demand for food. In 2014, there has been a significant difference in the NDVI and the NDWI between the wet and the dry season. The increase of the natural vegetation, cropland and water area in the wet season 2014 is mainly correlated to climatic conditions. Generally, the results indicate that during the dry (summer) season from 1976 to 2014, the area of the natural vegetation has undergone negligible or limited changes.

5 Acknowledgments

The research was supported by the Ministry of Higher Education and Scientific Research of Iraq (MoHESR), and the TU Bergakademie Freiberg. We are grateful to the Geological Survey of Iraq for providing the necessary data and support during field work. The authors are grateful to M.Sc. Hussein A. Jassas, M.Sc. Ahmed T. Al-Rubaiay, and M.Sc. Arslan A. Othman for their valuable comments. We also gratefully thank M.Sc. Mandy Hoyer for her very valuable and constructive comments and suggestions, which helped us to improve the paper.

6 References

Abubakar M and Anjide A (2012) Analysis of Land Use/Land Cover Changes to Monitor Urban Sprawl in Keffi-Nigeria. Environmental Research Journal, 6, 130–135.

Al-Mehaidi HM (1974) Geologicl Investigation of Mawat-Chuwarta Area, NE Iraq, GEOSURV, Baghdad, Iraq. Int. Rep. No. 609.

Al-Rowaily SL, El-Bana MI, Al-Dujain, FA (2012) Changes in vegetation composition and diversity in relation to morphometry, soil and grazing on a hyper-arid watershed in the central Saudi Arabia. CATENA, 97, 41–49. doi:10.1016/j.catena.2012.05.004

Al-Rubaiay TA, Al-Ma′amar AA, Hattab, AA (2010) Integration of remotely sensed data and GIS techniques to study Lesser Zab River Basin. Internalreport No. 3328, Geosurv, Iraq, Baghdad, 73 P. Baghdad.

Anderson BJ, Hardy EE, Roach J T, Witmer RE (1976) A Land Use And Land Cover Classification System For Use With Remote Sensor Data. U.S. Geological Survey Professional Paper 964 (Vol. 2001).

Aziz. MT, Ibraheem FA, Sebesta J, Hassan AR (1983) The Lesser Zab River basin project photo engineering geological and geomorphological mapping. Internal report. no. 1405, GEOSURV-IRAQ.

Barrios A (2000) Agriculture and Water Quality. American Farmland Trust, Center for Agriculture in the Environment.

Böer B, Sargeant D (1998) Desert perennials as plant and soil indicators in Eastern Arabia. Plant and Soil, 199(2), 261–266. doi:10.1023/A:1004318610230

Chander G, Markham B (2003) Revised Landsat-5 TM radiometric calibration procedures and postcalibration dynamic ranges. Geoscience and Remote Sensing, IEEE Transactions on, 41(11), 2674–2677.

Chen D, Stow D (2002) The effect of training strategies on supervised classification at different spatial resolutions. Photogrammetric Engineering and Remote Sensing, 68(11), 1155–1162.

Chen X, Vierling L, Deering D (2005) A simple and effective radiometric correction method to improve landscape change detection across sensors and across time. Remote Sensing of Environment, 98(1), 63–79. doi:10.1016/j.rse.2005.05.021

Clark RN (1999) Spectroscopy of rocks and minerals, and principles of spectroscopy. Manual of Remote Sensing, 3, 3–58.

Congalton RG (2001) Accuracy assessment and validation of remotely sensed and other spatial information. International Journal of Wildland Fire, 10(4), 321–328.

Congalton RG, Green K (2002) Assessing the Accuracy of Remotely Sensed Data: Principles and Practices. Taylor and Francis.

Cooper CM (1993) Biological effects of agriculturally derived surface water pollutants on aquatic systems - A review. Journal of Environmental Quality.

Cui L, Li G, Ren H, He L, Liao H, Ouyang N, Zhang Y (2014) Assessment of atmospheric correction methods for historical Landsat TM images in the coastal zone: A case study in Jiangsu, China. European Journal of Remote Sensing, 47, 701–716.

Del Valle HF, Elissalde NO, Gagliardini DA, Milovich J (1998) Status of desertification in the Patagonian region: Assessment and mapping from satellite imagery. Arid Land Research and Management, 12(2), 95–121.

Di Gregorio A, Jansen LJ (2000). Land cover classification system: LCCS: classification Nations, concepts and user manual. Food and Agriculture Organization of the United Rome. Rome, Italy.: FAO.

Eiumnoh A, Shrestha RP (2000) Application of DEM data to Landsat image classification: Evaluation in a tropical wet-dry landscape of Thailand. Photogrammetric Engineering and Remote Sensing, 66(3), 297–304.

El-Asmar HM, Hereher ME, El Kafrawy SB (2013) Surface area change detection of the Burullus Lagoon, North of the Nile Delta, Egypt, using water indices: A remote sensing approach. The Egyptian Journal of Remote Sensing and Space Science, 16(1), 119–123. doi:10.1016/j.ejrs.2013.04.004

Environment Canada (2001) Threats to Sources of Drinking Water and Aquatic Ecosystem Health in Canada. National Water Research Institute, Burlington, Ontario. NWRI Scientific Assessment Report Series No. 1. 72p. Page 69 – 15. Burlington, Ontario.

Ewel J, Berish C, Brown B, Price N, Raich J (1981) Slash and Burn Impacts on a Costa Rican Wet Forest Site. Ecology, 62(3), 816–829. doi:10.2307/1937748

Foody GM. (2002) Status of land cover classification accuracy assessment. Remote Sensing of Environment, 80(1), 185–201.

Foody GM (2008) Harshness in image classification accuracy assessment. International Journal of Remote Sensing, 29(11), 3137–3158. doi:10.1080/01431160701442120

Forghani A, Cechet B, Nadimpalli K (2007) Object-based classification of multi-sensor optical imagery to generate terrain surface roughness information for input to wind risk simulation. In 2007 IEEE International Geoscience and Remote Sensing Symposium (pp. 3090–3095). IEEE. doi:10.1109/IGARSS.2007.4423498

Forkuo EK, Frimpong A (2012) Analysis of forest cover change detection. International Journal of Remote Sensing Applicaions, 2(4), 82–92.

Fox J, Rindfuss RR, Walsh SJ, Mishra V (2007) People and the Environment: Approaches for Linking Household and Community Surveys to Remote Sensing and GIS. Springer US.

Frenken K (2009) Irrigation in the Middle East region in figures AQUASTAT Survey-2008. Water Reports, (34).

Giardina C, Sanford R, Døckersmith I, Jaramillo V (2000) The effects of slash burning on ecosystem nutrients during the land preparation phase of shifting cultivation. Plant and Soil, 220(1-2), 247–260. doi:10.1023/A:1004741125636

Griffith JA, Martinko EA, Whistler JL, Price KP (2002) Interrelationships among landscapes, ndvi, and stream water quality in the U.S. central plains. Ecological Applications, 12(6), 1702–1718. doi:10.1890/1051-0761(2002)012[1702:IALNAS]2.0.CO;2

Harris PM, Ventura SJ (1995) The integration of geographic data with remotely sensed imagery to improve classification in an urban area. Photogrammetric Engineering and Remote Sensing.

Havlin J, Schlegel A, Dhuyvetter KC, Shroyer JP, Kok H, Peterson D (1995) Great plains dryland conservation technologies Publication , Manhattan, KS: Kansas State University, Vol. S-81, 7–11.

Hölscher D, Ludwig B, Möller RF, Fölster H (1997) Dynamic of soil chemical parameters in shifting agriculture in the Eastern Amazon. Agriculture, Ecosystems and Environment, 66(2), 153–163. doi:http://dx.doi.org/10.1016/S0167-8809(97)00077-7

Ingram K, Knapp E, Robinson JW (1981) Change detection technique development for improved urbanized area delineation. Technical Memorandum CSC/TM-81, 6087.

Iqbal MF, Khan IA (2014) Spatiotemporal Land Use Land Cover change analysis and erosion risk mapping of Azad Jammu and Kashmir, Pakistan. The Egyptian Journal of Remote Sensing and Space Science, 17(2), 209–229. doi:10.1016/j.ejrs.2014.09.004

Jassim SZ, Goff JC (2006) Geology of Iraq. Geological Society of London.

Jensen JR (2000) Remote sensing of the environment: an earth resource perspective. Prentice Hall.

Jensen JR (1983) Urban/suburban land use analysis. Manual of Remote Sensing, 2, 1571–1666.

Ji L, Zhang L, Wylie B (2009) Analysis of dynamic thresholds for the normalized difference water index. Photogrammetric Engineering and Remote Sensing, 75(11), 1307–1317.

Jusoff K, Ismail MH, Ali NH (2009) Spectral separability of tropical forest tree species using airborne hyperspectral imager. Journal of Environmental Science and Engineering, 3(1), 37–41.

Leverington DW, Moon WM (2012) Landsat-TM-Based Discrimination of Lithological Units Associated with the Purtuniq Ophiolite, Quebec, Canada. Remote Sensing, 4(12), 1208–1231. doi:10.3390/rs4051208

Lillesand T, Kiefer RW, Chipman J (2014) Remote sensing and image interpretation. John Wiley and Sons.

Lindell L (2011) Environmental Effects of Agricultural Expansion in the Upper Amazon [Elektronisk resurs] : A study of river basin geochemistry and hydrochemistry, and farmers' perceptions. Växjö, Kalmar: Linnaeus University Press.

Liu C, Frazier P, Kumar L (2007) Comparative assessment of the measures of thematic classification accuracy. Remote Sensing of Environment, 107(4), 606–616.

Ma'ala KA (2007) The geology of Sulaimaniyah quadrangle sheet NI-38-3, GEOSURV, Baghdad, Iraq. Int. Rep. No.3095.

Macias LF (1995) Remote sensing of mafic-ultramafic rocks: examples from Australian Precambrian terranes. Australian Geological Survey Organisation.

Mancino G, Nolè, A, Ripullone F, Ferrara A (2014) Landsat TM imagery and NDVI differencing to detect vegetation change: assessing natural forest expansion in Basilicata, southern Italy. iForest - Biogeosciences and Forestry, 7(2), 75–84. doi:10.3832/ifor0909-007

Mather P, Koch M (2011) Computer processing of remotely-sensed images: an introduction. John Wiley and Sons.

McSween HY, Taylor GJ, Wyatt MB (2009) Elemental composition of the Martian crust. Science (New York, N.Y.), 324(5928), 736–9. doi:10.1126/science.1165871

Myneni RB, Hall FG, Sellers PJ, Marshak AL (1995) The interpretation of spectral vegetation indexes. IEEE Transactions on Geoscience and Remote Sensing, 33(2), 481–486.

Nian Y, Li X, Zhou J, Hu X (2014) Impact of land use change on water resource allocation in the middle reaches of the Heihe River Basin in northwestern China. Journal of Arid Land, 6(3), 273–286. doi:10.1007/s40333-013-0209-4

Ouyang W, Hao F, Skidmore AK, Groen TA, Toxopeus A G, Wang T (2012) Integration of multi-sensor data to assess grassland dynamics in a Yellow River sub-watershed. Ecological Indicators, 18(0), 163–170. doi:http://dx.doi.org/10.1016/j.ecolind.2011.11.013

Reed BC, Loveland TR, Tieszen LL (1996) An approach for using AVHRR data to monitor U.S. great plains grasslands. Geocarto International, 11(3), 13–22.

Rogan J, Franklin J, Roberts DA (2002) A comparison of methods for monitoring multitemporal vegetation change using Thematic Mapper imagery. Remote Sensing of Environment, 80(1), 143–156. doi:10.1016/S0034-4257(01)00296-6

Rogan J, Miller J (2006) Integrating GIS and Remotely Sensed Data for Mapping Forest Disturbance and Change. In Understanding Forest Disturbance and Spatial Pattern (pp. 133–171). CRC Press. doi:doi:10.1201/9781420005189.ch6

Russ JC (2011) The Image Processing Handbook, Sixth Edition. CRC Press.

Santillan J, Makinano M, Paringit E (2011). Integrated Landsat image analysis and hydrologic modeling to detect impacts of 25-year land-cover change on surface runoff in a Philippine watershed. Remote Sensing, 3(6), 1067–1087.

Scotter GW (1972) Fire as an ecological factor in boreal forest ecosystems of Canada.Scotter, G. W. 1972. Fire in the Environment. USDA Forest Service p. 15-24. (U. S. F. Service, Ed.). Dept. of Agriculture, Forest Service.

Serra P, Pons, X, Sauri D (2003) Post-classification change detection with data from different sensors: some accuracy considerations. International Journal of Remote Sensing, 24(16), 3311–3340.

Singh A (1989) Digital change detection techniques using remotely-sensed data. International Journal of Remote Sensing.

Sissakian VK (1993) The geology of Kirkuk Quadrangle sheet NJ-38- 2, GEOSURV, Baghdad, Iraq. Int. Rep. No. 2229.

Smits PC, Dellepiane, SG, Schowengerdt RA (1999) Quality assessment of image classification algorithms for land-cover mapping: A review and a proposal for a cost-based approach. International Journal of Remote Sensing, 20(8), 1461–1486. doi:10.1080/014311699212560

Sommer R, Vlek PG, Deane de Abreu Sá T, Vielhauer K, de Fátima Rodrigues Coelho R, and Fölster H. (2004) Nutrient balance of shifting cultivation by burning or mulching in the Eastern Amazon – evidence for subsoil nutrient accumulation. Nutrient Cycling in Agroecosystems, 68(3), 257–271. doi:10.1023/B:FRES.0000019470.93637.54

Song C, Woodcock CE, Seto, KC, Lenney MP, Macomber SA (2001) Classification and Change Detection Using Landsat TM Data. Remote Sensing of Environment, 75(2), 230–244. doi:10.1016/S0034-4257(00)00169-3

Stehman SV, Czaplewski RL (1998) Design and Analysis for Thematic Map Accuracy Assessment. Remote Sensing of Environment, 64(3), 331–344. doi:10.1016/S0034-4257(98)000108

Stone EL (1971) Effect of prescribed burning on long term productivity of Coastal Plain soils.Proc. USDA Forest Service, Southeastern Forest Experiment Station. Prescribed burning Symposium proceedings. 160 pp. Asheville, N.C. p. 115-138.

Tewolde MG, Cabral P (2011) Urban Sprawl Analysis and Modeling in Asmara, Eritrea. Remote Sensing, 3(12), 2148–2165. doi:10.3390/rs3102148

Thomlinson JR, Bolstad PV, Cohen WB (1999) Coordinating Methodologies for Scaling Landcover Classifications from Site-Specific to Global. Remote Sensing of Environment, 70(1), 16–28. doi:10.1016/S0034-4257(99)00055-3

Tucker CJ (1979) Red and photographic infrared linear combinations for monitoring vegetation. Remote Sensing of Environment, 8(2), 127–150. doi:10.1016/0034-4257(79)90013-0

Ulbricht KA, Teotia HS, Civco DL (1993) Supervised Classification to Land Cover Mapping in Semi-Arid Environment of NE Brazil Using Landsat-TM and SPOT Data. INTERNATIONAL ARCHIVES OF PHOTOGRAMMETRY AND REMOTE SENSING, 29, 821.

Van Der Meer F, de Jong SM (2001) Imaging Spectrometry:: Basic Principles and Prospective Applications (Vol. 1). Springer Science and Business Media.

Wang, L, Gong P, Ying Q, Yang Z, Cheng X, Ran Q (2010) Settlement extraction in the North China Plain using Landsat and Beijing-1 multispectral data with an improved watershed segmentation algorithm. International Journal of Remote Sensing, 31(6), 1411–1426. doi:10.1080/01431160903475332

Ward D, Phinn SR, Murray AT (2000) Monitoring growth in rapidly urbanizing areas using remotely sensed data. Professional Geographer, 52(3), 371–386.

Wardlow B, Egbert S, Kastens J (2007) Analysis of time-series MODIS 250 m vegetation index data for crop classification in the U.S. Central Great Plains. Remote Sensing of Environment, 108(3), 290–310. doi:10.1016/j.rse.2006.11.021

Wright GG, Morrice JG (1997) Landsat TM spectral information to enhance the land cover of Scotland 1988 dataset. International Journal of Remote Sensing, 18(18), 3811–3834. doi:10.1080/014311697216630

Zhang Q, Wang J, Peng X, Gong P, Shi P (2002) Urban built-up land change detection with road density and spectral information from multi-temporal Landsat TM data. International Journal of Remote Sensing, 23(15), 3057–3078. doi:10.1080/01431160110104728

Zheng JG, Chen YW, Wu GX (2013) Association of Vegetation Patterns and Environmental Factors on the Arid Western Slopes of the Helan Mountains, China. Mountain Research and Development, 33(3), 323–331. doi:10.1659/MRD-JOURNAL-D-12-00088.1

Zubair AO (2006) Change detection In land use and land cover using remote sensing data and GIS. Unpublished Master Thesis, University of Ibadan.

Land use and land cover dynamics in the dry Lake Haramaya Watershed in eastern Ethiopia using remote sensing

Shimelis, B. Gebere	Department of Hydrogeology, Institute of Geology, Technische Universität Bergakademie Freiberg, Gustav-Zeuner Str. 12, 09599 Freiberg, Germany. Email: shimelisberhanu@yahoo.com
Merkel, Broder	Department of Hydrogeology, Institute of Geology, Technische Universität Bergakademie Freiberg, Gustav-Zeuner Str. 12, 09599 Freiberg, Germany. Email: merkel@geo.tu-freiberg
Agumassie, Tena A.	Water and Land Resource Center, Addis Ababa, Ethiopia. Email: tena.a@wlrc-eth.org

Abstract: The knowledge of land use and land cover is important for properly managing, planning and monitoring natural resources. The aim of this study was to generate land use maps for the study area and to understand the land use and land cover changes using remotely sensed satellite imageries from 1985 to 2011. The images were geometrically corrected to a common map projection followed by image processing operations. In ERDAS, supervised classification based on the maximum likelihood algorithm was applied to the Landsat images acquired in 1985, 1995, 2006 and 2011. To check the accuracy of the classification, ground truth data was also collected. Post classification change detection was applied in order to assess changes in land use and land cover over time using IDRISI software. Rapid population growth has created land use misbalances. The results showed that dramatic changes in land use and land cover have occurred with shrinkage of water bodies, cultivated land, forests and grassland and at the same time expansion of *Catha edulis (chat)*/shrubs as well as settlement areas. The result revealed that an absolute shrinkage and loss of water bodies has occurred due to an extensive and massive clearance of forests and grasslands. Between 1985 and 2011, forests became smaller and more fragmented and declined from 202.6 ha to 101.6 ha. Only patches of mature forests are left. They are under threat from expansion of land for *chat* production and settlements. In the mentioned period, the total area of water bodies decreased from 3.5 % to 1.0 % while the area of grassland and cultivated land decreased from 29.2 % to 19.6 % and 42.4 % to 32.6 %, respectively. For a sustainable development of the watershed resources, proper land use planning is essential.

Keywords: Land use land cover changes, remote sensing, image analysis

1. Introduction

Land use and land cover changes are among the main causes for climate changes at local, regional and global scales (Etter et al. 2006; Manandhar et al. 2009). Decreases in soil productivity, biodiversity losses, shortages in water resources and global warming are often related to land use and land cover changes (Dwivedi et al. 2005; Mas et al. 2004; Zhao et al. 2004). The changes affect both human and

natural systems and are recognized as the key factor for global change (Bockstael 1996; Reis 2008; Yadav et al. 2012).

There is a variety of driving forces of land use and land cover changes such as urbanization, population growth and economic booming (Gong et al. 2013). The growing human population and its associated problems such as the rise in demand for land, water and forests along with poor resource management practices, are the major driving forces behind the land use and land cover changes (Hobbs et al. 1991; Lin and Ho 2003; Tanrivermis 2003). Hence, to meet the increasing demands of basic human needs and welfare, land use and land cover information and potentials for their best use is important for the selection, planning and implementation of land use systems (Fan et al. 2007; Manonmani and Suganya 2010; Pandey 2012; Yadav et al. 2012).

Over the last two or three decades, remote sensing techniques have been widely acknowledged as powerful tools to study land use and land cover changes at global to regional and local scales (Gong et al. 2011; Jensen 2007; Lambin et al. 2003; Manandhar et al. 2009; Mayaux et al. 2008). Remotely sensed imagery data provides reliable data at a more frequent interval and at relatively low costs. It makes it possible to obtain land use and land cover information and generates results that are more eye-catching than those obtained with traditional methods (Jat et al. 2008; Lu et al. 2004; Mahmoodzadeh 2007; Wang et al. 2010). Using satellite images is attractive due to their regular repetitive coverage, the recording of data from the same geographic area at the same time of the day, and the consistent scale and look-angle (Jensen 1986).

Valuable information on land use and land cover change can efficiently be extracted from remote sensing imageries. In this study, topographic maps, aerial photos, TM and ETM + Landsat images of the studied watershed and other supporting documents were used to prepare land use and land cover maps for years 1985, 1995, 2006 and 2011. Image classification was done using supervised image classification with a maximum likelihood classifier. Supervised classification is usually known as knowledge-based expert classification technique that depends on reference data to improve the accuracy of the classified image (Berberoglu et al. 2007; Chen et al. 2007). In order to see the nature of the changes of land use and land cover, maps were derived from satellite imageries, and post classification change detection was performed. Accuracy assessment was also done using an error or confusion matrix. An error matrix is the most commonly used method to present the accuracy of the classified images (Fan et al. 2007).

A rapid change in land use and land cover is one of the challenges, which seriously contribute to environmental degradation in Ethiopia in general and in the Haramaya catchment in particular. It is witnessed that extensive shifting and intensive cultivation and the continuous increase in population put significant stress not only on the land but also on water resources of the watershed. And also poor practices of water use, over-exploitation of surface water and groundwater, clearing of forests and siltation of lakes is continuing due to the increasing demand for water and biomass caused by the population growth. Maps drawn from a series of satellite images of the study area show the Lake Haramaya has disappeared completely.

Remote sensing data has been used for land use land cover dynamics analysis by (Assen 2011) in the study area. On his paper, *Catha edulis* (*chat*) is categorized under agricultural crops; moreover his findings reveal an increase in cultivated land but according to (Lemessa 2001) and (CESAR), *Catha edulis* (*chat*) is not an agricultural crop but a shrub, which requires high quantities of irrigation water compared with agricultural crops such as cereals or vegetables. In their study, (Taffesse et al. 2012) also stated that in 2003/04 *Catha edulis* (*chat*) production in Ethiopia used only 1.2 % of the total area cultivated; however, over five years, until 2008/09, its production increased by 6.1 % per year. Different from his findings, this paper also confirms a decrease in cultivated land from time to time

while *Catha edulis* (*chat*) farming increased significantly. Hence, based on intensive field visits and the collection of ground truth data, a more realistic land use land cover dynamics analysis is provided in this work.

Remotely sensed data in the form of Landsat images and aerial photographs is important for land use and land cover mapping and is cost-effective (Ali et al. 2012; Solaimani et al. 2010). However, little attention was paid to it in Ethiopia. Most of the land use and land cover maps developed in the country are based on traditional procedures. With this fact in mind, this study aimed at understanding land use and land cover changes and consequences for human activities in the dry Lake Haramaya watershed over the past 26 years.

2. Study area and dataset

2.1. Description of the study area

The study area is located in the eastern highlands of Ethiopia (9°22'58" to 9°31'22" N and 41°53'44" to 42°12'43" E) covering an area of 15,319.4 ha as shown in Fig. 1. The watershed consists of a vast depression area bounded by adjacent highlands. The elevation of the area ranges from 2460 m above sea level in the northeastern parts to 2006 m.a.s.l. close to the central depression area.

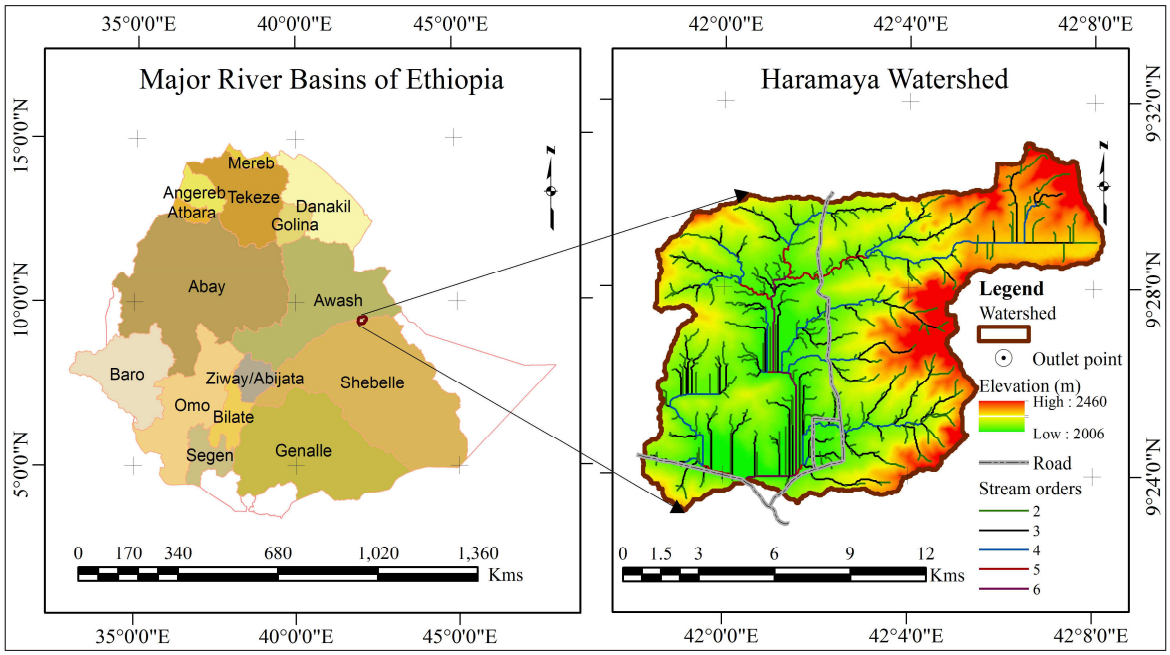

Fig. 1: Map of the study area

The climate in the study area is semi-arid with a mean annual rainfall of 743 mm. Rainfall is bimodal; its maxima occur in April and August with the highest peak in August (139.5 mm) while the smaller peak is in April (97.5 mm). January is the driest month with a rainfall amount of 8.5 mm. The elevation of the catchment causes is the reason why temperatures are moderate with an average temperature of 16.4°C. It varies from 12.6°C in December to 19.0°C in June. Fig. 2 shows the annual climatic variation in temperature and precipitation in the study area. The mean annual temperature between 1970 and 2010 ranged from 12.4°C to 19.8°C while the annual rainfall during same period ranged from 469 mm to 1104 mm.

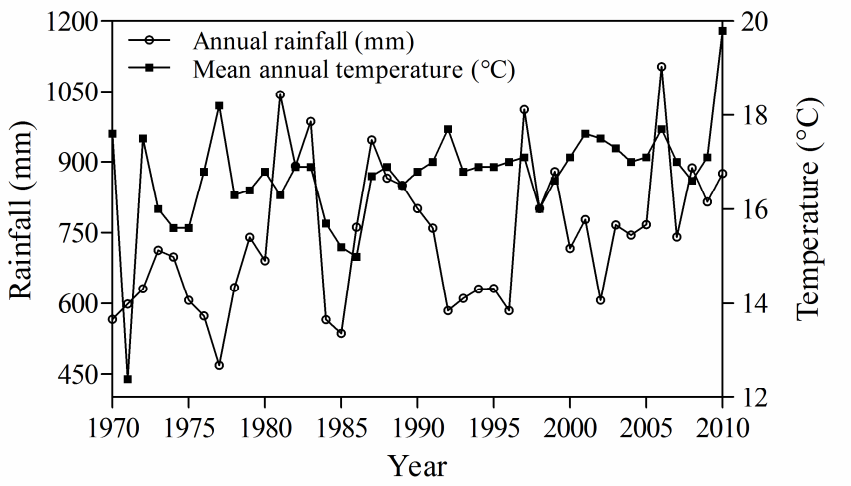

Fig. 2: Mean climate data of the study area in the period from 1970 to 2010

The watershed generally consists of rocks ranging in age from Precambrian to recent depositions. Stratigraphically, from the bottom to the top, the following order can be found: granite (Precambrian), sandstone and limestone (Mesozoic sedimentary rocks) and recent sediments (Quaternary). The predominant soil types of the watershed are characterized by medium to fine-textured materials.

Agriculture is the economic basis of the communities in the watershed (crop, vegetables, livestock and cash crops such as *Catha edulis* (*chat*)). According to (Mesfin et al. 2011), on average each household in the area owns about 0.74 ha of land. In general, activities other than agriculture seem to be very limited. Cattle, sheep, goats and poultry are the most common domestic animals raised in the rural area whereas the people in urban areas are mainly government, non-government, and private business employees or traders.

The increasing population size can contribute to many types of environmental stress (Grimm et al. 2008). Rapid population growth and unplanned human settlements are the major driving forces to the need of increased food production and stress for natural resources like soil, forests, water and fish. The Haramaya watershed is the main source of water for the towns of Harar and Haramaya and nearby communities. Rapid population growth in the area puts great stress on the limited resources available – water, land, forests, etc. According to the Central Statistical Agency of Ethiopia 1994 census report, the population living around the watershed was estimated to have been 166,597 while in 2007 the number increased to 271,018; i.e. it increased by 63 %. According to the report, 49,711 people lived in the watershed and the number increased by 74 % to 86,703 in 2007.

2.2. Cultivation of chat

Chat is an evergreen perennial shrub plant that belongs to the Celastraceae family. The plant is known under different vernacular names: *Khat* is used in English and in Arabic, and *chat* in Ethiopia (Lemessa 2001). In Ethiopia, *chat* is one of the main cash crops and is the major sources of country's foreign currency. There is a strong demand for it on local and foreign markets. It is cultivated for chewing its fresh leaves and young tender twigs (Belwal and Teshome 2011). Moreover, the other parts of the plant are used for various purposes such as fencing, as construction material for houses, as firewood, etc. It is planted in rows with row spacing of ½ m to 1 m.

The suckers or branches are used for vegetative propagation of *chat*. Due to the poor germination rate of the seeds, they are not used for propagation. *Chat* farms are being irrigated when there is water scarcity during dry season. In rainy season there is no need for irrigation since most parts of Ethiopia get adequate amounts of rainwater. Usually chat is intercropped with cereals and vegetables. *Chat* can be harvested all year round at any time of the day, but it is often harvested in the early morning or late afternoon. Generally, well-established, irrigated mature *chat* plants can possibly be harvested up to 2-3 times a year depending on the age, management practices and the fertility of the soil.

2.3. Preparation of datasets

Landsat scenes were acquired from the USGS (U.S. Geological Survey) GLOVIS (Global Visualization Viewer) website (http://glovis.usgs.gov/). While summer in Ethiopia is manly cloudy, winter days are usually relatively cloud-free. Hence, four predominantly cloud-free winter Landsat scenes between 1985 and 2011 were used. Three of these are Landsat TM scenes acquired in 1985, 1995 and 2011, while the last one is a Landsat ETM+ scene acquired in 2006. The dates of the images were chosen to be as closely to each other as possible, but at least in the same vegetation season.

Other materials used are aerial photos (1986, 1996 and 2005) and topographic maps (1986 and 1999) at a scale of 1:50,000 published by the Ethiopian Mapping Authority. ASTER 30 m resolution Digital Elevation Models (DEM) were used to delineate the catchment of the study area. The DEM data had some missing data points where no data was recorded by the mission due to some problems. Therefore, 3DEM Terrain Visualization Software was used to fill the gaps. Arc Hydro Tools 9, which is an extension for ArcGIS, was used to characterize the watershed of the study area. The results were compared with those obtained from SRTM 90 m resolution DEM using both Arc Hydro and Rivertools 2.4.

3. Methods

3.1. Image processing

In this study, supervised land use and land cover image classification was done. For image analysis, all visible and infrared bands (bands 1–5 and 7) were included. While the eye provides the best interpretation, computer algorithms are quicker and allow more consistent classifications. According to Eastman (Eastman 2006) and Mayaux et al. (Mayaux et al. 2008), the human eye is often used to guide digital classification or in conjunction with digital classification. For classification of images as well as for accuracy assessment, training areas (i.e. reference points) were collected.

A number of independent training areas were randomly collected during field survey using a GPS device. This survey was made to accurately determine the locations of the land use and land cover class references. As much as possible an effort was made to make the randomly selected points to be representative for the entire watershed. Also sufficient data was taken for land features such as water bodies, forests and settlements during the field visit. Initially visual interpretation of images including aerial photographs, land use maps, information from Google Earth was done and interviews were made with the elder community members, who are familiar with the land use and land cover history of the study area over long time periods. Features such as settlements and water bodies from topographic maps were also used for selecting the training areas.

Land use and land cover classification was performed in ERDAS software using supervised classification with the maximum likelihood algorithm. Compared with other classification algorithms, the supervised maximum likelihood classification method gives higher classification accuracies (Bolstad and Lillesand 1991; Lillesand and Kiefer 1994; Mengistu and Salami 2008; Reis 2008; Solaimani et al. 2010). It is the most commonly and most widely used technique (Dewan and

Yamaguchi 2009; Serra et al. 2003; Yacouba et al. 2009). This technique is based on the decision rule that unknown class pixels belong to the class with the highest likelihood among several classes (Foody 2002; Foody et al. 1992; Franklin et al. 2003; Solaimani et al. 2010).

Eight signature classes were created using the signature editor of ERDAS software. This process was performed for all four Landsat images. The spectral profile for the land use and land cover classes of the watershed is shown in Fig. 3. The following land use and land cover classes were identified: settlements, forest plantations, grassland, cultivated land, *Catha edulis (chat)*/shrubs, bare land, shallow water and water bodies. The descriptions of the land cover classes are presented in Tab. 1.

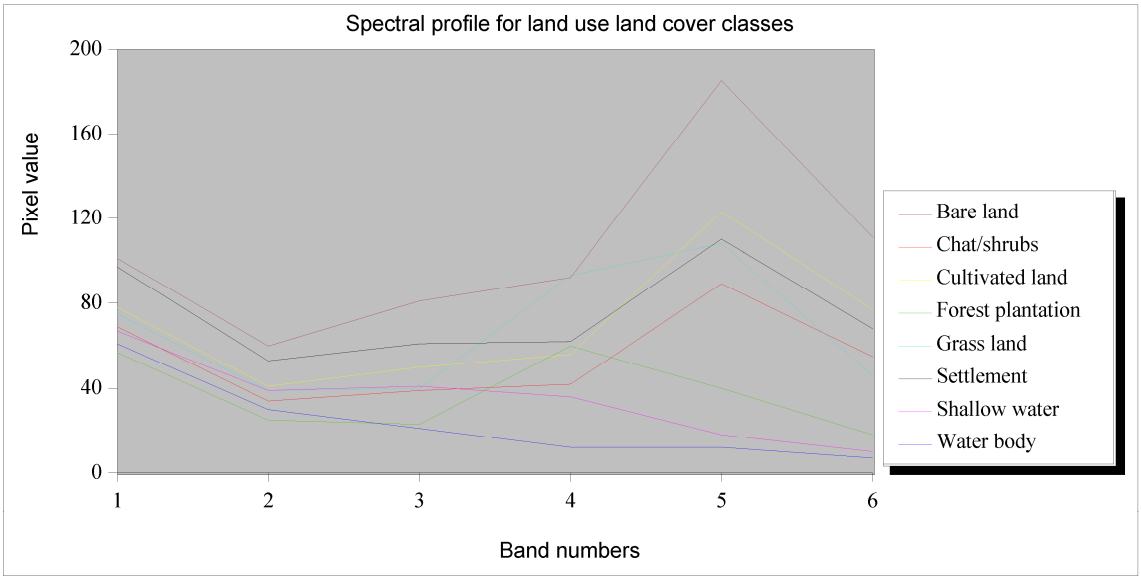

Fig. 3: Spectral profile of the land use and land cover classes

Tab. 1: Description of thesland cover classes

Land Cover Class	*Description*
Bare land	Area of exposed soils and bare exposed rocks
Shallow water	Swampy area where water is on the surface
Cultivated Land	Areas used for annual crop cultivation and fallow lands, which are permanently or not irrigated.
Forest Plantation	Represents both natural and enhanced plantation of forest areas that are stocked with trees capable of producing timber or other wood products that mainly are eucalyptus and conifers.
Water Body	All bodies of water are in this class. It is the area that remains water-logged throughout the year.
Settlement	Areas where there is a permanent concentration of people building and other man-made structures. Houses, roads, buildings, and bare soil.
Catha edulis (chat)/Shrub	*Catha edulis (chat)*, bushes, scrubs and tall herb communities.
Grass land	Area covered with grass that is used for grazing and that covered for a considerable period of the year.

3.2. Accuracy assessment

Accuracy assessment of the final image is important once the classifications are completed. It is important for post classification change detection analysis. Accuracy assessment of remotely sensed images involves the comparison of the classified map with reference data (Congalton 1991). It can give information on the quality of the map produced. In order to compare two classified images of different dates, an error matrix or confusion matrix can be used (Congalton 1991; Congalton and Green 2008). An error matrix is a c x c square array (c is the number of rows and columns), which is used for comparing information from the classified image (row data) with reference data (column data). Its most common application is land use and land cover change analysis using images of the same target land features from two dates (Congalton and Green 2008; Ismail and Jusoff 2008).

To assess the accuracy of the independently classified images, the produced land cover maps and reference data were compared as stated by (Congalton 1991). To check the accuracy of the produced land use and land cover maps, error matrices were created. More than 40 reference points (training areas) for each classified images were used for the accuracy assessment. The standard accuracy assessment criteria such as producer's accuracy, user's accuracy, overall classification accuracy and the Kappa statistics were used to show the accuracy of classification images.

The Kappa statistics were computed using the following equation:

$$\frac{N\sum_{i=1}^{r} x_{ii} - \sum_{i=1}^{r}\left(x_{i+}x_{+i}\right)}{N^2 - \sum_{i=1}^{r}\left(x_{i+}x_{+i}\right)} \qquad (1)$$

where r is number of rows in the error matrix, x_{ii} is number of observations in row i and column i, x_{i+} is the total number of observations in row i, x_{+i} is the total number of observations in column i and N is total number of observations included in the matrix.

3.3. Change analysis

Change detection is one of the most important applications of remote sensing. Post classification change detection analysis is ideally one of the most simple change detection methods (Xu et al. 2009). It is a comparative analysis of independently classified images of different dates. For the post classification change detection in this study, each image was classified independently followed by a thematic overlay of the classified images. The method results in a "from-to" change matrix showing the transitions between the individual classes in a certain time period (Fichera et al. 2012).

In this study, post classification change detection was carried out to quantitatively show from-to changes. In order to detect and quantify the extent of changes from one land cover category to another at a later date, in IDRISI software the cross tabulation technique was used. For cross tabulation operations, IDRISI was found to be better than ERDAS Imagine. Microsoft Excel was used to organize some of the data for change detection analysis and to quantitatively determine the change dynamics. The general workflow of the supervised classification is shown in Fig. 4.

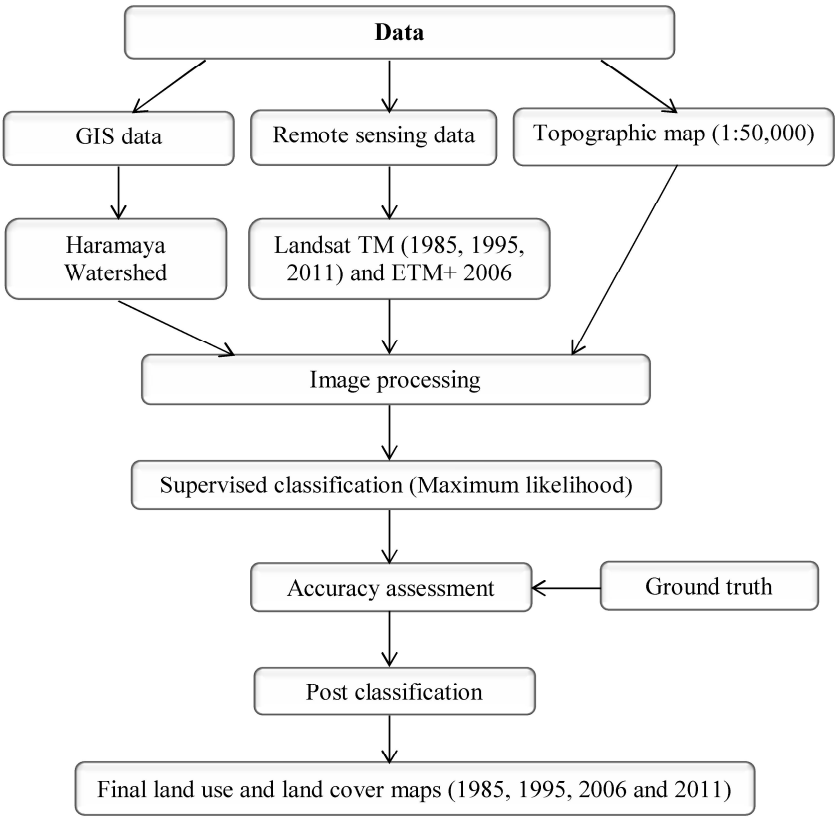

Fig. 4: General workflow for a supervised land use land cover classification

4. Results and discussion

4.1. Results

This study gives a better understanding of land use and land cover changes in the study area of the watershed for a period of more than two decades due to rise in number of population. To understand the changes in the watershed, the land use and land cover categories were extracted for the year 1985, 1995, 2006 and 2011 using supervised maximum likelihood classification technique as a means of image classification. All the images were classified into eight thematic classes: forest plantation, water body, settlement, cultivated land, grassland, bare land, shallow water and chat/shrubs. The results from the study indicate that the land use and land cover of the watershed has considerably changed.

As shown in Tab. 2, the majority of the area was covered by cultivated land in 1985 but from time to time, much of the cultivated land was converted to *Catha edulis (chat)*/shrubs and settlements. For example, from 1985 to 2011, the cultivated land cover decreased by 1,503.2 ha whereas the *Chat*/shrubs cover increased by 3,144.0 ha. In 1985, 42.4 % of the watershed were covered by cultivated land. This number decreased to 32.6 % in 2011. The area covered with *Catha edulis (chat)*/shrubs increased from 20.7 % in 1985 to 41.2 % in 2011. Settlement areas also increased from 0.7 % in 1985 to 1.6 % in 2011. Bare land increased from 2.1 % in 1985 to 2.4 % in 2011. Water bodies covered 3.5 % of the study area in 1985 but they decreased to 2.3 % in 1995; it further decreased to 1.5 % in 2006, and in 2011 it covered only 1.0 %. It is obvious that the majority of the cultivated land was converted to *Catha edulis (chat)*/shrubs as Fig. 5 shows.

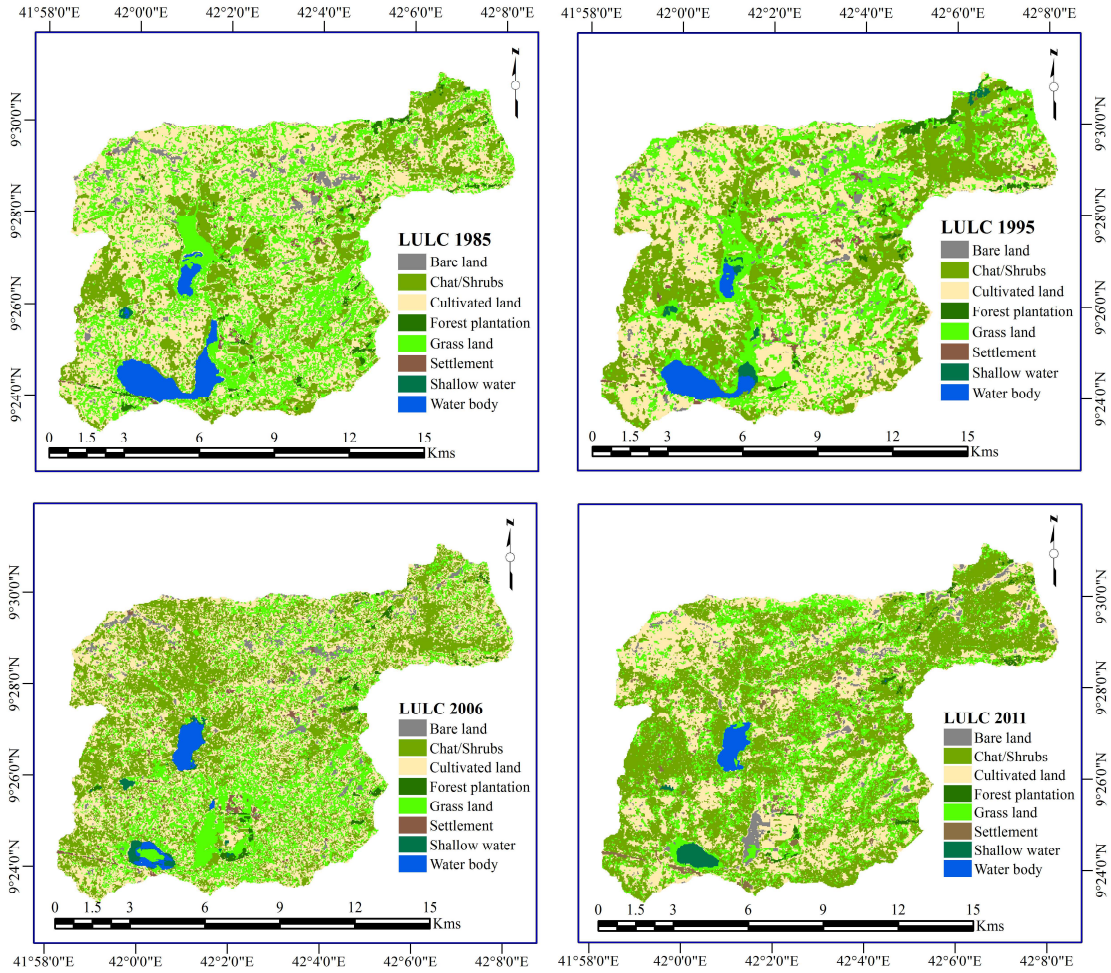

Fig. 5: Land use and land cover maps of the study area in the period from 1985 until 2011

Tab. 2: Extent and percentage of land use and land cover between 1985 and 2011

LULC Categories	*1985*		*1995*		*2006*		*2011*	
	ha	*%*	*ha*	*%*	*ha*	*%*	*ha*	*%*
Bare land	314.1	2.1	323.2	2.1	329.8	2.2	367.0	2.4
Chat/Shrubs	3170.9	20.7	4377.3	28.6	5145.6	33.6	6314.9	41.2
Cultivated land	6499.6	42.4	6231.3	40.7	5809.5	37.9	4996.4	32.6
Forest plantations	202.6	1.3	172.0	1.1	139.8	0.9	101.6	0.7
Grassland	4472.8	29.2	3626.2	23.7	3381.3	22.1	3005.1	19.6
Settlements	103.9	0.7	129.9	0.8	186.6	1.2	252.3	1.6
Shallow water	14.8	0.1	102.3	0.7	96.0	0.6	124.1	0.8
Water bodies	540.7	3.5	357.1	2.3	230.9	1.5	158.1	1.0
Total	15319.4	100	15319.4	100	15319.4	100	15319.4	100

Tab. 3 shows the extent of changes in land use and land cover between 1985 and 1995. A significant amount of the cultivated land was converted to *Chat*/shrubs. For example, in 1985 cultivated land covered 6,499.6 ha of the watershed and about 3,197.0 ha of the land remained unchanged in 1995. This means that the cultivated land was partly converted to different land use and land cover classes

such as 1.5 ha to water bodies, 1,251.7 ha to grassland, 1,849.3 ha to *Catha edulis*/shrubs, 43.1 ha to settlements, 122.3 ha to bare land, 3.6 ha to shallow water and 31.2 ha to forest plantations. A significant amount of the cultivated land was converted to *Catha eduli*/shrubs.

Tab. 3: Change matrix of land use and land cover (ha) from 1985 (columns) to 1995 (rows)

	Classes	*1985*								
		BL	*CS*	*CL*	*FP*	*GL*	*ST*	*SW*	*WB*	*Total*
1995	BL	**90.5**	3.2	122.3	1.7	100.5	5.0	0.0	0.1	323.2
	CS	0.5	**2014.0**	1849.3	34.9	438.3	11.3	0.9	28.1	4377.3
	CL	88.2	595.9	**3197.0**	40.4	2259.0	37.9	0.1	12.8	6231.3
	FP	0.9	50.6	31.2	**45.3**	43.9	0.0	0.0	0.2	172.0
	GL	130.7	474.5	1251.7	76.1	**1568.1**	21.9	6.3	97.0	3626.2
	ST	3.2	10.4	43.1	1.4	43.8	**27.8**	0.0	0.1	129.9
	SW	0.0	21.2	3.6	2.7	9.8	0.0	**7.5**	57.5	102.3
	WB	0.0	1.2	1.5	0.0	9.5	0.0	0.0	**345.0**	357.1
	Total	314.1	3170.9	6499.6	202.6	4472.8	103.9	14.8	540.7	**15319.4**

Overall Kappa Index of Agreement = 69.8 %

Note: WB = water bodies, SW = shallow water, BL = bare land, GL = grassland, CS = *Catha edulis (chat)*/shrubs, CL = cultivated land, ST = settlements and FP = forest plantations

The land use and land cover changes from 1995 to 2006 can be derived from Tab. 4. For instance, of 6,231.3 ha which were covered by cultivated land in 1995, 2,785.3 ha remained unchanged in 2006. Hence, 3,446.0 ha of the cultivated land were converted to other land use and land cover classes such as 3.7 ha to water bodies, 1,353.5 ha to grassland, 1,895.8 ha to *Chat*/shrubs, 84.1 ha to settlements, 84.8 ha to bare land, 5.9 ha to shallow water and 18.3 ha to forest plantations. In fact, a significant amount of the cultivated land was converted to *Chat*/shrubs. In the same time period, out of 4,377.3 ha, 2,287.9 ha of *Chat*/shrubs remained unchanged.

Tab. 4: Change matrix of land use and land cover (ha) from 1995 (columns) to 2006 (rows)

	Classes	*1995*								
		BL	*CS*	*CL*	*FP*	*GL*	*ST*	*SW*	*WB*	*Total*
2006	BL	**91.0**	2.9	84.8	3.8	140.7	4.1	0.0	2.5	329.8
	CS	12.8	**2287.9**	1895.8	54.1	830.8	19.1	19.8	25.3	5145.6
	CL	129.3	1406.9	**2785.3**	49.9	1355.9	47.2	5.9	29.3	5809.5
	FP	0.5	48.2	18.3	**29.3**	40.7	2.7	0.0	0.2	139.8
	GL	78.3	618.0	1353.5	34.5	**1112.1**	23.0	44.0	117.8	3381.3
	ST	11.3	7.7	84.1	0.5	48.6	**33.9**	0.0	0.5	186.6
	SW	0.0	1.4	5.9	0.0	25.5	0.0	**11.3**	51.8	96.0
	WB	0.0	4.2	3.7	0.0	71.9	0.0	21.2	**129.8**	230.9
	Total	323.2	4377.3	6231.3	172.0	3626.2	129.9	102.3	357.1	**15319.4**

Overall Kappa Index of Agreement = 66.7 %

The changes in land use and land cover in the study area between 2006 and 2011 can be obtained from Tab. 5. For example, *Catha edulis (chat)*/shrubs covered 5,145.6 ha in 2006 and 3,120.8 ha remained unchanged in 2011. However, 2,024.8 ha were converted to different land use and land cover classes like 20.3 ha to settlement areas, 846.1 ha to grasslands, 1,127.4 ha to cultivated land, 3.8 ha to bare land, 3.7 ha to shallow water and 20.3 ha to forests. A significant increase in the *Catha edulis*

(chat)/shrubs cover from 2006 to 2011 was noticed, from 5,145.6 ha to 6,314.9 ha. Again, the shrinkage in cultivated land had the largest contribution to the expansion of *Catha edulis (chat)* farm.

Tab. 5: Change matrix of land use and land cover (ha) from 2006 (columns) to 2011 (rows)

	Classes	*2006*								
		BL	*CS*	*CL*	*FP*	*GL*	*ST*	*SW*	*WB*	*Total*
2011	BL	**132.3**	3.8	65.5	0.0	152.2	12.6	0.4	0.1	367.0
	CS	2.3	**3120.8**	2139.0	57.7	975.9	10.0	8.1	1.1	6314.9
	CL	149.5	1127.4	**2340.5**	18.3	1255.0	81.8	18.7	5.0	4996.4
	FP	0.3	20.7	21.6	**42.6**	16.5	0.0	0.0	0.0	101.6
	GL	32.1	846.1	1133.2	18.5	**901.3**	15.5	32.3	26.1	3005.1
	ST	13.3	20.3	106.0	2.3	43.7	**66.7**	0.0	0.0	252.3
	SW	0.0	3.7	1.4	0.0	35.5	0.0	**27.9**	55.5	124.1
	WB	0.0	2.8	2.2	0.4	1.2	0.0	8.6	**143.1**	158.1
	Total	329.8	5145.6	5809.5	139.8	3381.3	186.6	96.0	230.9	**15319.4**

Overall Kappa Index of Agreement = 67.8 %

In 1985, the watershed was dominated by cultivated land (6,499.6 ha) but later in 2011, 2,629.5 ha of the cultivated land had been converted to *Catha edulis (chat)*/shrubs. The result in Tab. 6 shows an increase in *Catha edulis (chat)*/shrubs from 1985 to 2011. In 1985 *Catha edulis (chat)*/shrubs covered about 3,170.9 ha of the land; it increased to 6,314.9 ha in 2011. The increase in *Catha edulis (chat)*/shrubs is, recorded in 2011, due to the transformation of other land use and land cover classes to it. For instance, water bodies covered 98.9 ha of the land, grassland contributed 1,121.1 ha, cultivated land contributed 2,629.5 ha and forest plantations occupied 76.3 ha of the entire study area. The settlement area also increased from 103.9 ha to 252.3 ha during the same time period. It was noticed that the shrinkage in cultivated land to a large extent contributed to the increase in *Catha edulis (chat)*.

Tab. 6: Change matrix of land use and land cover (ha) from 1985 (columns) to 2011 (rows)

	Classes	*1985*								
		BL	*CS*	*CL*	*FP*	*GL*	*ST*	*SW*	*WB*	*Total*
2011	BL	**83.3**	4.6	82.3	0.6	129.9	6.0	0.0	60.2	367.0
	CS	2.6	**2365.1**	2629.5	76.3	1121.1	17.9	3.4	98.9	6314.9
	CL	190.5	365.6	**2354.0**	31.6	1945.2	38.0	5.5	66.0	4996.4
	FP	0.3	27.8	19.4	**34.1**	19.7	0.2	0.0	0.1	101.6
	GL	32.3	390.9	1316.9	49.2	**1083.0**	15.2	0.8	116.9	3005.1
	ST	5.1	15.5	90.8	10.4	100.9	**26.6**	0.0	2.9	252.3
	SW	0.0	0.3	0.3	0.0	1.0	0.0	**5.0**	117.5	124.1
	WB	0.0	1.2	6.4	0.3	71.9	0.0	0.0	**78.3**	158.1
	Total	314.1	3170.9	6499.6	202.6	4472.8	103.9	14.8	540.7	**15319.4**

Overall Kappa Index of Agreement = 65.0 %

Post classification of land use and land cover changes was performed to see the change from one land use and land cover type to another land use and land cover type during the time periods 1985–1995, 1995–2006, 2006–2011 and 1985–2011 as compiled in Tables 3, 4, 5 and 6, respectively. All possible changes and no changes were identified, with no changes shaded in grey color along the diagonals. For example, between 1985 and 2011 (Table 6), more than 100 ha of forest plantations were cleared. During the time period 1985 – 2011, the majority of the cultivated land (2,629.5 ha), water bodies (98.9 ha), bare land (2.6 ha) and grassland (1,121.1 ha) was converted to *Catha edulis (chat)*/shrubs. Bare land and settlements have never been transformed to shallow water or water bodies. Most of the

land in the watershed was converted to *Catha edulis (chat)*/shrubs. The overall Kappa index agreement of the change detections ranges from 65.0 % to 69.8 %.

The assessment of the results for the classification accuracy for the four sets of Landsat images is presented in Tab. 7. The overall classification accuracies for 1985, 1995, 2006 and 2011 are 86.0 %, 88.3 %, 82.8 % and 88.2 % respectively, with overall Kappa statistics of 0.798, 0.827, 0.753 and 0.811. The producer's and user's accuracies also showed consistently high results, accounting for 66 % to 100 % and 77 % to 100 %, respectively.

Tab. 7: Accuracy assessment for the classified images

Year	*Type of Landsat*	*Date*	*Path/Row*	*Resolution*	*Overall classification accuracy*	*Overall Kappa statistics*
1985	TM	21 Feb, 1985	166 – 54	30 m	86.0 %	0.798
1995	TM	17 Feb, 1995	166 – 54	30 m	88.3 %	0.827
2006	ETM+	06 Nov, 2006	166 – 54	30 m	82.8 %	0.753
2011	TM	12 Jan, 2011	166 – 54	30 m	88.2 %	0.811

Data source: USGS Global Visualization Viewer http://glovis.usgs.gov/

4.2. Discussion

In this study, four land use and land cover maps were produced using remotely sensed data through supervised image classification with maximum likelihood classification. The main idea of image classification is to automatically assign all pixels in an image to specific land use and land cover classes (Lillesand and Kiefer 1994). The results of the supervised classification into eight land use and land cover classes are shown in Fig. 6. Post classification change detection was also employed in order to compare the four independently classified images. Eight land use and land cover classes were identified in the studied watershed: forest plantations, water bodies, settlements, cultivated land, grassland, bare land, shallow water and chat/shrubs.

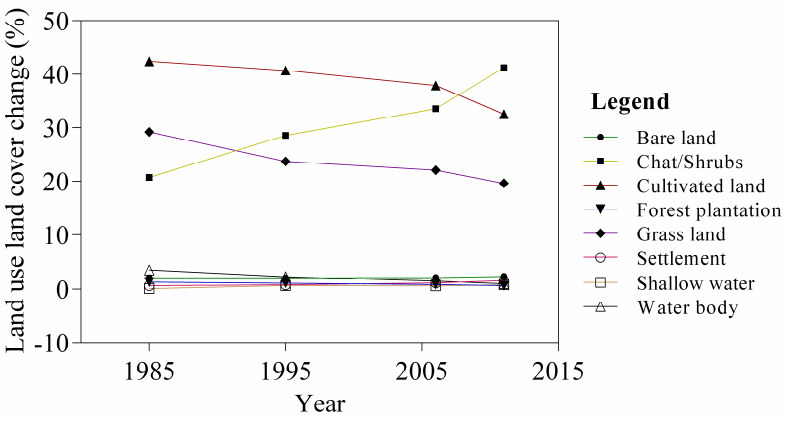

Fig. 6: Land use and land cover changes in percent

The rising population number and increasing socioeconomic demands create pressure on land use and land cover which results in unplanned and uncontrolled changes in land use and land cover (Ikiel et al. 2013). The study result reveals that shifting large shares of the agriculture to *Catha edulis* (*chat*)/shrubs cultivation and clearing forests for settlements is one of the causes of deforestation in the watershed. The transformation of forest areas is related to human activities that affect the environment (Gong et al. 2013; GUO et al. 2006). Forest lands are exploited extremely for housing and firewood production as well as for satisfying the land demand for *Catha edulis* (*chat*) production. If the present trend of deforestation in the study area keeps continuing, it is just a matter of time when the whole forest cover will have been converted.

The study area is well known for extensive *Catha edulis (chat)* production due to availability of basic infrastructure such as roads and due to the proximity of markets (Lemessa 2001). The rapid decline of cultivated land may be largely attributed to land use conversions to *Catha edulis (chat)* production and to the expansion of settlement areas. Presently *Catha edulis (chat)* is more and more being produced by the local people and sold on local markets as well as exported to neighboring countries. This creates the opportunity for local farmers to be able to improve their standard of living by earning significant amounts of benefit instead of growing cereal crops or other vegetables.

All in all, this study revealed an increase in *Chat*/shrubs, bare land, settlements and shallow water whereas cultivated land, grassland, water bodies and forest plantations decreased. A large share of the water bodies were converted to shallow water and grasslands. Agriculture is the economic mainstay in the study area and multiple cropping is practiced in most parts of it. Most of the farmers in the watershed are small-scale farmers engaged in mixed farming, i.e. cropping and livestock production. All marginal and grazing lands were brought under cultivation of *Chat*. Currently, *Chat* production now occupies a significant amount of the watershed area. The production of this plant requires substantial amounts of water mostly using surface irrigation.

Continuous population growth with an increasing individual demand for water used for irrigation, municipal and industrial uses result in strong competition in the allocation of the scarce water resources of the watershed. Between 1994 and 2007, the number of people living in the watershed grew by 74 %. Changes in land use and land cover and improper use of the watershed's resources have also caused a substantial decline of the wetland resources of the study area. These may be major causes for the complete demise of the lake. Lake Haramaya does no longer exist (the storage capacity decreased to zero) for subsistence irrigation, domestic and industrial uses.

5. Conclusions

This study provides land use and land cover changes that occurred in Lake Haramaya watershed between 1985 and 2011 using remotely sensed images. Remote sensing techniques are useful and detailed ways for producing land use and land cover maps. Post classification change detection was employed to analyze the land use and land cover changes in the study area. Information of land use and land cover and its changing patterns over time is very important especially for the management of natural resources of the watershed such as forests, water and soil. The main objective of the study was to detect spatial and temporal land use and land cover changes using satellite imagery.

It was shown that the *Catha edulis (chat)*/shrubs cover increased, as well as the area occupied by bare land, shallow water and settlements while the cultivated land, grassland, water body and forest plantation cover decreased. The most important reason for the expansion of *Catha edulis (chat)* production is that it is an attractive plant for increasing the income of the local farmers, who sell it to local market and neighboring countries, and that it creates employment opportunities for the local communities. Moreover, the climate pattern of the region is very suitable for growing *Catha edulis*

(chat). Although the plant is an important economic resource in the watershed, its high water demand remained unknown and unexplored.

Rapid population growth along with the scarce natural resources and unmanaged cultivation practices cause environmental changes in the watershed. The extent of cultivated land, water bodies, forest plantations and grasslands are shrinking in favor of settlements and *Catha edulis (chat)*/shrubs farms. According to the Central Statistics Agency reports, the population of the watershed annually increased at a rate of 4 % between 1994 and 2007, a very high figure, compared with the national average being 2.7 %. The population in the towns of Harar, Awoday and Haramaya showed an annual growth rate of about 3.2 %, which is still higher than the national growth rate.

Currently, uncontrolled and unplanned construction activities along with a high rate of population growth cause an extensive depletion of water resources, which may lead to serious food scarcity and misery for the rising population in the area in the near future unless immediate measures are taken. These land use maps could be used as valuable means for monitoring changes in land use and land cover patterns, for providing water resource information, for evaluating the extent of deforestation and for dealing with lake rehabilitation in the study area as well. Information on land use and land cover pattern changes is therefore critically important for land resources management and for future planning activities. So, remote sensing is a powerful tool that can be used to extract information on land use for monitoring, assessing, managing and planning natural resources.

Acknowledgements

This study was funded by the Engineering Capacity Building Program of Ethiopia (ECBP). The authors gratefully acknowledge the support rendered by Haramaya University in providing office facilities, materials helpful for this study and a vehicle for field data collection.

References

Ali Z, Tuladhar A, Zevenbergen J (2012) An integrated approach for updating cadastral maps in Pakistan using satellite remote sensing data International Journal of Applied Earth Observation and Geoinformation 18(0):386-398 doi:http://dx.doi.org/10.1016/j.jag.2012.03.008

Assen M (2011) Land use/cover dynamics and its implications in the dried Lake Alemaya watershed, eastern Ethiopia J Sustain Dev Africa 13(267-284

Belwal R, Teshome H (2011) Chat exports and Ethiopian economy: opportunities, dilemmas and constraints Afr J Bus Manage 5(9):3635-3648

Berberoglu S, Evrendilek F, Ozkan C, Donmez C (2007) Modeling forest productivity using Envisat MERIS data Sensors 7(10):2115-2127

Bockstael NE (1996) Modeling economics and ecology: the importance of a spatial perspective American Journal of Agricultural Economics:1168-1180

Bolstad PV, Lillesand TM (1991) Rapid maximum likelihood classification vol 57. vol 1. American Society for Photogrammetry and Remote Sensing, Bethesda, MD, ETATS-UNIS

CESAR Khat. Center for Substance Abuse Research. http://www.cesar.umd.edu/cesar/drugs/khat.asp. Accessed June 23, 2015 2015

Chen X, Cai X, Li H (2007) Expert classification method based on patch-based neighborhood searching algorithm Geo-spat Inf Sc 10(1):37-43 doi:10.1007/s11806-006-0145-y

Congalton RG (1991) A review of assessing the accuracy of classifications of remotely sensed data Remote sensing of environment 37(1):35-46

Congalton RG, Green K (2008) Assessing the accuracy of remotely sensed data: principles and practices. CRC press,

Dewan AM, Yamaguchi Y (2009) Land use and land cover change in Greater Dhaka, Bangladesh: Using remote sensing to promote sustainable urbanization Applied Geography 29(3):390-401

Dwivedi R, Sreenivas K, Ramana K (2005) Cover: Land-use/land-cover change analysis in part of Ethiopia using Landsat Thematic Mapper data International Journal of Remote Sensing 26(7):1285-1287

Eastman JR (2006) Idrisi Andes Guide to GIS and image processing:87-131

Etter A, McAlpine C, Pullar D, Possingham H (2006) Modelling the conversion of Colombian lowland ecosystems since 1940: Drivers, patterns and rates Journal of environmental management 79(1):74-87

Fan F, Weng Q, Wang Y (2007) Land use and land cover change in Guangzhou, China, from 1998 to 2003, based on Landsat TM/ETM+ imagery Sensors 7(7):1323-1342

Fichera CR, Modica G, Pollino M (2012) Land cover classification and change-detection analysis using multi-temporal remote sensed imagery and landscape metrics European Journal of Remote Sensing 45(1):1-18

Foody GM (2002) Status of land cover classification accuracy assessment Remote sensing of environment 80(1):185-201

Foody GM, Campbell NA, Trodd NM, Wood TF (1992) Derivation and applications of probabilistic measures of class membership from the maximum-likelihood classification LLLTLL 58(9):1335-1341

Franklin J, Rogan J, Phinn SR, Woodcock CE (2003) Rationale and conceptual framework for classification approaches to assess forest resources and properties. In: Remote Sensing of Forest Environments. Springer, pp 279-300

Gong C, Chen J, Yu S (2011) Spatiotemporal dynamics of urban forest conversion through model urbanization in Shenzhen, China International journal of remote sensing 32(24):9071-9092

Gong C, Yu S, Joesting H, Chen J (2013) Determining socioeconomic drivers of urban forest fragmentation with historical remote sensing images Landscape and urban planning 117(57-65

Grimm NB, Faeth SH, Golubiewski NE, Redman CL, Wu J, Bai X, Briggs JM (2008) Global change and the ecology of cities Science 319(5864):756-760

GUO L, XIA B-C, YU S-X, GONG C-F (2006) Effect of anthropogenic disturbances on the temporal-spatial changes of landscape patterns at Taishan Mountain Chinese Journal of Eco-Agriculture 4(060

Hobbs NT, Schimel DS, Owensby CE, Ojima DS (1991) Fire and grazing in the tallgrass prairie: contingent effects on nitrogen budgets Ecology 72(4):1374-1382

Ikiel C, Ustaoglu B, Dutucu AA, Kilic DE (2013) Remote sensing and GIS-based integrated analysis of land cover change in Duzce plain and its surroundings (north western Turkey) Environmental monitoring and assessment 185(2):1699-1709

Ismail MH, Jusoff K (2008) Satellite data classification accuracy assessment based from reference dataset International Journal of Computer and Information Science and Engineering 2(2):96-102

Jat MK, Garg PK, Khare D (2008) Monitoring and modelling of urban sprawl using remote sensing and GIS techniques International journal of Applied earth Observation and Geoinformation 10(1):26-43

Jensen JR (1986) Introductory digital image processing: a remote sensing perspective. Pearson Prentice-Hall,

Jensen JR (2007) Remote Sensing of the Environment: An Earth Resource Perspective. Second edn. Pearson Prentice Hall,

Lambin EF, Geist HJ, Lepers E (2003) Dynamics of land-use and land-cover change in tropical regions Annual review of environment and resources 28(1):205-241

Lemessa D (2001) Khat (Catha edulis): Botany, distribution, cultivation, usage and economics in Ethiopia Addis Ababa: United Nations Development Programme, Emergencies Unit for Ethiopia (UNDP-EUE)

Lillesand TM, Kiefer RW (1994) Remote Sensing and Image Interpretation. John Willey & Sons Inc., United States of America

Lin GCS, Ho SPS (2003) China's land resources and land-use change: insights from the 1996 land survey Land use policy 20(2):87-107

Lu D, Mausel P, Brondizio E, Moran E (2004) Change detection techniques International journal of remote sensing 25(12):2365-2401

Mahmoodzadeh H (2007) Digital change detection using remotely sensed data for monitoring green space destruction in Tabriz International Journal of Environmental Research 1(1):35-41

Manandhar R, Odeh IOA, Ancev T (2009) Improving the accuracy of land use and land cover classification of Landsat data using post-classification enhancement Remote Sensing 1(3):330-344

Manonmani R, Suganya GMD (2010) Remote sensing and GIS application in change detection study in urban zone using multi temporal satellite International Journal of Geomatics and Geosciences 1(1):60-65

Mas J-F et al. (2004) Assessing land use/cover changes: a nationwide multidate spatial database for Mexico International Journal of Applied Earth Observation and Geoinformation 5(4):249-261 doi:http://dx.doi.org/10.1016/j.jag.2004.06.002

Mayaux P, Eva H, Brink A, Achard F, Belward A (2008) Remote sensing of land-cover and land-use dynamics. In: Earth Observation of Global Change. Springer, pp 85-108

Mengistu DA, Salami AT (2008) Application of remote sensing and GIS inland use/land cover mapping and change detection in a part of south western Nigeria African Journal of Environmental Science and Technology 1(99-109

Mesfin W, Fufa B, Haji J (2011) Pattern, trend and determinants of crop diversification: empirical evidence from smallholders in eastern Ethiopia Journal of Economics and Sustainable Development 2(8):78-89

Pandey D (2012) Land Use and Land Cover Planning of Gondia Municipal City, Maharashtra State, India Using Remote Sensing & GIS Techniques Int J Life Sc Bt & Pharm Res 1(4):46-64

Reis S (2008) Analyzing land use/land cover changes using remote sensing and GIS in Rize, North-East Turkey Sensors 8(10):6188-6202

Serra P, Pons X, Sauri D (2003) Post-classification change detection with data from different sensors: some accuracy considerations International Journal of Remote Sensing 24(16):3311-3340

Solaimani K, Arekhi M, Tamartash R, Miryaghobzadeh M (2010) Land use/cover change detection based on remote sensing data (A case study; Neka Basin) Agric Biol JN Amer 1(1148-1157

Taffesse AS, Dorosh P, Gemessa SA (2012) Crop Production in Ethiopia: Regional Patterns and Trends Food and agriculture in Ethiopia: Progress and policy challenges 74(53

Tanrivermis H (2003) Agricultural land use change and sustainable use of land resources in the Mediterranean region of Turkey Journal of Arid Environments 54(3):553-564

Wang K, Franklin SE, Guo X, Cattet M (2010) Remote sensing of ecology, biodiversity and conservation: A review from the perspective of remote sensing specialists Sensors 10(11):9647-9667

Xu L, Zhang S, He Z, Guo Y The comparative study of three methods of remote sensing image change detection. In: Geoinformatics, 2009 17th International Conference on, 2009. IEEE, pp 1-4

Yacouba D, Guangdao H, Xingping W (2009) Assessment of land use cover changes using ndvi and dem in Puer and Simao counties, Yunnan Province, China World Rural Observations 1(2):1-11

Yadav PK, Kapoor M, Sarma K (2012) Land use land cover mapping, change detection and conflict analysis of Nagzira-Navegaon corridor, Central India using geospatial technology International Journal of Remote Sensing and GIS 1(2):90-98

Zhao GX, Lin G, Warner T (2004) Using Thematic Mapper data for change detection and sustainable use of cultivated land: a case study in the Yellow River delta, China International Journal of Remote Sensing 25(13):2509-2522

The influence of volatile organic components on the stable isotopic composition of the groundwater in Tanjero area - Kurdistan region, Iraq

Kareem, Aras — Department of Hydrogeology, Institute of Geology, Technische Universität Bergakademie Freiberg, Gustav-Zeuner Str. 12, 09599 Freiberg, Germany. Email: arasomer@yahoo.com

Merkel, Broder — Department of Hydrogeology, Institute of Geology, Technische Universität Bergakademie Freiberg, Gustav-Zeuner Str. 12, 09599 Freiberg, Germany. Email: merkel@geo.tu-freiberg

Abstract: Landfills in urban areas are among the major sources for organic contamination. Seasonal weather changes accelerate the disintegration of organic matter and precipitation increases the risk of leakage through the subsurface into the groundwater. BTEX compounds are among the most common organic contaminants in the environment, particularly on industrial sites. In this study, they were found in Tanjero's industrial area southeast of Sulaimani city near Tanjero River. BTEX are present there as a result of random dumping of volatile solvents by petroleum refineries on the waste dump site as well as dumping of municipal waste rich in organics from Sulaimani city. The stable isotopes of water in the wells around the waste site show an evaporation effect as compared to wells that are more than 1 kilometer away from the landfill site. The seasonal variations of BTEX concentrations in groundwater are correlated with the stable isotopes of water ($\delta^{18}O$, $\delta^{2}H$) as a result of increasing bio-degradation, the lack of rainfall and dropping groundwater table in summer. Due to heat developed by the microbial degradation of BTEX and other organic components, seepage water evaporates and leads to a shift of the signature of the stable isotopes of water. This changed isotope signature can also be traced in the groundwater in the downstream plume of the dump site.

Keywords: Landfill; petroleum refinery; stable isotopes; BTEX; groundwater contamination

1 Introduction

The growing population in Sulaimani city (Kurdistan region, northern Iraq) led to an increase in solid waste generation that reached up to 1000 tons per day (Rashid 2010) (Fig. 1). In the last decade the industrial zone in Tanjero area was characterized by an increasing number of petroleum refineries. The area is located to the southwest of Sulaimani city (12 km from the city center). Waste, warehouses, and fuel tanks are randomly spread without any control measures in place or any concept for environmental protection. The industrial remains are dumped uncontrolledly on a fenced but non-supervised and not constructed landfill site. The area of the landfill is about 50 hectares allocated for the municipal waste dumping. The wells around the waste dump area are contaminated with benzene, toluene, ethylbenzene and xylenes (BTEX) that caused changes in the quality of the pumped water and the suitability for human consumption.

The seasonal weather changes are significant in Kurdistan region of Iraq. The climate is characterized by cold and snowy winters and long, warm dry summers. Autumn and spring are short. During summer, the day temperature may reach 45°C. The main characteristic of the seasonal rainfall distribution is the absence of precipitation in summer (June-September). Rainy season usually starts in mid-October and ends in the beginning of May. The month with the greatest amount of precipitation in the

whole region is January (Stevanovic and Markovic 2003) (Tab. 1). The area of interest consists of clastic rocks (Tanjero formation) with a thickness approximately 140 m and clastic alluvium sediments that contain gravel, sand, and clay (Budy et al. 1980; Ali 2007). Tanjero is a river flowing permanent along the southern margin of Sulaimani city and feeding Darbadikhan Lake in the east-southeast (Habib 2003). This small river is polluted by the sewage of the city and some villages around (NI 2008).

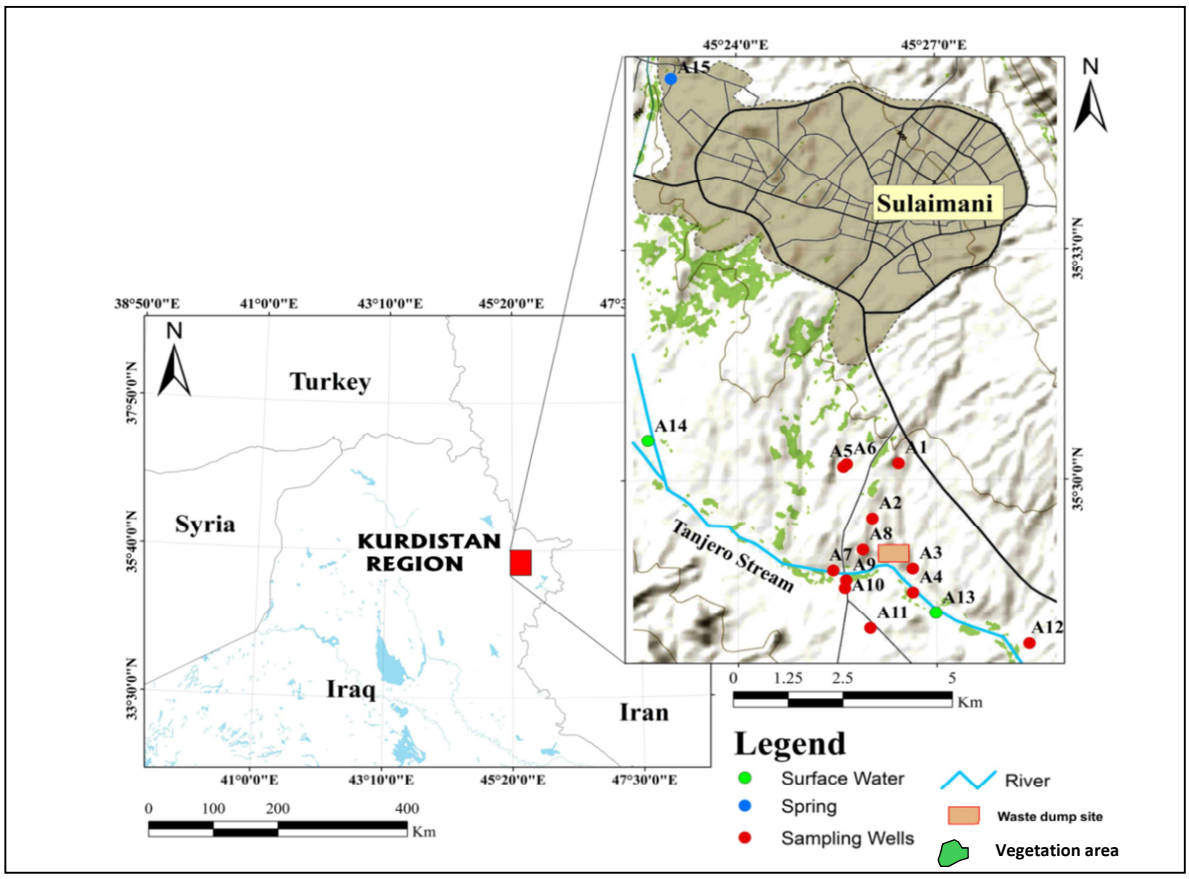

Fig. 1: Map of the study area

Tab. 1: Average monthly climate parameters of the study area over a period of 25 years (Mustafa 2006).

Month	Air temperature (°C)	Relative humidity (%)	Water vapor pressure (mbar)	Rainfall (mm)	Sunshine (h)	Evaporation (mm)
January	5.7	68.4	6.89	125.4	4.9	51.8
February	6.7	64.9	6.7	107.7	5.7	57.5
March	10.8	58.7	7.8	112.1	6.9	108.5
April	16.6	54.3	9.9	77.6	6.3	143.6
May	22.4	39.4	10.9	37.2	9.5	250.7
June	29	24.6	7.1	4.6	11.6	342.1
July	33.1	22.6	11.8	0.7	11.5	416.9
August	32.1	22.9	11.1	0	11.8	368.8
September	28.3	25	9.7	3.9	10.5	263.5
October	22	37.4	9.5	26	7.9	165.8
November	13.7	59.2	9	96.6	6.2	78.6

December	8.2	68.5	6.3	111.6	5.8	51

The groundwater contamination in the study area is caused by the dumping of solid and liquid waste and contaminants spread by surface runoff, river drainage systems, wastewater discharges, eutrophication and littering (Patrick et al. 2002). The increased amount of waste and contaminants endangers local environments, natural resources, public health, local economies, and proper living conditions. Various diseases like cancer result from the exposure to hazardous emissions mainly from waste incineration without proper technologies. Especially the worker faces high health risks (EPA 2007). Waste water discharges damage the soil and irrigation system (Green, Jammenjad 1997). The relative share different components contribute to the total sum of municipal garbage dumped on the landfill site is showed in Tab. 2 (Ray 1958).

Tab. 2: Main components of the municipal garbage (modified after (Ray 1958)).

Category	%
Paper	30
Putrescible	25
Fines	10
Glass	8
Metal	8
Plastics	8
Textile	3
Rubber	3
Miscellaneous	5

The oil refinery industry produces several types of hydrochloric and sulfochloric acid leachate waste. The refining and processing of crude oil requires water; one gallon of crude oil generates 30 gallons of wastewater (Ray 1958).

Benzene, toluene, ethylbenzene and xylene (BTEX) are often found together and all have their origin in the petroleum production and leaks from underground fuel storages and landfills. These compounds are relatively mobile and can easily dissolve in water and hence contaminate groundwater (Davis et al. 1999; Kennedy 1992; Batlle-Aguilar 2008). BTEX compounds have been reported to be toxic compounds having hazardous effects on terrestrial biota as well as aquatic organisms (An 2004). Some regional environmental isotope studies have been done around the study area. Results from Haji Omaran (Mawlood 2003) and Rania area (Al Manmi 2008) yielded a LMWL (Local meteoric water line) defined by the equation:

$$\delta^2H=7.7\delta^{18}O+14.4 \qquad \text{(Hamamin, Saeed 2012)}$$

While the GMWL (Global meteoric water line) is defined by the equation:

$$\delta^2H = 8\ \delta^{18}O +10 \qquad \text{(Craig 1961).}$$

Data from stable isotope analysis can be used to determine the origin of contaminants, the combination of different sources contributing to a multi-source plume, but also to characterize their complex transport processes and to assess measures for contaminated site remediation. Quantitatively assessing isotopic fractionation can be done for studying the progress of environmental processes like biodegradation. (North et al. 2006).

2 Materials and methods

15 water samples were collected from several wells around the landfill site (Fig.1 and Tab. 3) according to the standards for water sampling for BTEX and stable isotope analyses (Borden et al. 1996; Headley and Rae 1992). Sample A13 was taken southeast of the waste dump site and refineries and sample A14 was taken from Tanjero River northwest of the waste dump site and refineries. A15 was collected from Sarchnar spring 10 km away from the dump site. The rest of the samples were collected from water wells in the industrial area at various distances from the waste dump site. For the GC-MS determination, a 50 ml glass tube was filled with 25 ml of sample and sealed with caps using a crimper. The volume of the stable isotopes analysis glass tube was 30 ml. The sample glass tubes filled completely and firmly closed. All samples were with vials containing 1.5 ml in the auto sampler and the average of the results calculated from 10 runs.

Tab. 3: Names and locations of the water samples.

Sample No.	Name of the location	Latitude			Longitude		
A1	Yellow house well	35°	30′	12.7′′	45°	26′	11.5′′
A2	Metal melting factory well	35°	29′	30.1′′	45°	26′	2.1′′
A3	Livestock warehouse (well depth 42 m)	35°	28′	50.6′′	45°	26′	38.6′′
A4	Livestock warehouse (well depth 15 m)	35°	28′	32′′	45°	26′	38.6′′
A5	A house south of scrape location (well depth 75 m)	35°	30′	10′′	45°	25′	36′′
A6	The well of the School	35°	30′	12.2′′	45°	25′	39′′
A7	The well of the pebble factory	35°	28′	49.4′′	45°	25′	26.4′′
A8	The well of the pebble crushing factory	35°	29′	5.7′′	45°	25′	53.3′′
A9	The well beside the stream at the west bank	35°	28′	41.7′′	45°	25′	38.1′′
A10	The well of the oil factory	35°	28′	35.6′′	45°	25′	36.9′′
A11	The well of the building material warehouse	35°	28′	4′′	45°	25′	59.8′′
A12	Qaywan oil warehouse	35°	27′	51.7′′	45°	28′	23.9′′
A13	Tanjero Stream south the waste site	35°	28′	15.9′′	45°	26′	59.3′′
A14	Tanjero Stream above the industrial area	35°	30′	30.9′′	45°	22′	38.8′′
A15	Sarchnar Spring	35°	35′	14′′	45°	23′	0.9′′

BTEX was determined by headspace technique with gas chromatography and detection by mass spectrometry (Thermo Scientific Ultra-ISQ GC-MS) in the laboratory of the Department of Hydrogeology of TU Bergakademie Freiberg according to the procedures described by (Butler et al. 2010). The stable isotopes $\delta^{18}O$ and $\delta^{2}H$ were measured by a liquid-water isotope analyzer based on cavity ring down spectroscopy with a reproducibility of 0.3 ‰ for $\delta^{2}H$ and 0.1 ‰ for $\delta^{18}O$ (LGS, Los Gatos Research) in the laboratory of the Department of Hydrogeology of TU Bergakademie Freiberg.

3 Results and discussion

The stable isotope analysis data for winter and summer is shown in Fig. 2 and Fig. 3. The standard deviation and error bars are included as well for indicating the uncertainty of the stable isotopes data whose importance (Donald et al. 2001) underlined.

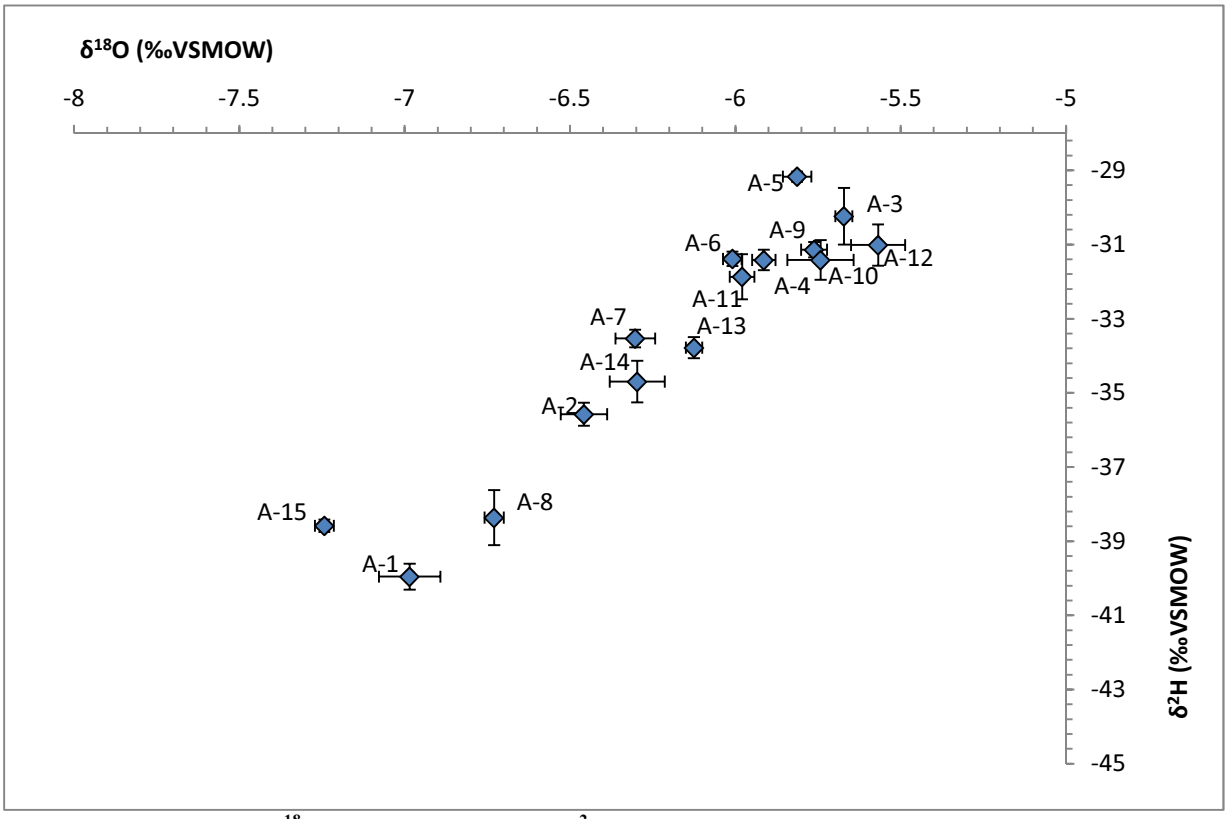

Fig. 2: Scatter-gram of $\delta^{18}O$ (‰VSMOW) versus $\delta^{2}H$ with error bars for winter samples

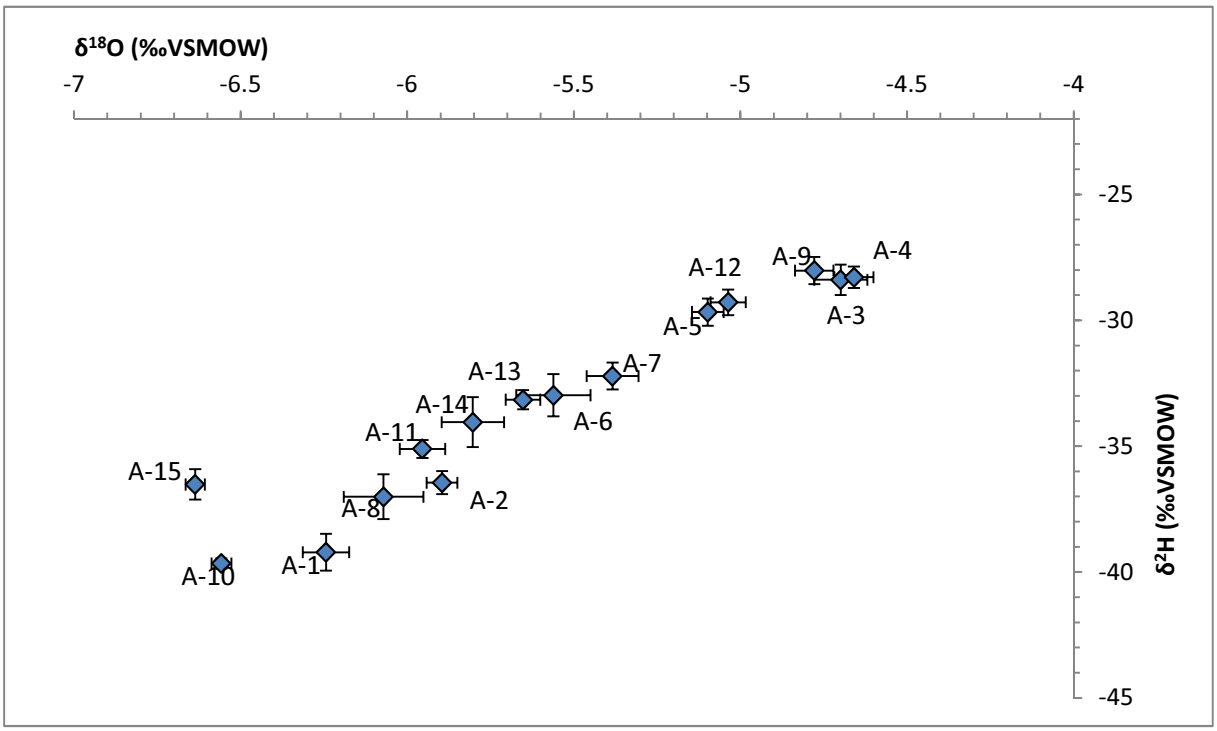

Fig. 3: Scatter-gram of δ18O (‰VSMOW) versus δ2H with error bars for summer samples

In summer, two leachate samples were collected from two interflow drainages on the waste dump site and analyzed for BTEX as shown in Tab. 4.

Tab. 4: BTEX concentrations in the leachate of the drainages.

	Benzene	Toluene	Ethylbenzene	Total xylene	Sum
Northern waste drainage 1	14.25	23.93	<0.01	2.71	40.89
Southern waste drainage 2	2.54	27.93	2.28	8.23	40.98

Note: The waste drainage data is not plotted in the following figures.

3.1 BTEX and stable isotopes results for the end of December 2012 samples

BTEX components revealed rather low concentrations (< 0.55 ppb) during winter (Fig. 4) and elevated concentrations of up to 3.4 ppb during summer (Fig. 6). During winter, the sampling point A4 showed some higher BTEX values while in summer A3, A4, A9, A10, and A12 showed significantly higher BTEX concentrations. During winter season, the xylene contents in the water samples A3 and A4 were elevated with 0.54 and 0.11 ppb, respectively, as compared to the other well and surface water samples. The wells from which sample A3 and A4 were taken are located at 15 m distance from the eastern fence of the landfill site. In the other groundwater samples xylene concentrations were equal to or less than 0.11 ppb and the concentrations of the other BTEX components (benzene, toluene, and ethylbenzene) were less than 0.1 ppb except for sample A4.

The average rainfall was 119.1 mm and the air temperature was 7.8 °C from November 2012 until the end of January 2013. The stable isotopes plot around the LMWL except for those of sample A3 and A4, which plot below the LMWL. The GMWL is used for understanding the distribution of the stable isotopes signatures of the area and the evaporation (Clark, Fritz 1997). The samples A3, A4, A5, A9, and A12 show high levels of BTEX contamination compared to the samples A15, A10, and A1. Water sample A15 plots above the LMWL (Fig. 5). These water samples were collected from springs and wells far from the waste dump site and the industrial area (2 to 10 km north and northwest of the waste dump site). Sample A4 and A3 represent the effect of dump site leaching as BTEX plume in the groundwater. The precipitation during rainy season diluted the concentration of the dump site contamination plume in the groundwater especially in the shallow aquifer. This was found by (Castañeda et al. 2012) in a similar scenario.

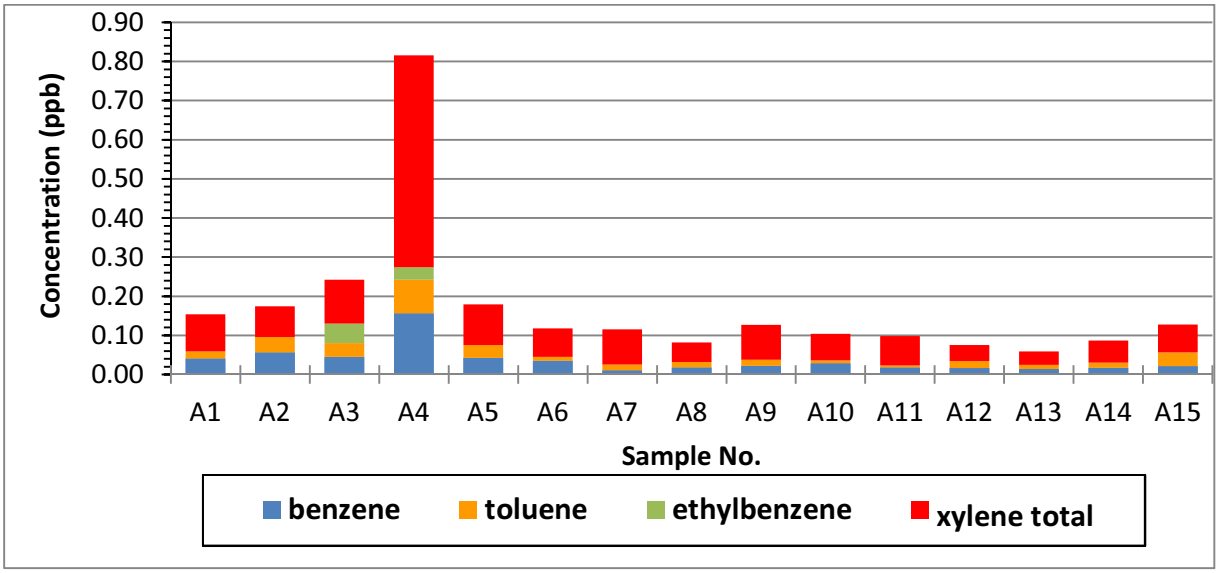

Fig. 2: Concentration of the BTEX components in the water samples taken during winter season

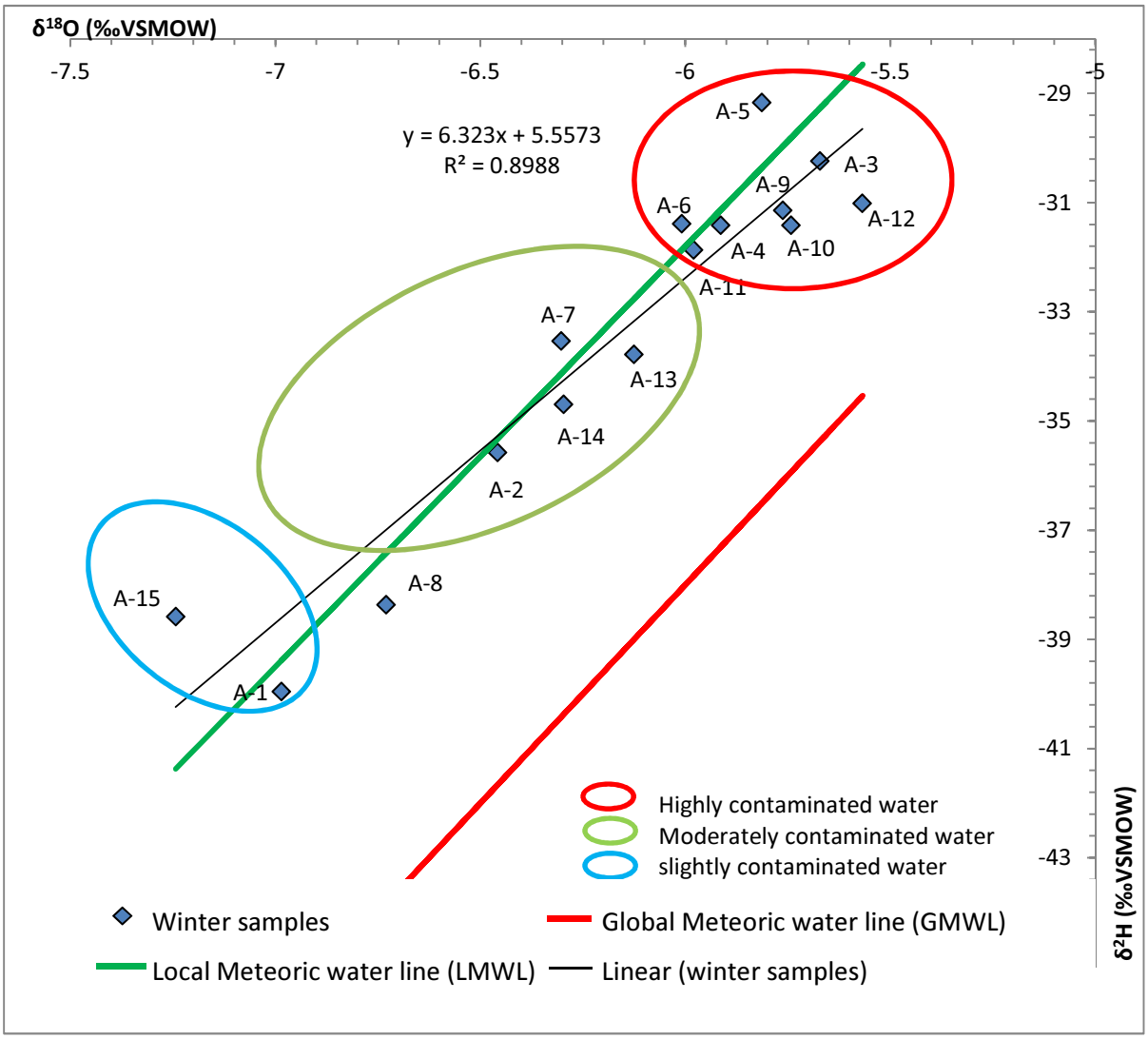

Fig. 3: Stable water isotopes during winter

3.2 BTEX and stable isotopes results for the end of June 2013 samples

All water samples except for A15 plot below the LMWL, which indicates elevated biodegradation of the contaminants in the groundwater. The heat generated by this elevated biodegradation caused a stronger isotopic fractionation, i.e. lighter isotopes evaporated more rapidly than heavier isotopes ((Delleur Jacques 2007); Miljević 2007) (Fig. 7 and Fig. 9)). These samples represent the water of the wells around the waste dump site and near the refineries and oil warehouses in the industrial area. Some of these facilities had been running during the last 8 months as in sample A9 and A10. And this might have had an effect on the results of the BTEX and the stable isotopes values in summer.

The average rainfall has been very low in the period between the beginnings of June and the end of August 2013 with only 4.1 mm. The average temperature was high and reached 32°C. But still the water samples A15 and A1 show low BTEX concentrations compared to the other samples. The reason for the temperature increase during summer is that under favorable conditions microorganisms increase their activity easily by several orders of magnitude and produce additional heat. A similar scenario was observed by (Hackley et al. 1996) in a study area in Illinois landfill-USA.

The water samples A2, A7, A8 and A14 show moderate BTEX concentrations and moderate shifting of the stable isotopes signature. Relative to the other water samples, the samples A2, A7 and A8 represent samples that are located north and west of the waste dump site. The water samples A3, A4, and A9 have higher BTEX concentrations and plot below the high end of the LMWL (Fig. 6). The recharge shortage in the study area in summer is a result of the rainfall shortage in summer. The static water table of the wells A3 and A4 in winter was 3 m and 5 m below surface but only 8 m and 11 m, respectively, in summer.

The summer samples show more strongly depleted δ^2H isotope signatures than the winter samples. This can be explained by the fact that the summer samples were subjected to stronger evaporation than the winter samples, by the action of biodegradation of the organic contaminants in groundwater and additionally by the increased BTEX input (Fig. 8).

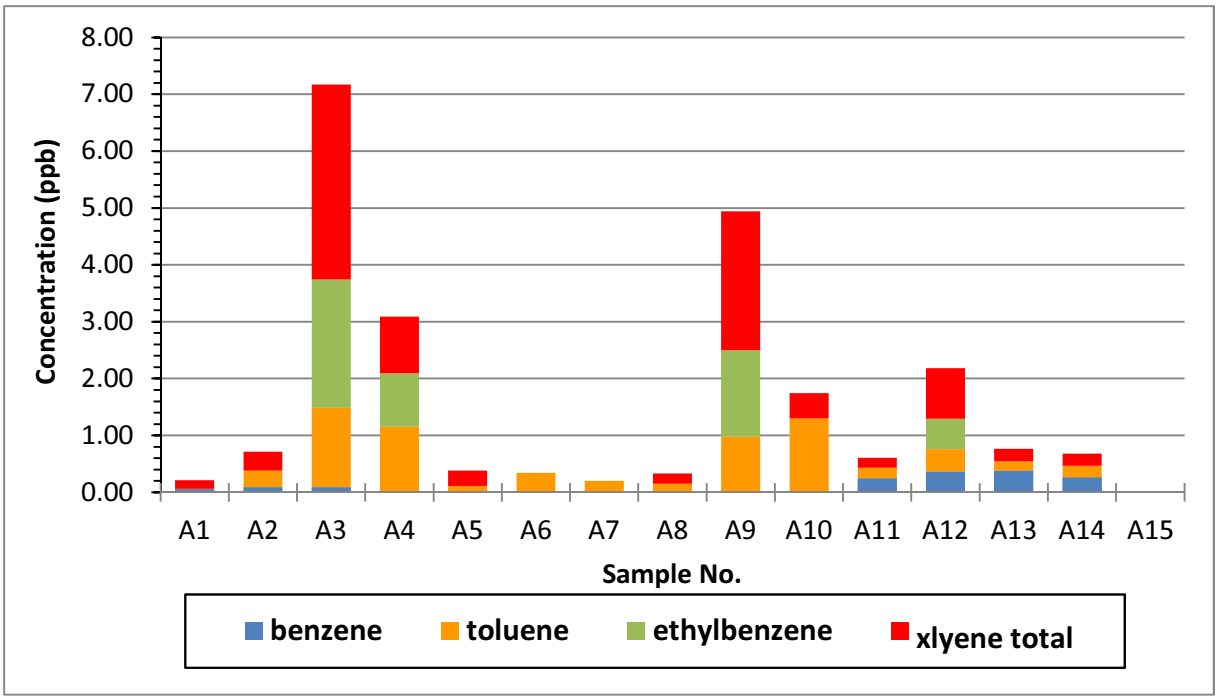

Fig. 4: Concentration of the BTEX components in the water samples taken during summer season

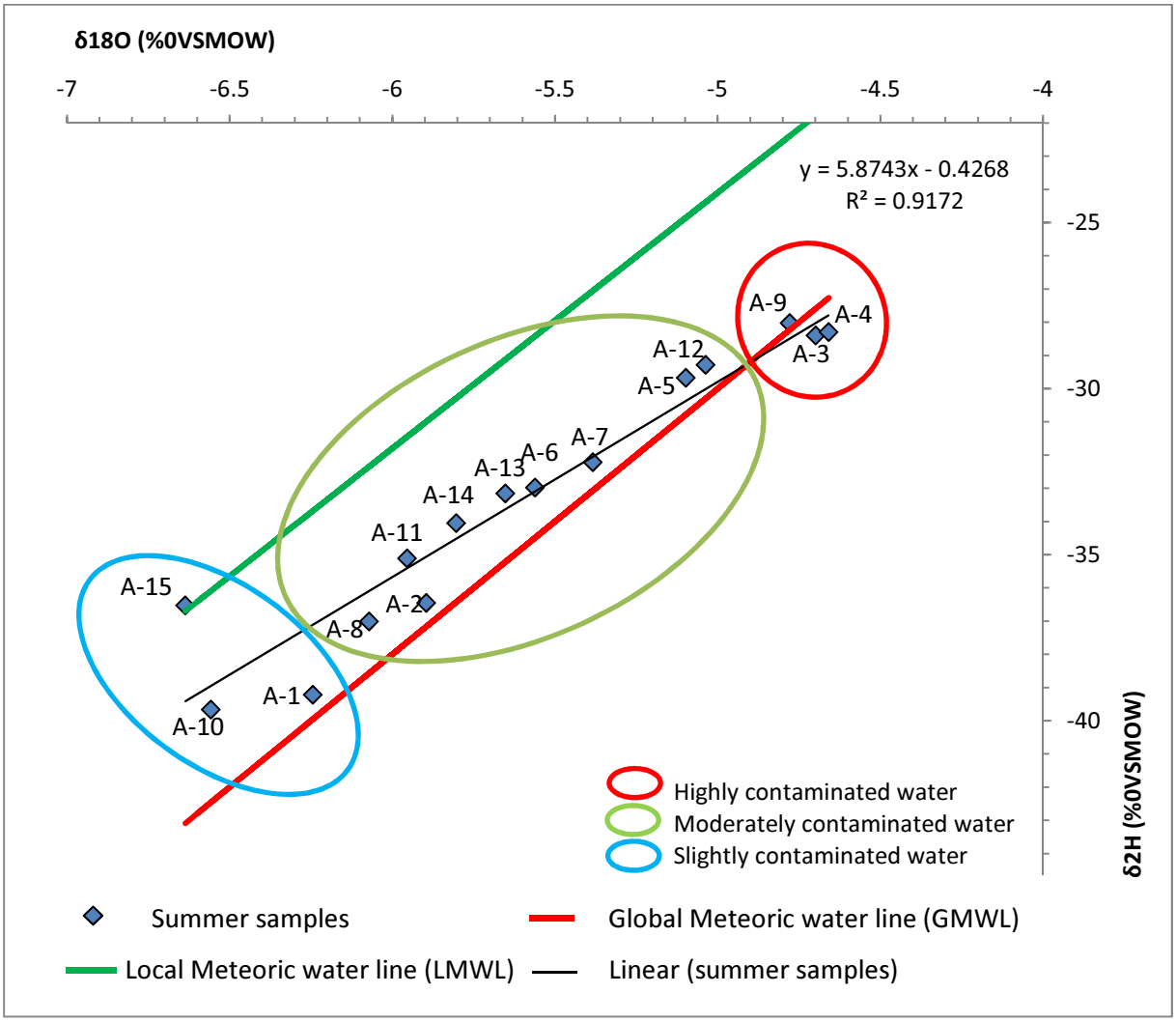

Fig. 5: Stable water isotopes during summer

The relationship between the average of the sum of the BTEX components and the average of $\delta^{18}O$ signatures of winter and summer seasons reveals that the water samples that are highly contaminated with BTEX (such as A3 and A4) show lighter $\delta^{18}O$ values than the less strongly BTEX-contaminated water samples like A15 and A1 (Fig. 8).

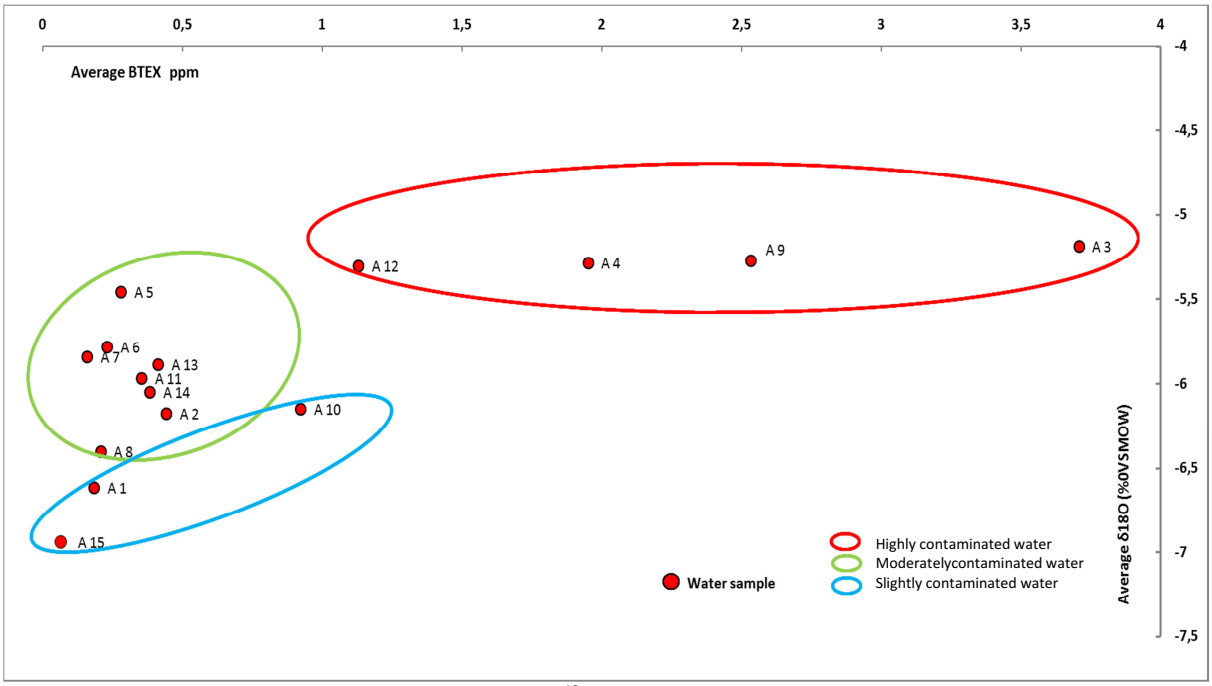

Fig. 6: Relationship between the mean of BTEX and $\delta^{18}O$

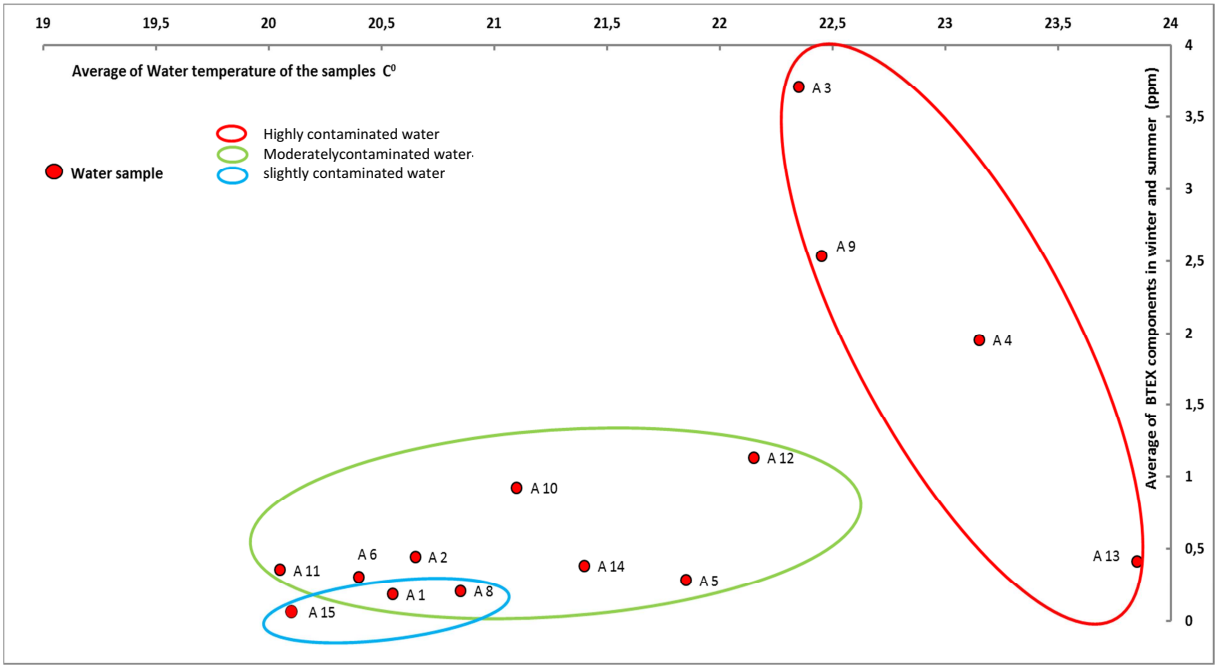

Fig. 7: Relationship between the mean of BTEX and mean of water temperature

4 Conclusions

Stable isotopes in groundwater are significantly correlated with the BTEX concentrations in groundwater. The biodegradation of BTEX and probably other organic contaminants produces heat, which triggers an increase of evaporation and fractionation of r isotopes in soil water and groundwater. Stable isotopes in groundwater can thus be used as an indication for additional evaporation resulting from organic contaminations in soil- and groundwater. The study of BTEX and stable isotopes in groundwater can be used as a tracer for determining the contamination flow and contaminated groundwater plume around the source of contamination.

5 Acknowledgments

This work was supported and funded by the ministry of higher education (MHE) - Kurdistan region government (KRG). A special thank goes to Mr. Rudi Abo for his help und discussions during the BTEX analysis.

6 List of references

Al Manmi, D. A. (2008): Water resources management in Rania area, Sulaimaniyah NE-Iraq. Unpublished Ph.D. thesis. University of Baghdad.

Ali, S. S. (2007): Geology and hydrogeoloy of Sharzoor-Piramagroon basin-Sulaimani. Unpublished Ph.D. thesis. Belgrade Univeristy.

An, Y. J. (2004): Toxicity of Benzene, Toluene, Ethylbenzene, and Xylene (BTEX) Mixtures to Sorghum bicolor and Cucumis sativus, Bull Environ Contam Toxicol (72), pp. 1006–1011.

Batlle-Aguilar, J. (2008): Groundwater flow and contaminant transport in an alluvial aquifer: in-situ investigation and modelling of a brownfield with strong groundwater - surface water interaction. Ph.D. thesis. University of Liège, Belgium.

Borden, C. R.; Goin, R. T.; Chih-Ming, K.; Charlita G. R. (1996): Enhanced Bioremediation of BTEX Using Immobilized Nutrients: Field Demonstration and Monitoring.

Budy, T.; Jassim, S. Z.; Kassab, I. I. (1980): Regional geology of Iraq Vol. 1, p. 445.

Butler, J.; Steiniger, D.; Robarge, T.; Phillips, E. (2010): Combining Hardware, Software, and Chromatography to Improve the GC/MS Analysis of Semi-Volatile Compounds. Austin, TX, USA.

Castañeda, S. S.; Sucgang, R. J.; Almoneda, R. V.; Mendoza, N.D.S.,David C.P.C. (2012): Environmental isotopes and major ions for tracing leachate contamination from a municipal landfill in Metro Manila, Philippines Vol. 110, pp. 30–37.

Clark, I.; Fritz, P. (1997): Environmental Isotopes in Hydrogeology: CRC press LLC.

Craig, H. (1961): Isotopic variations in meteoric waters (133), pp. 1702–1708.

Davis, G. B.; Barber, C.; Power, T. R.; Thierrin, J.; Patterson, B. M.; Rayner, J. L.; Wu, Q. (1999): The variability and intrinsic remediation of a BTEX plume in anaerobic sulphate-rich groundwater (36), pp. 265–290.

Delleur Jacques, W. (2007): The Handbook of Groundwater Engineering. 2nd ed.: CRC press LLC (Chapter 17).

EPA (2007): Mercury-containing products, mercury: spills, disposal and site cleanup.

Green, D. C.; Jammenjad, G. (1997): Settlement characters of Domestic waste. Lonclon: Thomas Telford.

Habib, I. (2003): La politique agraire en Irak de 1920 a 1980 et ses consequences sur les soiceoetes rurales. Paris: Publibook.

Hackley, K. C.; Liu, C. L.; Coleman, D. D. (1996): Environmental Isotope Characteristics of Landfill Leachates and Gases. doi: 10.1111/j.1745-6584.1996.tb02077.x. Groundwater Vol. 34, pp. 827–836.

Hamamin, D.; Saeed, Ali.S. (2012): Hydrodynamic studyof karstic and intergranular aquifers using isotope geochemisty in Basara basin, Sulaimani, North-Eastern of Iraq. With assistance of Arabic Journal of Geosciences.

Headley, J. V.; Rae, W. E. (1992): Sampling and Analytical Strategies for Delineating Petroleum Contaminated Soils and Ground Water. Bulletin of Canadian Petroleum Geology Vol. 40 (4), pp. 295–302.

Kennedy, L. (1992): Site characterisation at pipeline spill at Park City, Kansas: estimating hydraulic and geochemical constraints on bioremediation. Bioremediation of Hazardous Wastes. US-EPA document EPA/600/R-92/126, pp. 7–9.

Mustafa, O. (2006): Impact of sewage wastewater on the environment of Tanjero river and its basin within Sulamiani city/ NE-Iraq. M.Sc. degree. Sulamani University, Sulamani.

Mawlood, D. (2003): Application of isotope hydrology studies considering the specific climate, hydrogeological and geological conditions in order to research underground water resources in a specific area in the near East. Unpublished Ph.D. Vienna University of Technology, Vienna.

Miljević, N.; Golobočanin, D. (2007): Potential Use of Environmental Isotopes in Pollutant Migration Studies. Archives of Industrial Hygiene and Toxicology. doi: 10.2478/v10004-007-0015-5 Vol. 58 (2), pp. 251–262, checked on 5/3/2015.

NI (2008): survey of water quality, sediment, benthic macro invertebrate and fisheries for Qara Ali dam irrigation project (QDIP). Nature Iraq field and lab. Report. Environmental impact assessment.

North, J. C.; Frew, R. D.; van Hale, R. (2006): Can stable isotopes be used to monitor landfill leachate impact on surface waters? Journal of Geochemical Exploration, Elsevier, pp. 49–52.

Patrick, R.; Ford, E.; Quarles, J. (2002): Groundwater contamination in the united states. 2nd ed.

Phillips, D. L.; Gregg, J. W. (2001): Uncertainty in source partitioning using stable isotopes Vol. 127 (2), pp. 171–179.

Rashid, Kh. (2010): Environmental Implication of Tanjero waste disposal site of Sulaimani. Unpublished Ph.D. Sulaimani University, Sulaimani.

Ray, F. E. (1958): Oil Refining Wastes. Sewage and Industrial Wastes Vol. 30 (11), pp. 1390–1393. Available online at http://labs.jstor.org/demo/stable/25033746.

Stevanovic, Z.; Markovic, M. (2003): Hydrogeology of northern Iraq. Climate, Hydrology, Geomorphology, Geology. Ed. “Field documents” Vol. 1.